SIMULATION OF GLOBAL TSUNAMI HAZARD ALONG THE U.S. EAST COAST

BY

STEPHAN T. GRILLI, LAUREN SCHAMBACH AND ANNETTE GRILLI

DEPT. OF OCEAN ENGINEERING, UNIVERSITY OF RHODE ISLAND

RESEARCH REPORT NO. CACR-20-02

NTHMP AWARD #NA18NWS4670073

NATIONAL WEATHER SERVICE PROGRAM OFFICE

CENTER FOR APPLIED COASTAL RESEARCH

Ocean Engineering Laboratory
University of Delaware Newark,
Delaware 19716

Contents

Methodology

Global tsunami coastal hazard along the US East Coast (USEC) is simulated and assessed based on a series of extreme tsunamigenic sources, identified in past work (e.g., Hornbach et al., 2007; Gica et al., 2008; Barkan et al., 2009; Chaytor et al., 2009; Grilli et al., 2009, 2010, 2013, 2015, 2017a,b; Abadie et al., 2012; Grilli and Grilli 2013a,b,c; ten Brink et al., 2014; Tehranirad et al., 2015; Schnyder et al., 2016; Schambach et al., 2018, Abadie et al., 2019). The sources detailed and modeled below are divided into three groups: 1) co-seismic, 2) submarine mass failure (SMF), and 3) volcanic flank collapse (Figure 1). These sources were individually simulated and their tsunami impact assessed for some areas of the USEC as part of work performed since 2010 under the auspices of the US National Tsunami Hazard Mitigation Program (NTHMP). However, the global impact of these tsunamigenic sources along the entirety of the USEC had not been systematically assessed. This assessment is the object of this work. Using the best available digital elevation models (DEMs) of bathymetric/topographic data in each respective area, two levels of tsunami model grids are developed (Figure 2), with a coarser ocean-basin scale 1 arc-min level spherical coordinate grid G0, and three 450 m resolution Cartesian grids G1-G3 encompassing the USEC. Simulations are performed based on a one-way grid nesting technique to increase model resolution along the coast, and the global tsunami coastal hazard is calculated along the 5 m isobaths, in the form of maximum elevation, current velocity and momentum force. These parameters are graphically represented as color-coded classes in a series of figures prepared in each grid for each modeled tsunami source.

Specifically, co-seismic sources considered here include the extreme:

(i) hypothetical Mw 9.0 earthquake in the Puerto Rico Trench (PRT; Figure 1), developed and used by Grilli et al. (2010, 2013, 2016, 2017b), based on 12 sub-fault planes with parameters obtained from the Short-term Inundation Forecast for Tsunamis (SIFT; Gica et al., 2008) database;

(ii) historical 1755 Lisbon (LSB) co-seismic source, within the Azores Convergence Zone (ACZ; Figure 1), whose magnitude was estimated at Mw 8.5-9.0 (here the largest value is used), and exact location was unknown. Barkan et al. (2009) found that the most likely location was the Horseshoe Plane area, and estimated the source parameters for a Mw 9 magnitude. Grilli and Grilli (2013a) modeled the tsunami caused by a dozen Mw 9.0 co-seismic sources sited in this area, with different slip and strike angle, based on Barkan et al. (2009). They determined that strike angles of 15° and 345° caused maximum impact on the upper USEC and lower USEC respectively (with the lower USEC always being the most impacted); both strike angles for this source are considered here.

Initial surface elevations caused by these co-seismic sources are computed using Okada's (1985) method, based on fault plane parameters. These are specified as initial condition in grid G0 (with

no velocity) and tsunami propagation is computed with the two-dimensional (2D) fully nonlinear dispersive Boussinesq wave model FUNWAVE-TVD (Shi et al., 2012). Okada's method solves a three-dimensional elasticity problem for a homogenous half-space with a dislocation specified over an oblique plane, given the fault plane width, length, depth, centroid location, dip, rake, strike, shear modulus of the medium, and either the moment magnitude or the fault slip value.

Chaytor et al.'s (2009) and ten Brink et al.'s (2014) field surveys showed the presence of widespread historical SMFs (most of them very old) along the USEC shelf break and slope (particularly north of the Carolina's). One dominant historical failure is the entire Currituck slide complex, off of Chesapeake Bay whose combined volume was about 165 km^3 (Geist et al., 2009; Locat et al., 2009; Grilli et al., 2015). Here, SMF sources are modeled in four areas of the upper USEC continental shelf break (Figure 1), which were identified by Grilli et al. (2015), based on the Monte Carlo simulations of Grilli et al. (2009) and an analysis of the availability and nature of seafloor sediment by Eggeling (2012), as having higher risk of a large SMF failure. In earlier NTHMP work, in the absence of detailed guidance for selecting extreme SMF sources, these 4 SMF parameters were selected identical to those of the Currituck slide, and then modeled by Grilli et al. (2015, 2017a,b) and Schambach et al. (2018), as rigid slumps or deforming slides. Rigid slump SMFs, however, were found to trigger worst-case scenario tsunamis. Hence in this work, rigid slump SMFs are modeled in areas 1-4.

Hornbach et al. (2007) present analysis of the Cape Fear slide complex, which is located about 200 km southeast of Cape Fear, NC. At least 5 major escarpments were identified, and a large SMF here would pose particular hazard to the highly populated Myrtle Beach, SC region. Grilli et al. (2013d) modeled a rigid slump SMF here with parameterization based on the work of Hornbach et al. (2007) as a proxy for an extreme SMF in this area. This case is considered in this work.

Schnyder et al. (2016) investigate and model historical and potential future SMFs and a margin collapse located on the slopes of Great Bahama Bank, concluding that failures here pose hazard to the southeastern Florida coastline. The potential future SMF they identified is modeled as a rigid slide with kinematics based on the work of Grilli and Watts (2005) and Enet and Grilli (2007). This case is considered in this work, as well as a case where the same SMF volume is treated as a deforming slide.

SMF tsunami generation is modeled using the three-dimensional (3D) non-hydrostatic model NHWAVE (Ma et al., 2012), in which the rigid SMF geometry and motion are specified as bottom boundary conditions. SMF kinematics is specified based on the analytical laws developed by Grilli and Watts (1999, 2005) and Watts et al. (2005) from a balance of forces, and the geometry is idealized as having a quasi-Gaussian shape (below seafloor) as proposed by Enet and Grilli (2007) and used in earlier work (Grilli et al., 2015; Schambach et al., 2018; see details in appendix of the latter paper). For the deforming SMF case, the SMF is modeled as a dense

Newtonian fluid, coupled with the overlying fluid layer (Kirby et al., 2016). Once the tsunami is fully generated, simulations of wave propagation are pursued in FUNWAVE-TVD.

A volcanic flank collapse of the Cumbre Vieja Volcano (CVV; Figure 1) was identified by Ward and Day (2001) as a potentially devastating tsunamigenic source, able to cause a "mega-tsunami" in the Atlantic Ocean. They proposed an extreme scenario for the western flank collapse of this volcano, with a volume of 500 km^3 of material falling into the ocean. While geological scenarios and landslide rupture kinematics for a CVV flank collapse are still the subject of debate, Abadie et al. (2012) modeled various flank collapse scenarios using the incompressible multi-fluid three-dimensional volume of fluid 3D Navier-Stokes model THETIS considering collapse volumes of 20, 40, 80, and 450 km^3. The slide was considered as a Newtonian fluid with very low viscosity (quasi-inviscid). After waves had propagated far enough from the source, results were reinterpolated into FUNWAVE-TVD grids, to be propagated across the Atlantic Ocean. Based on this source, Tehranirad et al. (2015) further computed tsunami impact in finer nested grids along the USEC. The tsunamis caused by the 80 km^3 and 450 km^3 CVV sources were used in earlier detailed tsunami inundation mapping work performed for NTHMP. Abadie et al. (2019) recomputed the CVV sources to make them more realistic; the slide is considered as a Newtonian fluid whose viscosity is adjusted to approximate a granular behavior, with validation based on experiments of Viroulet et al. (2013) and Grilli et al. (2017a). Here, as in past work, we similarly model 2 scenarios, the 80 km^3 and 450 km^3 flank collapses, using the new results of Abadie et al. (2019). However, note that the extreme 450 km^3 case is not included in our global tsunami hazard assessment as it is considered highly unlikely.

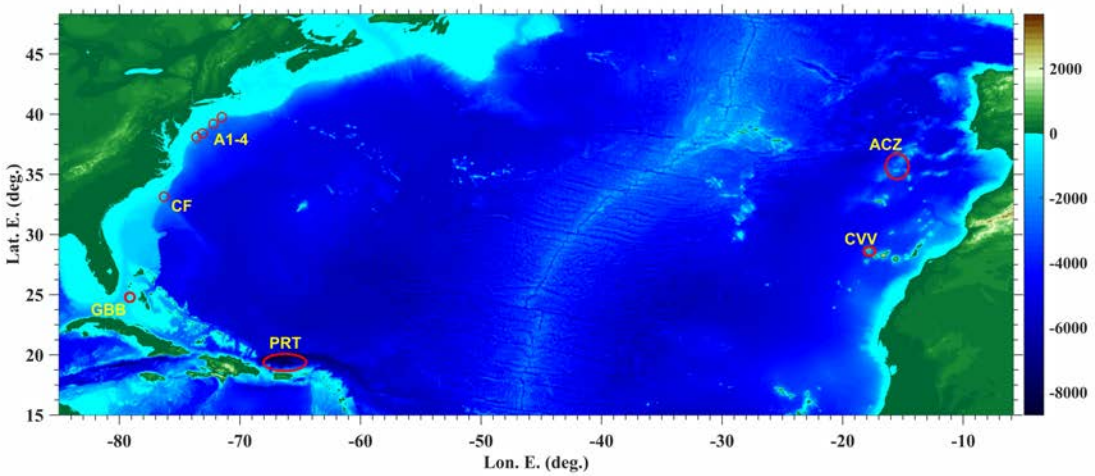

Figure 1: Extreme sources used in USEC global tsunami hazard assessment, including co-seismic (PRT, ACZ), SMFs (in areas referred to as A1-4, Cape Fear (CF), and Great Bahama Bank (GBB)), and volcanic flank collapse (CVV) sources. Color scale shows bathymetry/topography in meters.

After the sources are generated, they are initialized in the 1 arc-minute resolution spherical grid G0 and propagated with FUNWAVE-TVD (Shi et al., 2012). Results for the surface elevation and velocity are saved at thousands of points along the 450 m resolution G1-G3 nested grid boundaries for further one-way coupling simulations (Figure 2). Coastal hazard is quantified

through maximum surface elevations, velocities, and momentum force along the coast. Detailed maps are provided as well as values along the 5 m isobath contour.

This report is organized as follows: in the next section, the computational grids and bathymetric data are detailed. Then, an overview of the specific co-seismic, SMF, and volcanic flank collapse sources is given. Finally, simulation results are shown and discussed.

Bathymetric Data and Computational Grids

Five computational grids are used for simulation work (Figure 2, Figure 3, Table 1). G0 grids are 1 arc-minute resolution spherical grids ranging from 15° – 48.31° latitude. The Large G0 grid is used for transoceanic tsunami propagation, for example, to simulate the propagation of the Lisbon 1755 (ASZ) Mw 9 coseismic and Cumbre Vieja flank collapse (80 or 450 km^3) generated tsunamis. The Local G0 grid is used for sources that are located within the northwestern Atlantic Basin, for example, to simulate the propagation of Puerto Rico (PRT) Mw 9 coseismic and local SMF tsunamis. Three Cartesian computational grids of 450 m resolution are nested within the G0 grids and cover the entirety of the contiguous USEC from Maine to Florida (Figure 3). Grid G1 covers Maine to New Jersey, grid G2 covers New Jersey to South Carolina, and grid G3 covers South Carolina to Florida.

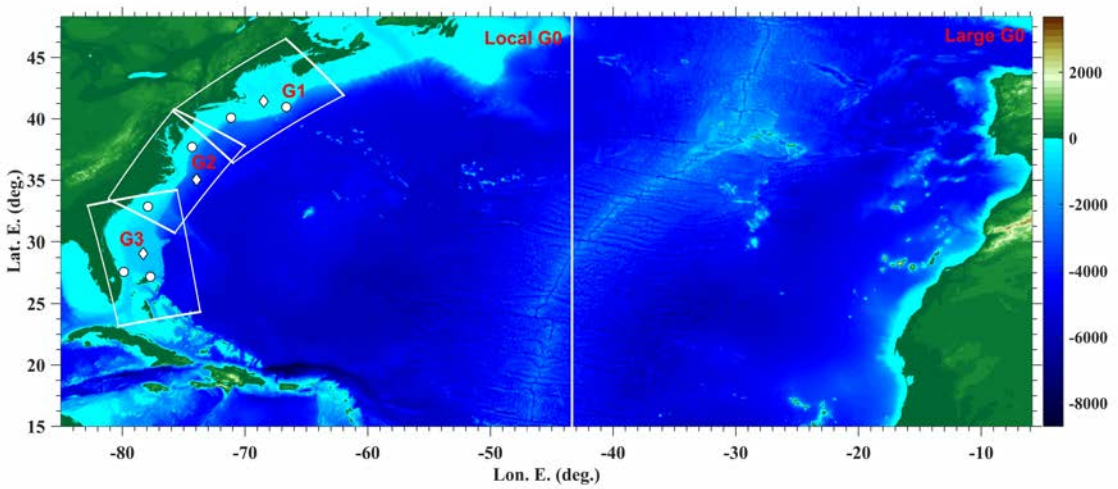

Figure 2: Computational grids used in tsunami simulations, to develop global coastal hazard products for the USEC. Large and Local G0 grids are 1 arc-minute resolution spherical grids, and G1-G3 are 450 m resolution Cartesian grids nested within them (see also Figure 3). White dots mark locations of wave gauge stations located along the 200 m isobath contour, and white diamonds are sub-grid save points used for time series analysis and grid nesting validation. Color scale shows bathymetry/topography in meters.

Grid/Type	Lat (°N)	Lon (°E)	Angle (°)	Resolution	N_x	N_y
G0 Large/S	15.000 (SW)	-85.000 (SW)	-	1 arc min	4750	2000
G0 Local/S	15.000 (SW)	-85.000 (SW)	-	1 arc min	2500	2000
G1/C	41.500 (Center)	-69.000 (Center)	39.66	450 m	2200	1416
G2/C	35.750 (Center)	-75.750 (Center)	57.90	450 m	2100	1332
G3/C	28.705 (Center)	-78.050 (Center)	-258.8	450 m	2472	1536

Table 1: Computational grid parameters. Grid rotation angle is CCW from E.

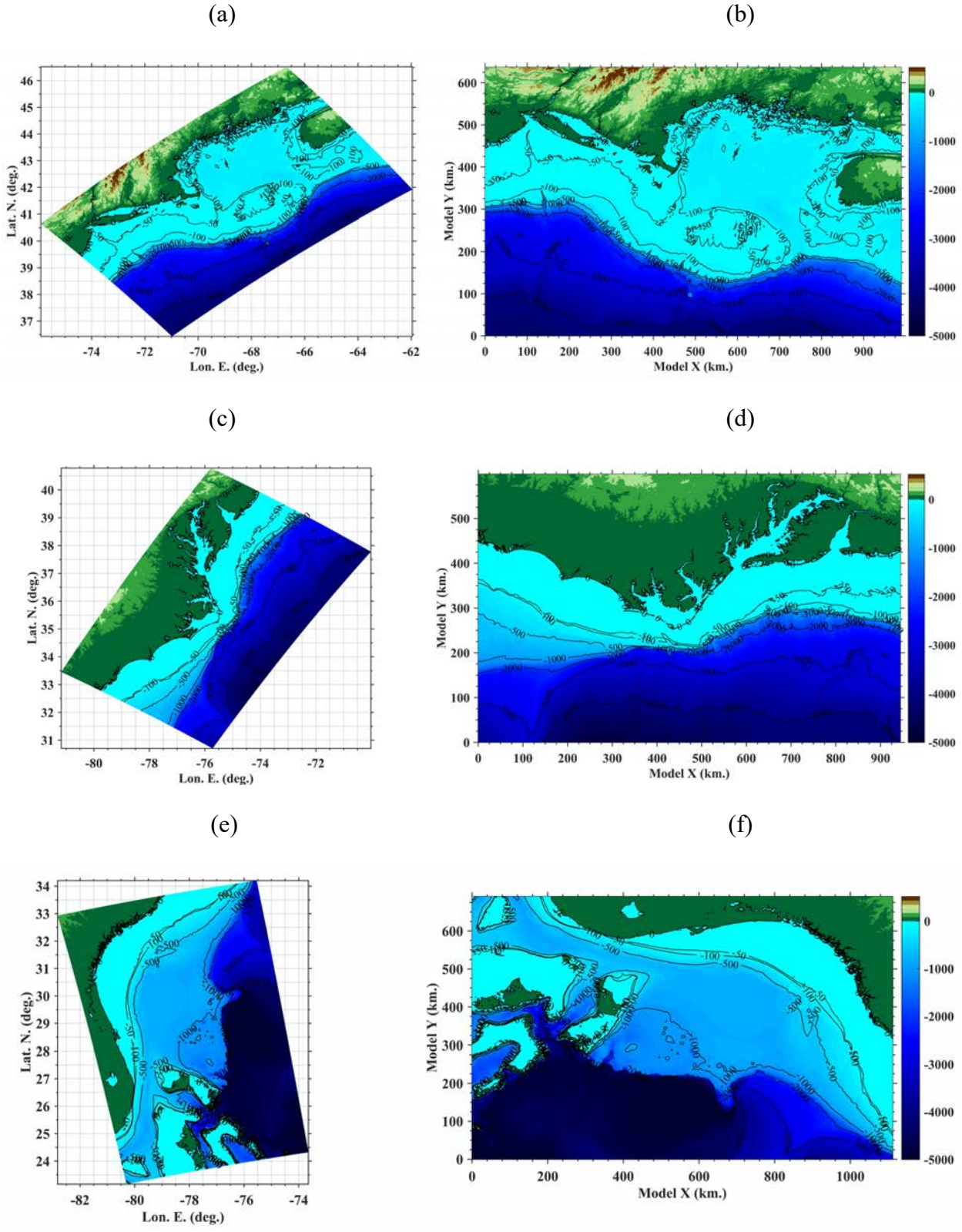

Figure 3: 450 m resolution grids (a, b) G1 (c, d) G2 and (e, f) G3 plotted in (a,c,e) spherical coordinates and (b,d,f) Cartesian model grid coordinates; colorscale and contours show depth in m.

Bathymetric data was obtained from the National Geophysical Data Center (NGDC) Northeast Atlantic (NGDC, 1999), Southeast Atlantic (NGDC, 1998), Florida and East Gulf of Mexico (NGDC, 2001), and Puerto Rico (NGDC, 2004) 3 arc-second resolution Coastal Relief Models (CRM), combined with the ETOPO1 1 arc-minute resolution Global Relief Model (Amante and Eakins, 2009) for areas outside of the CRM coverage. These datasets were combined and interpolated onto each computational grid.

Nine grid save points are defined in Table 2, three of which are located near the center of each respective nested grid (white diamonds, P-G1, P-G2, and P-G3 in Table 2, Figure 2) and used for grid nesting time series verification, and six others, which are located along the 200m isobaths contour (white dots, P1 to P6 from North to South in Table 2, Figure 2), to extract and compare tsunami wave train time series for each source.

Save Point	Lat (°N)	Lon (°E)
P-G1	41.430	-68.480
P-G2	35.050	-73.950
P-G3	29.070	-78.300
P1	40.954	-66.632
P2	40.084	-71.143
P3	37.709	-74.309
P4	32.842	-77.910
P5	27.579	-79.888
P6	27.183	-77.711

Table 2: Grid save points (white diamonds/dots, Figure 2)

Tsunamigenic Sources

Puerto Rico Trench Coseismic Source

Grilli et al. (2010) demonstrated that a large earthquake in the Puerto Rico Trench could generate a large tsunami that would impact the USEC. Their work indicated that an extreme event of magnitude Mw 9.0 may have an estimated return period of about 300 years. Recent discussions with USGS, however, indicate that part of the PRT fault could be locked, thus increasing the return period for an event of this magnitude. Grilli and Grilli (2013b) modeled this event using a combination of 12 NOAA SIFT sources (Gica et al., 2008) scaled to give the appropriate moment magnitude. Okada's (1975) method was used to generate the initial surface elevations. The same procedure and parameters are used here, with the SIFT source parameters given in Table 3 and the resultant initial surface displacement shown in Figure 4. Simulations are performed until t = 24h in the spherical implementation of FUNWAVE-TVD (Kirby et al., 2013) in the Local G0 grid and, by one-way coupling, using the Cartesian model implementation in the nested coastal grids G1-G3. Sponge layers were used in the Local G0 grid boundary to prevent reflections, and were set to 200 km on the west, south, and north boundaries, and 400 km on the east boundary.

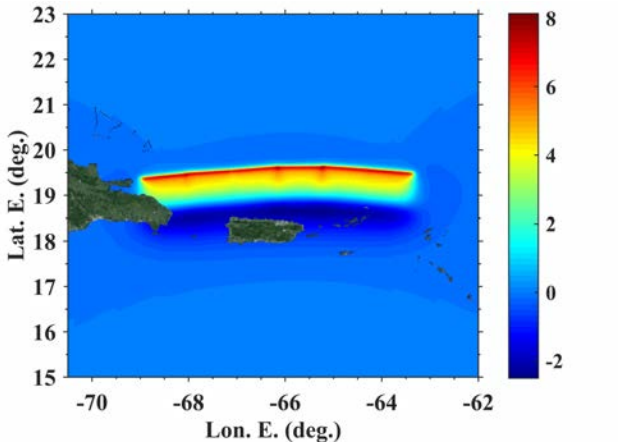

Figure 4: Initial surface elevation (m) computed with Okada's (1985) method for a Mw 9.0 PRT coseismic source consisting of 12 SIFT sub-faults, located at the Puerto Rico Trench (see parameters in Table 3).

Sub-fault	Lat. (°N)	Lon. (°E)	Depth (km)	Strike (°)	Length (km)	Width (km)	Rake (°)	Dip (°)	Slip (m)
1	18.8870	-63.8800	22.1	95.37	100	50	90	20	14.8
2	19.3072	-63.8382	5	95.37	100	50	90	20	14.8
3	18.9650	-64.8153	22.1	94.34	100	50	90	20	14.8
4	19.3859	-64.7814	5	94.34	100	50	90	20	14.8
5	18.9848	-65.6921	22.1	89.59	100	50	90	20	14.8
6	19.4069	-65.6953	5	89.59	100	50	90	20	14.8
7	18.9484	-66.5742	22.1	84.98	100	50	90	20	14.8
8	19.3688	-66.6133	5	84.98	100	50	90	20	14.8
9	18.8738	-67.5412	22.1	85.87	100	50	90	20	14.8
10	19.2948	-67.5734	5	85.87	100	50	90	20	14.8
11	18.7853	-68.4547	22.1	83.64	100	50	90	20	14.8
12	19.2048	-68.5042	5	83.64	100	50	90	20	14.8

Table 3: Source parameters for a Mw 9.0 PRT coseismic source based on 12 SIFT sub-faults (Gica et al., 2008). Corresponding surface elevation computed with Okada's (1985) method is shown in Figure 4.

Azores Convergence Zone Coseismic Source

The 1755 Lisbon Mw 8.5-9.0 earthquake caused a transoceanic tsunami that was recorded in Newfoundland, Canada, the Lesser Antilles, and as far south as Brazil. Although there are no records of tsunami waves hitting the USEC for this event, Barkan et al. (2009) demonstrated through numerical tsunami modeling of different earthquake locations and strike angles within the region of the presumed epicenter of the 1755 Lisbon earthquake, that tsunami waves from earthquake events in this area would have impacted the USEC. Grilli and Grilli (2013a) modeled a dozen sources of magnitude Mw 9.0 located at potential source locations, varying the slip and strike angle while holding the other fault plane parameters constant to those given by Barkan et al. (2009). They found that a strike angle of 15° led to maximum impact on the upper USEC, while a strike angle of 345° caused maximum impact on the lower USEC. Maximum impact on

the USEC was created by a source sited west of the Madeira Tore Rise, while a source located at the Horseshoe Plain area, the most likely location of the epicenter of the 1755 Lisbon earthquake, did not have as much of an impact due to the effects of the local bathymetry near the earthquake redirecting the tsunami energy towards the NW and SW parts of the Atlantic Ocean.

In this work, two strike angles (15°, 345°) are considered for a Mw 9.0 1755 Lisbon (ASZ) earthquake event located in the Horseshoe Plain thrust area. Figure 5 shows the initial surface elevations computed for these sources using Okada's (1985) method, with the source parameters given in Table 4. Simulations are performed until t = 24h in the spherical implementation of FUNWAVE-TVD (Kirby et al., 2013) in the Large G0 grid and, by one-way coupling, using the Cartesian model implementation in the nested coastal grids G1-G3. Sponge layers were used in the Large G0 grid boundary to prevent reflections, and were set to 200 km on the west and east boundaries, and 400 km on the south and north boundaries.

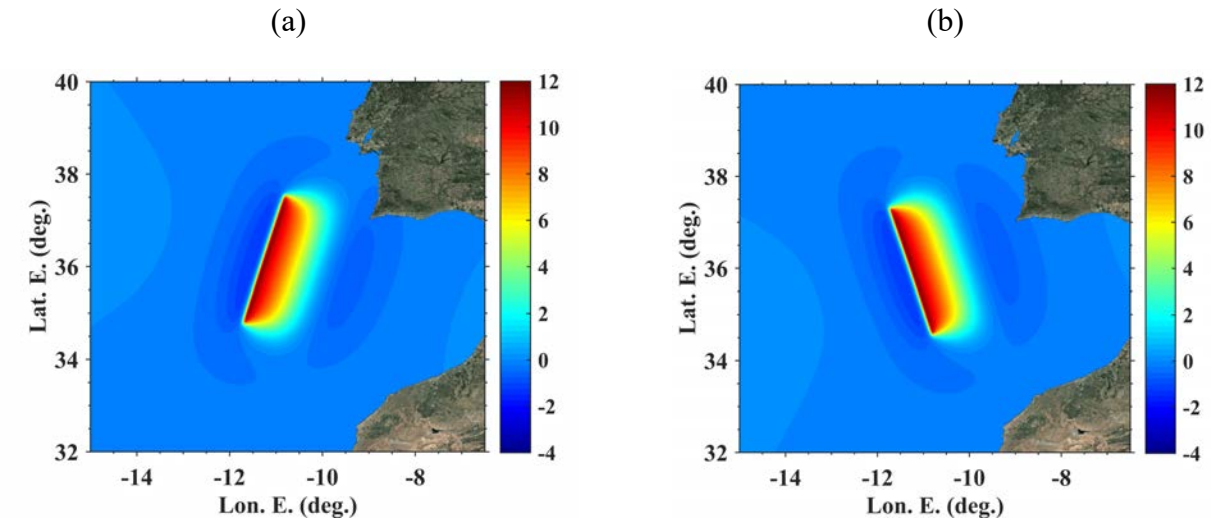

Figure 5: Initial surface elevations (m) computed with Okada's (1985) method for a Mw 9.0 Lisbon (ACZ) 1755 proxy coseismic source located in the Horseshoe Plain area with a strike angle of: (a) 15°, or (b) 345° (see parameters in Table 4).

Lat. (°N)	Lon. (°E)	Depth (km)	Strike (°)	Length (km)	Width (km)	Rake (°)	Dip (°)	Slip (m)	Mw
36.042	-10.753	5	15	317	126	90	40	20	9.0
36.042	-10.753	5	345	317	126	90	40	20	9.0

Table 4: Source parameters for two Mw 9.0 Lisbon (ASZ) 1755 proxy coseismic sources, based on Barkan et al. (2009) and Grilli and Grilli (2013a). Corresponding surface elevations computed with Okada's (1985) method is shown in Figure 5.

Areas 1-4 Submarine Mass Failures

The 1929 Grand Banks landslide tsunami was caused by the largest earthquake ever measured in the USEC area, with a magnitude of Mw 7.2. Chaytor et al. (2009) and ten Brink et al. (2014) mapped numerous paleo-SMFs on the US Atlantic continental shelf and margin, confirming that the 1929 landslide was not an isolated event. The largest paleo-SMF off the USEC is the Currituck slide complex, whose geology and slide triggering has been extensively studied (e.g. Locat et al., 2009 and references therein). Tsunami generation from the Currituck SMF was modeled in NHWAVE by Grilli et al. (2015) assuming rigid slump motion. Grilli et al. (2009) performed Monte Carlo simulations of tsunami triggered by slope failure (slumps and slides) triggered by seismicity and causing tsunami generation and coastal impact to evaluate the first order SMF tsunami hazard along the USEC. This study, however, did not take into account if there was sufficient sediment accumulation for large SMFs to occur off the coast where large runup was predicted. Eggeling (2012) identified 4 areas with large bottom slopes and sediment thickness for large SMFs given sufficient seismicity (Areas 1-4, marked in Figure 1 and by black ellipses in Figure 6). Grilli et al. (2015) and Schambach et al. (2018) modeled SMFs in these study areas using NHWAVE considering rigid slump motion, and in the latter work, slightly deforming SMFs. Each had an initial elliptical footprint on the seafloor, with a downslope length b = 30 km, width w = 20 km, and thickness T = 750 m; assuming a quasi-Gaussian geometry this yielded a total volume V = 158 km^3 for each SMF. In the present work, the free surface elevations computed with NHWAVE by Schambach et al. (2018), for rigid slump SMFs having this geometry and other identical parameters (see Table 5), at t = 13.3 min after triggering (Figure 6) are used to initialize FUNWAVE-TVD and compute tsunami propagation to shore in the 450 m grids. Details on rigid slump kinematics can be found in the appendix of Schambach et al. (2018).

Simulations are performed until t = 24h in the spherical implementation of FUNWAVE-TVD (Kirby et al., 2013) in the Local G0 grid and, by one-way coupling, using the Cartesian model implementation in the nested coastal grids G1-G3. Sponge layers were used in the Local G0 grid boundary to prevent reflections, and were set to 200 km on the west and north boundaries, and 500 km on the east and south boundaries.

Grids and SMFs	Area 1	Area 2	Area 3	Area 4
Grid SW Corner (Lon., Lat.)	-75.00°E, 36.90°N	-74.32°E, 37.47°N	-75.97°E, 36.12°N	-76.37°E, 35.80°N
SMF Center (Lon., Lat.)	-72.19°E, 39.19°N	-71.49°E, 39.76°N	-73.10°E, 38.41°N	-73.60°E, 38.09°N
SMF Azimuth (CW from N)	136°	153°	140°	126°

Table 5: Parameters of NHWAVE grids used by Schambach et al. (2018) to generate rigid slump SMF tsunamis in Areas 1-4 (Figure 1). $\Delta x = \Delta y$ = 500 m resolution; N_σ = 5 σ-layers; 1000 by 1000 cells, and locations (center) of SMFs of length b = 30 km, width w = 20 km, and thickness T = 0.75 km, the average local slope is assumed $\alpha = 4°$.

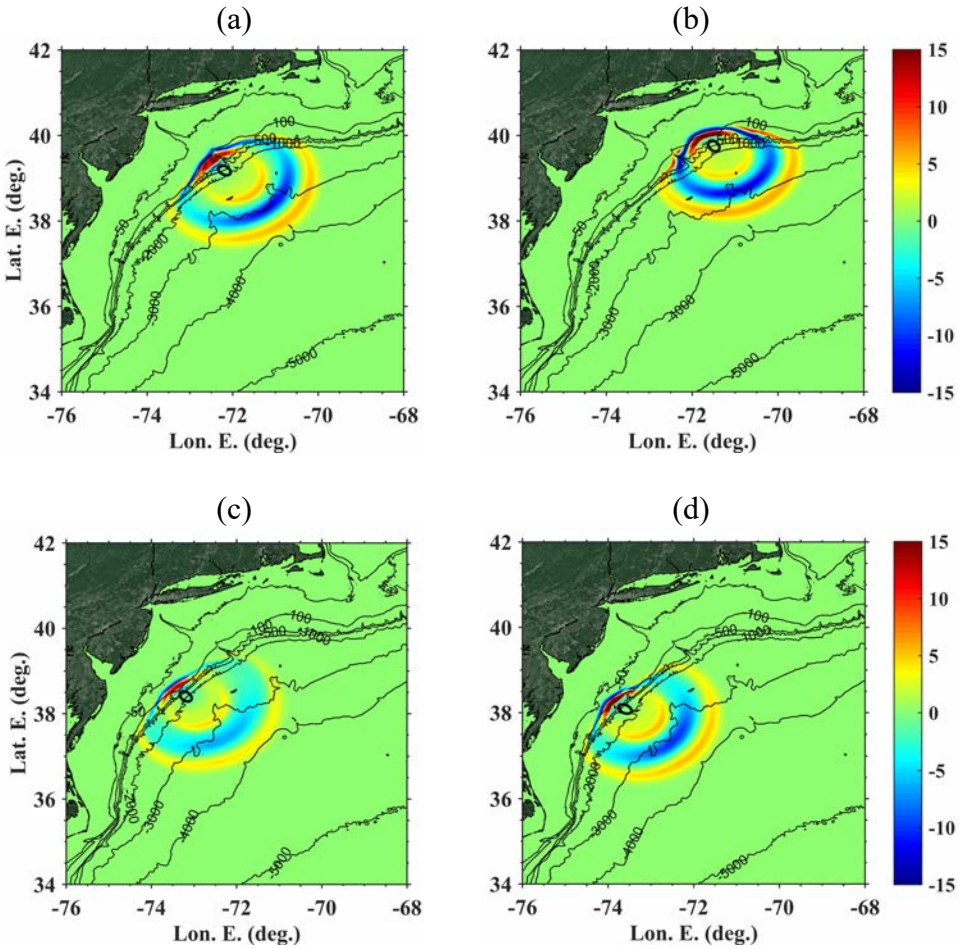

Figure 6: Initial surface elevations (m) computed with NHWAVE at t = 13.3 min, for rigid SMFs sited in areas 1-4 (a-b) (see Figure 1)**,** by Schambach et al. (2018). These are used as inputs to FUNWAVE-TVD (along with horizontal velocities at $z = 0.531\ h$). Black ellipses mark the initial footprint of each SMF with downslope length b = 30 km and width w = 20 km.

Cape Fear Submarine Mass Failure

Hornbach et al. (2007) studied the triggering and tsunamigenic potential of the Cape Fear Slide complex off of South Carolina, and determined that at least five major SMFs have occurred at this site over the past 30,000 years, some of which may have been associated with a significant tsunami. A tsunami triggered at this site would pose a large hazard to the South Carolina coast, particularly to the Myrtle Beach area.

SMF characteristics are determined for this site based on Hornbach et al. (2007) and geologic interpretation of GLORIA (Geological Long Range Inclined ASDIC) data from this region. Grilli et al. (2013d) modeled a rigid SMF in this area as a proxy for an extreme SMF for this region. The SMF had a downslope length b = 30 km, width w = 20 km, thickness T = 375 m; assuming a quasi-Gaussian geometry gives a volume V = 80 km^3. Note that the SMF footprint is similar to the Currituck proxy footprint, but the thickness is reduced from the Currituck proxy and set to approximate failure along the upper limit of the bottom simulating reflector depth. The SMF is initially centered at 33.191°N, -76.165°W. At t = 1020 s (17 min; Figure 7) the results

from NHWAVE (surface elevation and horizontal velocities at $z = 0.531h$) are passed into FUNWAVE-TVD grids.

Simulations are performed until t = 24h in the spherical implementation of FUNWAVE-TVD (Kirby et al., 2013) in the Local G0 grid and, by one-way coupling, using the Cartesian model implementation in the nested coastal grids G1-G3. Sponge layers were used in the Local G0 grid boundary to prevent reflections, and were set to 200 km on the west and north boundaries, and 500 km on the east and south boundaries.

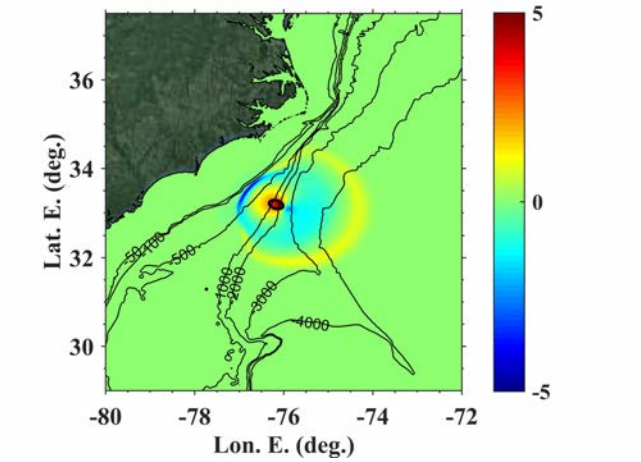

Figure 7: Initial surface elevations (m) computed with NHWAVE at t = 17 min, for rigid SMFs sited off Cape Fear. These are used as inputs to FUNWAVE-TVD (along with horizontal velocities at $z = 0.531\ h$). The black ellipse marks the initial footprint of the SMF.

Great Bahama Bank Submarine Mass Failures

Schnyder et al. (2016) studied and modeled tsunami generation from SMFs and margin collapses of Bahamian platforms. SMFs in this region have the potential to cause large impacts on the low lying areas in and near the Florida Keys and on the Floridian mainland. Short distance and travel time from the source areas to densely populated coastal areas, such as Miami, makes these areas vulnerable to these low probability but high impact events.

Two slides on the western Bahamian platform are modeled in this analysis, a past event modeled as a single large slide (SLS), and a potential future slide (PFS), after the work of Schnyder et al. (2016). The slides used in this analysis is estimated to have downslope length b = 3.5 km SLS (6 km PFS), width w = 9 km SLS (40 km PFS), thickness T = 150 m SLS (80 m PFS). Assuming a quasi-Gaussian geometry this gives a volume of V = 1.6 km^3 SLS (6.7 km^3 PFS). The SMFs are initially centered at 24.850°N, 79.235°W SLS (24.670°N, 79.235°W PFS) with azimuth of 270° CW from N. The local seafloor slope is 3.3°. Differing from the work of Schnyder et al. (2016), for these cases the SMF is modeled as a dense Newtonian fluid in NHWAVE (Kirby et al., 2016) with a bulk sediment density ρ_s = 1845 kg/m^3 (estimated by Schnyder et al. 2016) and viscosity = 0.5 m^{2}s (set to the upper range of debris flows). The results from NHWAVE (surface elevation and horizontal velocities at $z = 0.531\ h$) are passed into FUNWAVE-TVD grids when

the SMF is no longer significantly tsunamigenic; at t = 650 s (10.8 min; Figure 8a) for the SLS case and at t = 1000 s (16.7 min; Figure 8b) for the PFS case.

Simulations are performed until t = 8.3h in the spherical implementation of FUNWAVE-TVD (Kirby et al., 2013) in the Local G0 grid and, by one-way coupling, using the Cartesian model implementation in the nested coastal grid G3 [note that these sources only impact southern Florida]. Sponge layers were used in the Local G0 grid boundary to prevent reflections, and were set to 200 km on the west and north boundaries, and 500 km on the east and south boundaries.

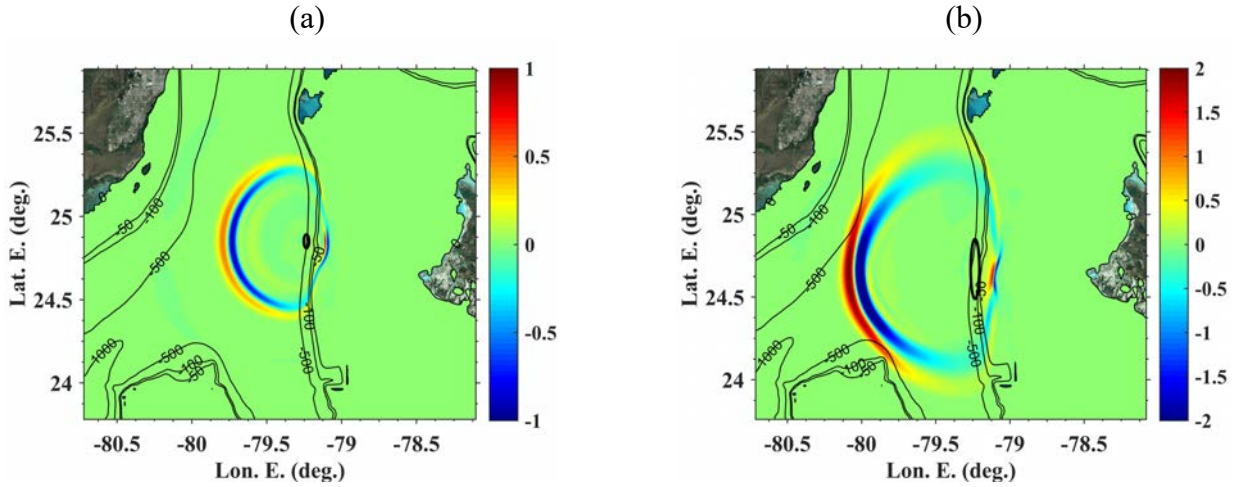

Figure 8: Initial surface elevations (m) computed with NHWAVE at (a) t = 10.8 min for the SLS case, and (b) at t = 16.7 min for the PFS case, both sited off the western platform of Great Bahama Bank. These are used as inputs to FUNWAVE-TVD (along with horizontal velocities at z = 0.531 h). Black ellipses mark the initial footprints of the SMFs.

Cumbre Vieja Volcanic Flank Collapse

Ward and Day (2001) first studied and performed simulations for a 500 km^3 CVV flank collapse, predicting that the USEC could face up to 10-25 m inundation from such an event. Abadie et al. (2009; 2012) modeled several CVV flank collapse scenarios as subaerial slides represented by a heavy Newtonian fluid with very low viscosity (quasi-inviscid) and volumes of 20, 30, 80, and 450 km^3 using the 3D multi-material Navier-Stokes model THETIS (Abadie et al., 2010). Abadie et al. (2012) performed slope stability analyses and indentified the 80 km^3 collapse as the "most credible worst case scenario". Abadie et al. (2019) recomputed the CVV flank collapse scenarios, this time calibrating the rheology to experiments of Viroulet et al. (2013) and Grilli et al. (2017a) so that the slide motion is more realistic, with a large dynamic viscosity, set to μ = 2x10^7 Pa-s, finding that the new wave source is reduced in half compared to previous estimations.

For the present simulations, similar to the previous modeling work of Grilli and Grilli (2013b) and Tehranirad et al. (2015), the results of Abadie et al. (2019) are used to simulate the propagation to the USEC of the tsunami due to the CVV flank collapse for two scenarios, 80 km^3 and the extreme 450 km^3 volume events. Once the slide stopped moving and most of its energy

was transferred to the water motion, at t = 5 min, surface elevation and depth-averaged currents (at $z = 0.531h$) were reinterpolated from THETIS into a FUNWAVE-TVD horizontal grid of 500 m resolution to further compute tsunami propagation, up to $t = 20$ min into the event. The surface elevation and depth-averaged currents at $t = 20$ min are used here as the initial condition for the Large G0 grid (Figure 9, Figure 10).

Simulations are performed until $t = 24$h in the spherical implementation of FUNWAVE-TVD (Kirby et al., 2013) in the Large G0 grid and, by one-way coupling, using the Cartesian model implementation in the nested coastal grids G1-G3. Sponge layers were used in the Large G0 grid boundary to prevent reflections, and were set to 200 km on the west and east boundaries, and 400 km on the south and north boundaries.

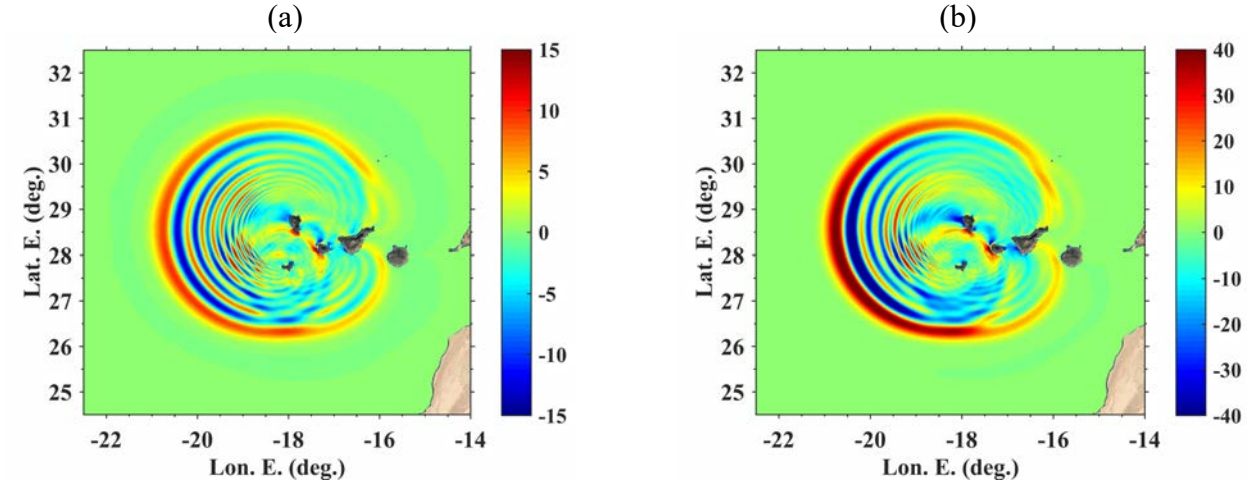

Figure 9: Initial surface elevations (m) computed with THETIS and FUNWAVE-TVD (Abadie et al., 2019) at t = 20 min, for Cumbre Vieja volcanic flank collapse of volumes: (a) 80 km^3, or (b) 450 km^3. These are used as inputs to FUNWAVE-TVD (along with horizontal velocities at $z = 0.531\ h$; Figure 10).

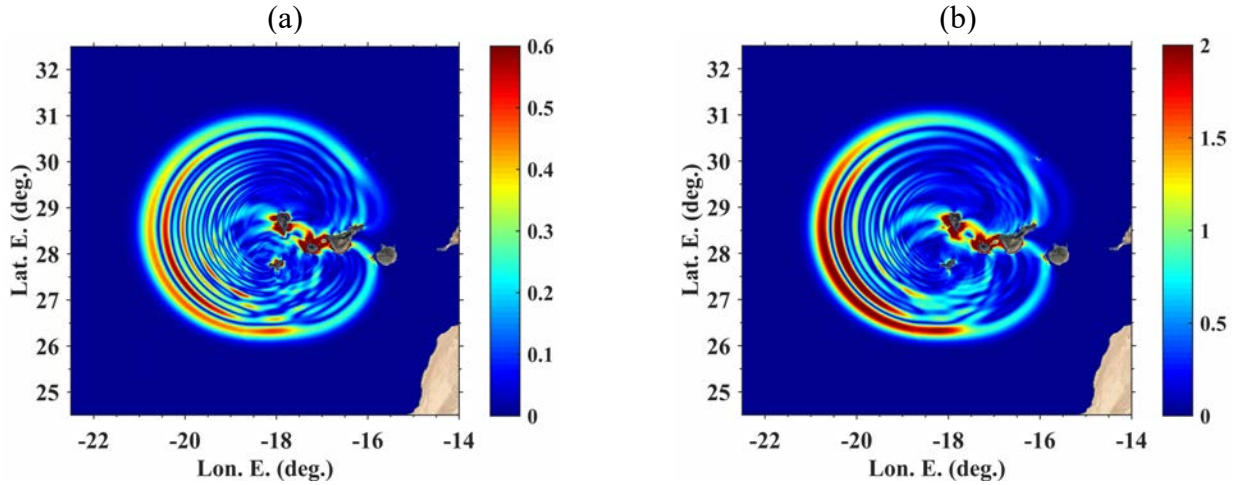

Figure 10: Horizontal water velocity magnitude (m/s) at $z = 0.531h$ computed with THETIS and FUNWAVE-TVD (Abadie et al., 2019) at t = 20 min, for Cumbre Vieja volcanic flank collapse of volumes: (a) 80 km^3, or (b) 450 km^3. These are used as inputs to FUNWAVE-TVD (along with initial surface elevation; Figure 9).

Simulations and Results

In this section, results of each simulation are presented as maps of maximum envelope of surface elevation, velocity, and impulse force. For each map in grids G1-G3, color coding along the 5 m isobath contour indicates magnitude of impact. Values along the 5 m contour for each result are also plotted as a function of latitude. Time series of surface elevation at the grid save points and other points selected along the 200 m isobath contour (Table 2) are also shown.

Puerto Rico Trench Mw 9.0 Coseismic Source

Maximum Surface Elevation, Velocity, and Impulse Force

Figure 11 shows an overview of the maximum surface elevation in grids Local G0, G1, G2, and G3 computed with FUNWAVE-TVD for a PRT Mw 9.0 coseismic source (Figure 4, Table 3) with a simulation time of t = 86400 s (24 h).

Figure 12 shows the surface elevation time series at the grid save points (Table 2).

Figure 13, Figure 14, and Figure 15 show the maximum surface elevation, velocity, and impulse force respectively in grids Local G0, G1, G2, and G3 with values along the 5 m isobath contour (calculated in G1-G3) plotted as a function of latitude.

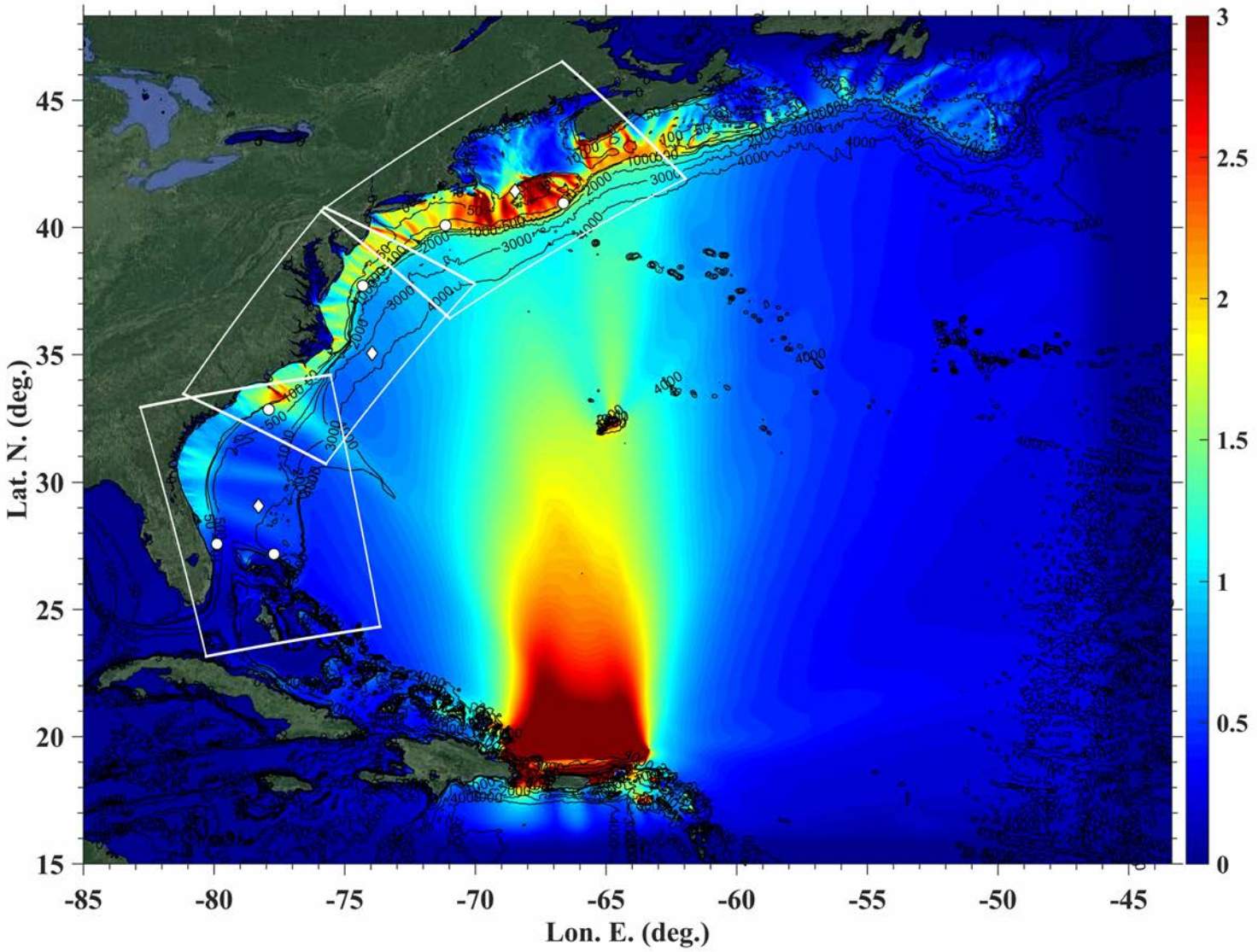

Figure 11: Maximum surface elevation for PRT Mw 9.0 coseismic source

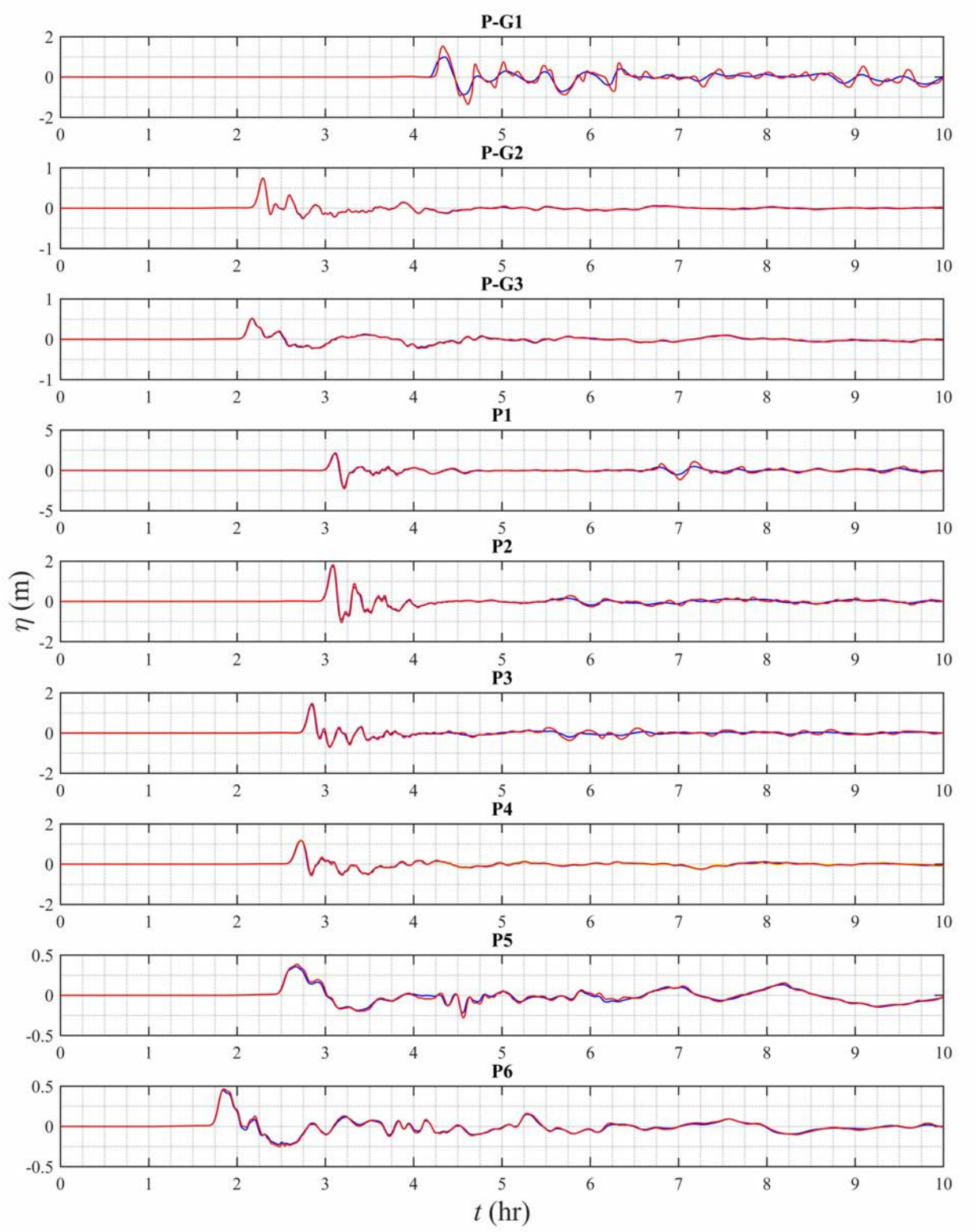

Figure 12: Tsunami wave time series at grid save points. Blue indicates surface elevation computed in grid Local G0, red indicates surface elevation computed in nested grids G1-G3. For point P4, yellow indicates surface elevation computed in G2, red indicates surface elevation computed in G3.

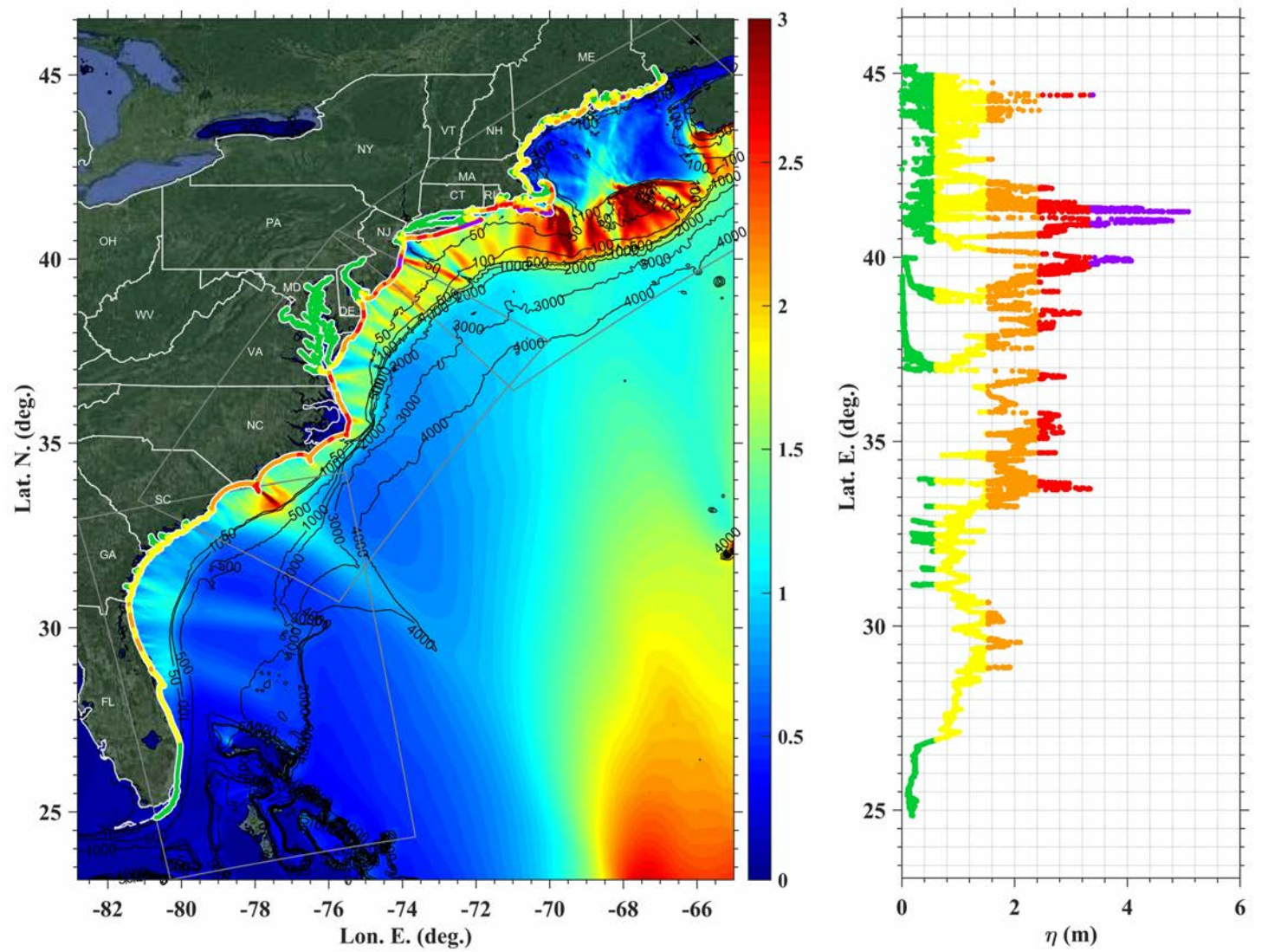

Figure 13: Maximum surface elevation for PRT Mw 9.0 coseismic source in grid G1, G2, G3 with color-coded hazard along the 5m isobath contour. Color-coding reflects elevation classes: below 2 ft (green); 2-5 ft (yellow); 5-8 ft (orange); 8-11 ft (red); over 11 ft (purple).

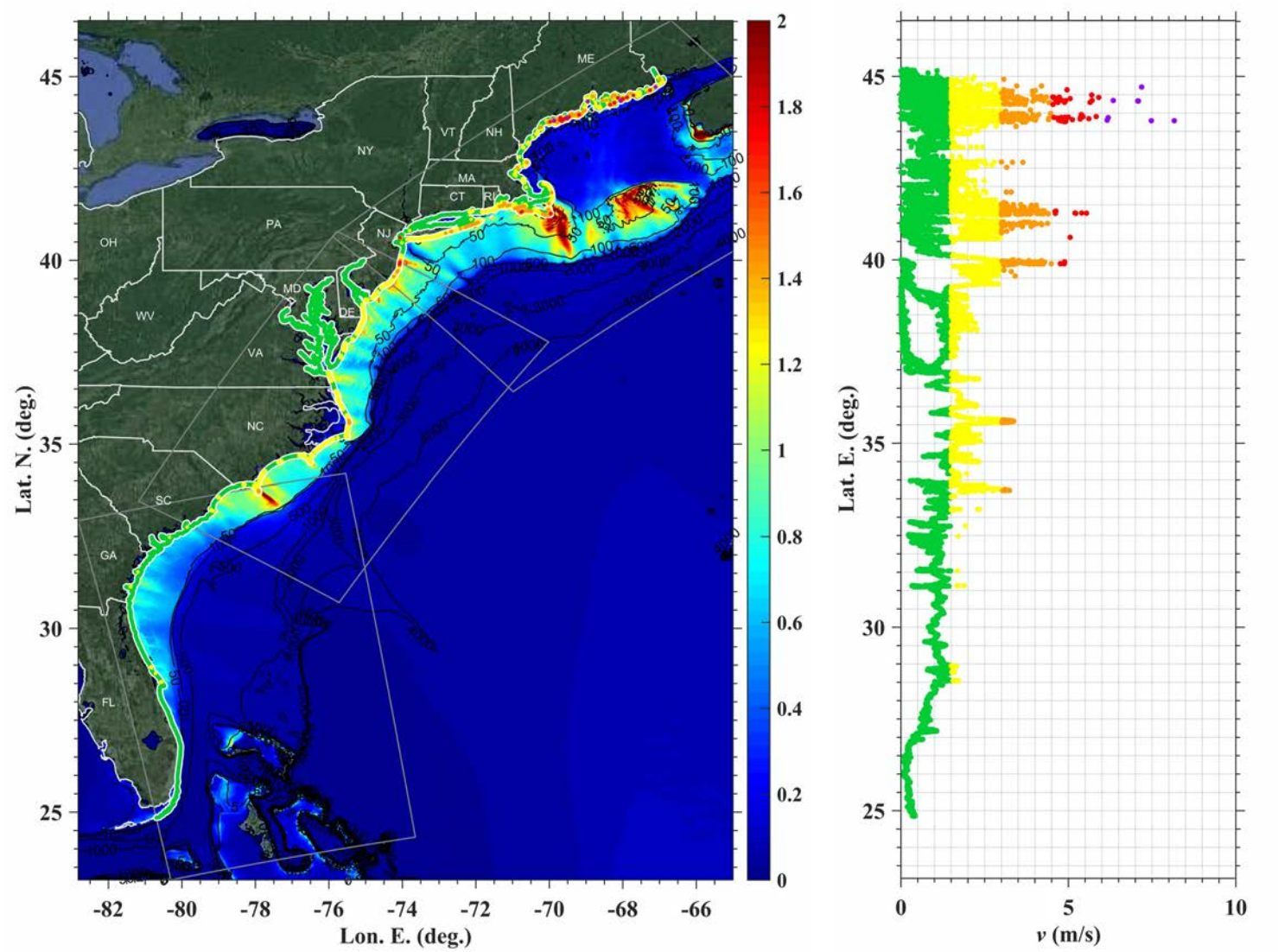

Figure 14: Maximum velocity for PRT Mw 9.0 coseismic source in grid G1, G2, G3 with color-coded hazard along the 5m isobath contour. Color-coding reflects velocity classes: below 1.5 m/s (green); 1.5-3 m/s (yellow); 3-4.5 m/s (orange); 4.5-6 m/s (red); over 6 m/s (purple).

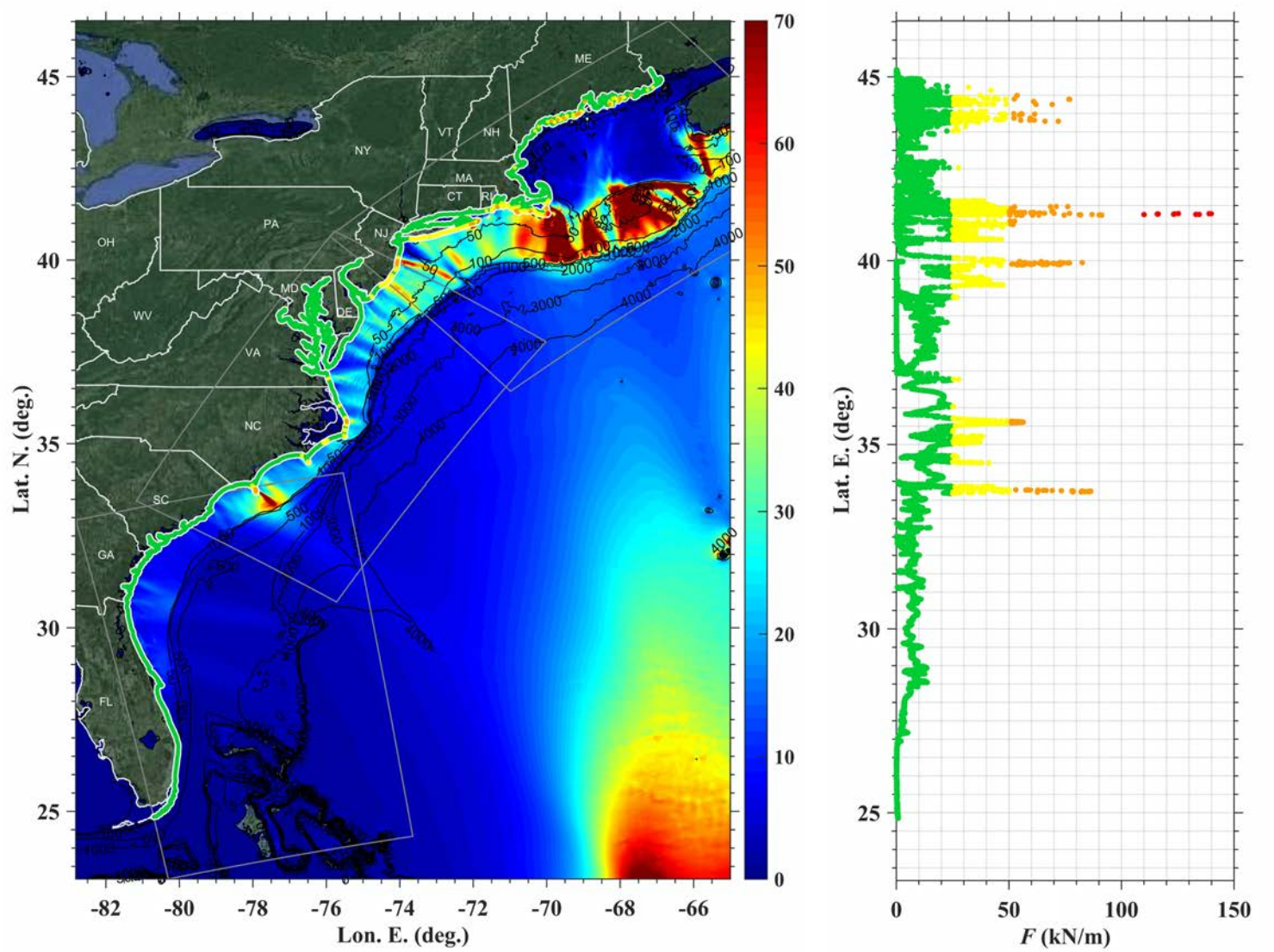

Figure 15: Maximum impulse force for PRT Mw 9.0 coseismic source in grid G1, G2, G3 with color-coded hazard along the 5m isobath contour. Color-coding reflects impulse force classes: below 25 kN/m (green); 25-50 kN/m (yellow); 50-100 kN/m (orange); 100-200 kN/m (red); over 200 kN/m (purple).

Azores Convergence Zone 15° Strike Mw 9.0 Coseismic Source

Maximum Surface Elevation, Velocity, and Impulse Force

Figure 16 shows an overview of the maximum surface elevation in grids Large G0, G1, G2, and G3 computed with FUNWAVE-TVD for a LSB Mw 9.0 15° strike coseismic source (Figure 5, Table 4) with a simulation time of t = 86400 s (24 h).

Figure 17 shows the surface elevation time series at the grid save points (Table 2).

Figure 18, Figure 19, and Figure 20 show the maximum surface elevation, velocity, and impulse force respectively in grids Large G0, G1, G2, and G3 with values along the 5 m isobath contour (calculated in G1-G3) plotted as a function of latitude.

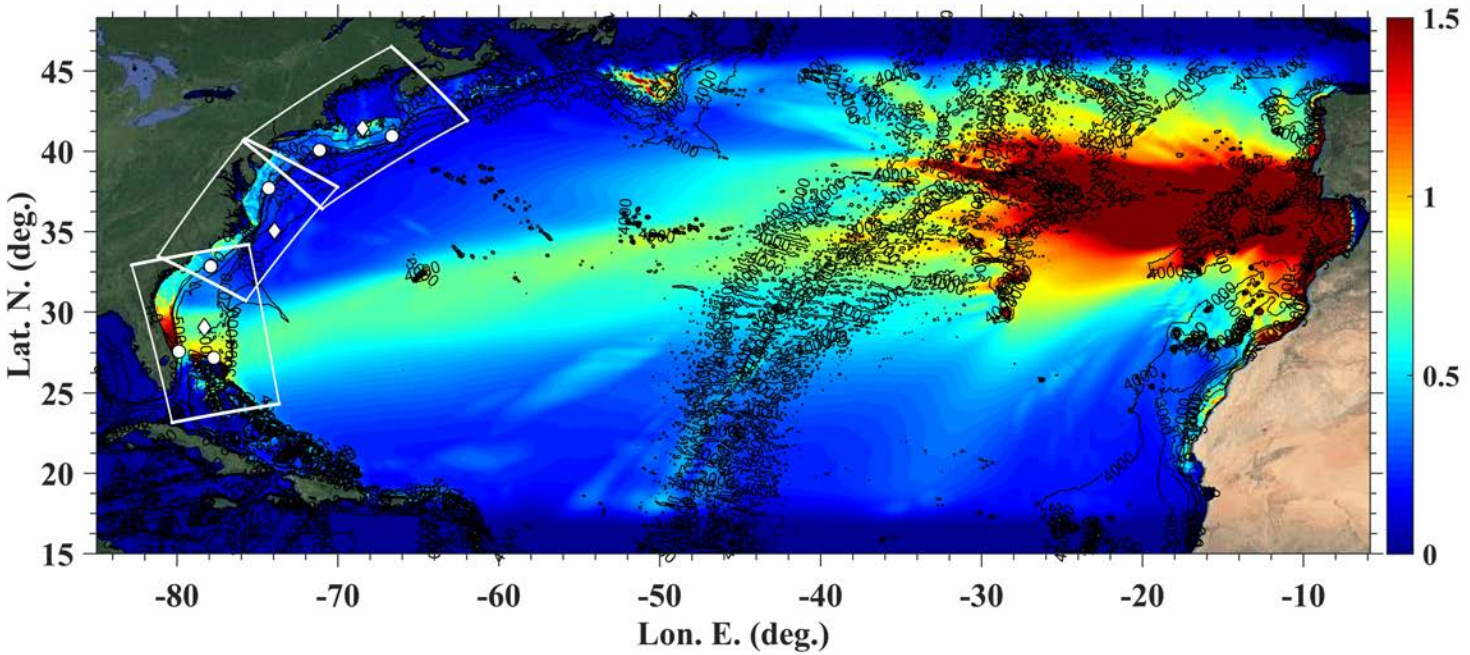

Figure 16: Maximum surface elevation for LSB Mw 9.0 15° strike coseismic source

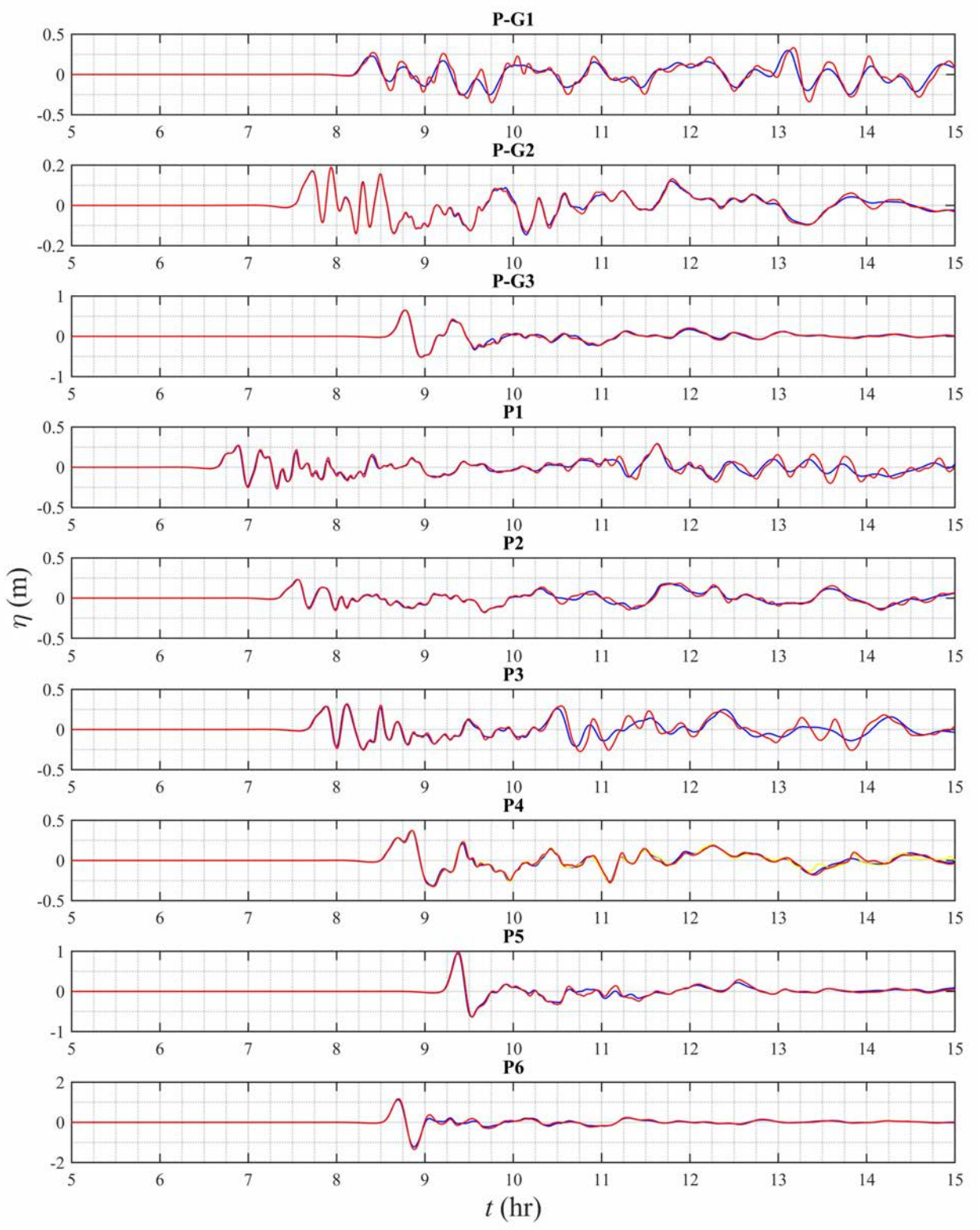

Figure 17: Tsunami wave time series at grid save points. Blue indicates surface elevation computed in grid Large G0, red indicates surface elevation computed in nested grids G1-G3. For point P4, yellow indicates surface elevation computed in G2, red indicates surface elevation computed in G3

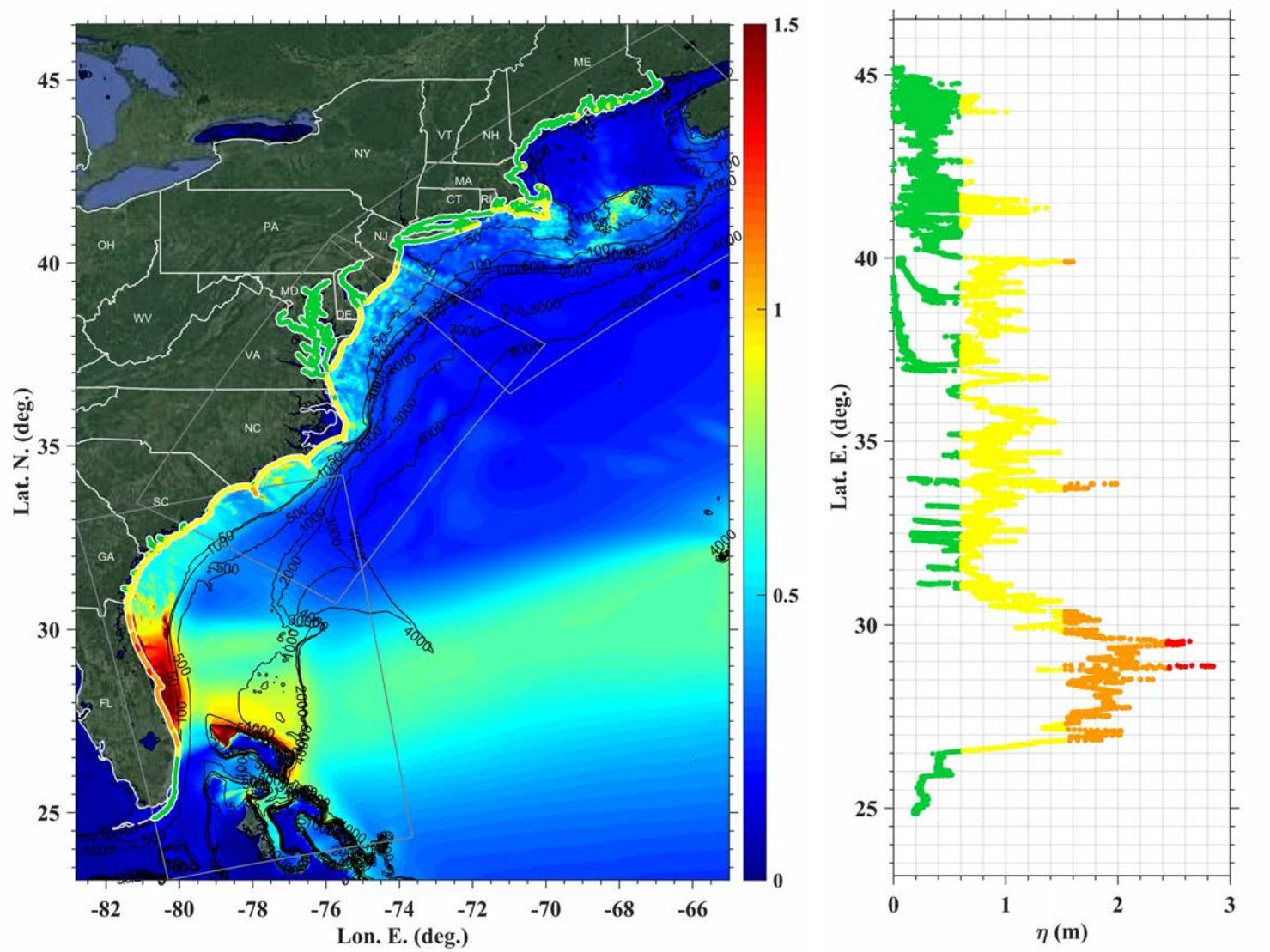

Figure 18: Maximum surface elevation for LSB Mw 9.0 15° strike coseismic source in grid G1, G2, G3 with color-coded hazard along the 5m isobath contour. Color-coding reflects elevation classes: below 2 ft (green); 2-5 ft (yellow); 5-8 ft (orange); 8-11 ft (red); over 11 ft (purple).

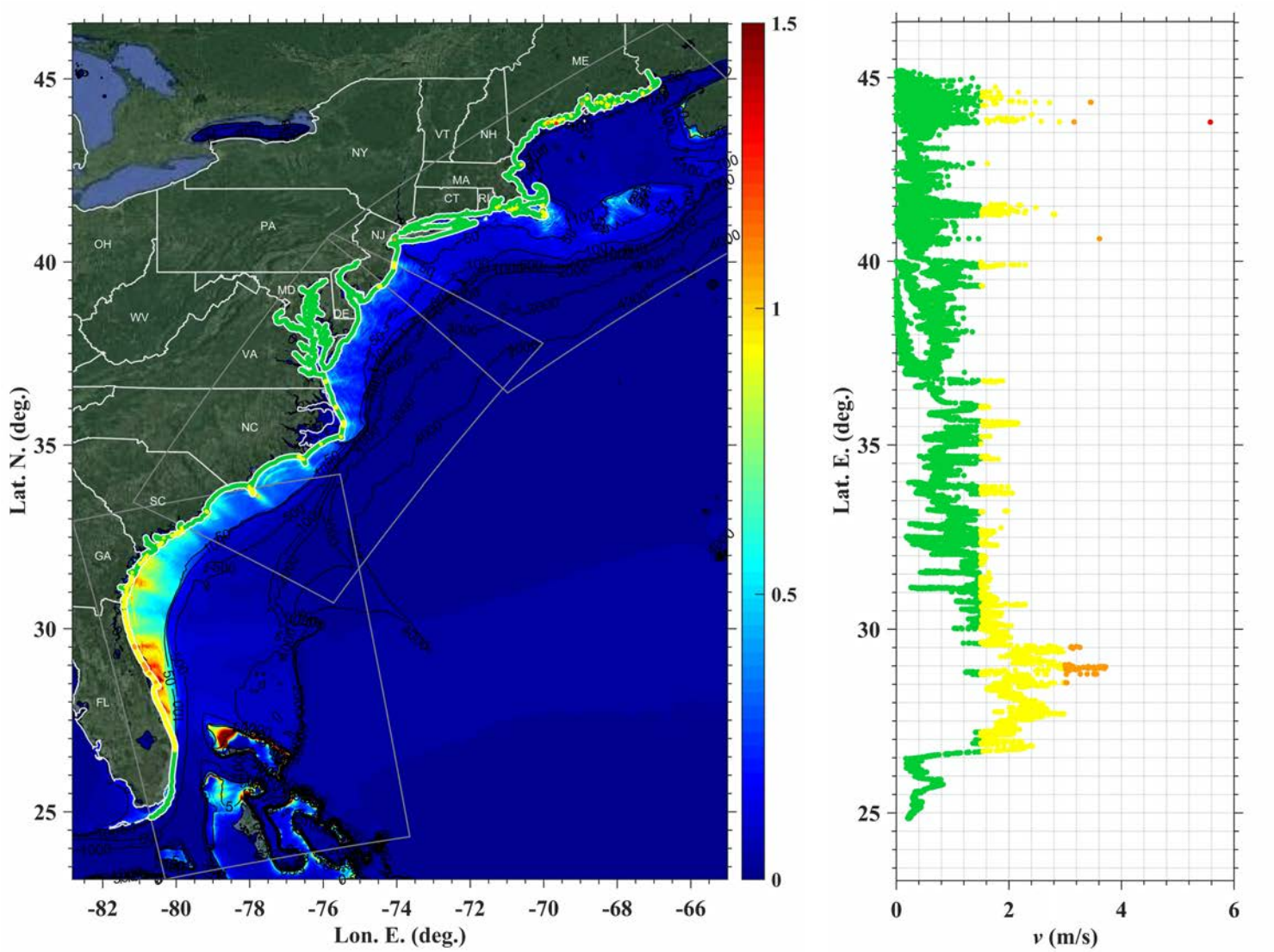

Figure 19: Maximum velocity for LSB Mw 9.0 15° strike coseismic source in grid G1, G2, G3 with color-coded hazard along the 5m isobath contour. Color-coding reflects velocity classes: below 1.5 m/s (green); 1.5-3 m/s (yellow); 3-4.5 m/s (orange); 4.5-6 m/s (red); over 6 m/s (purple).

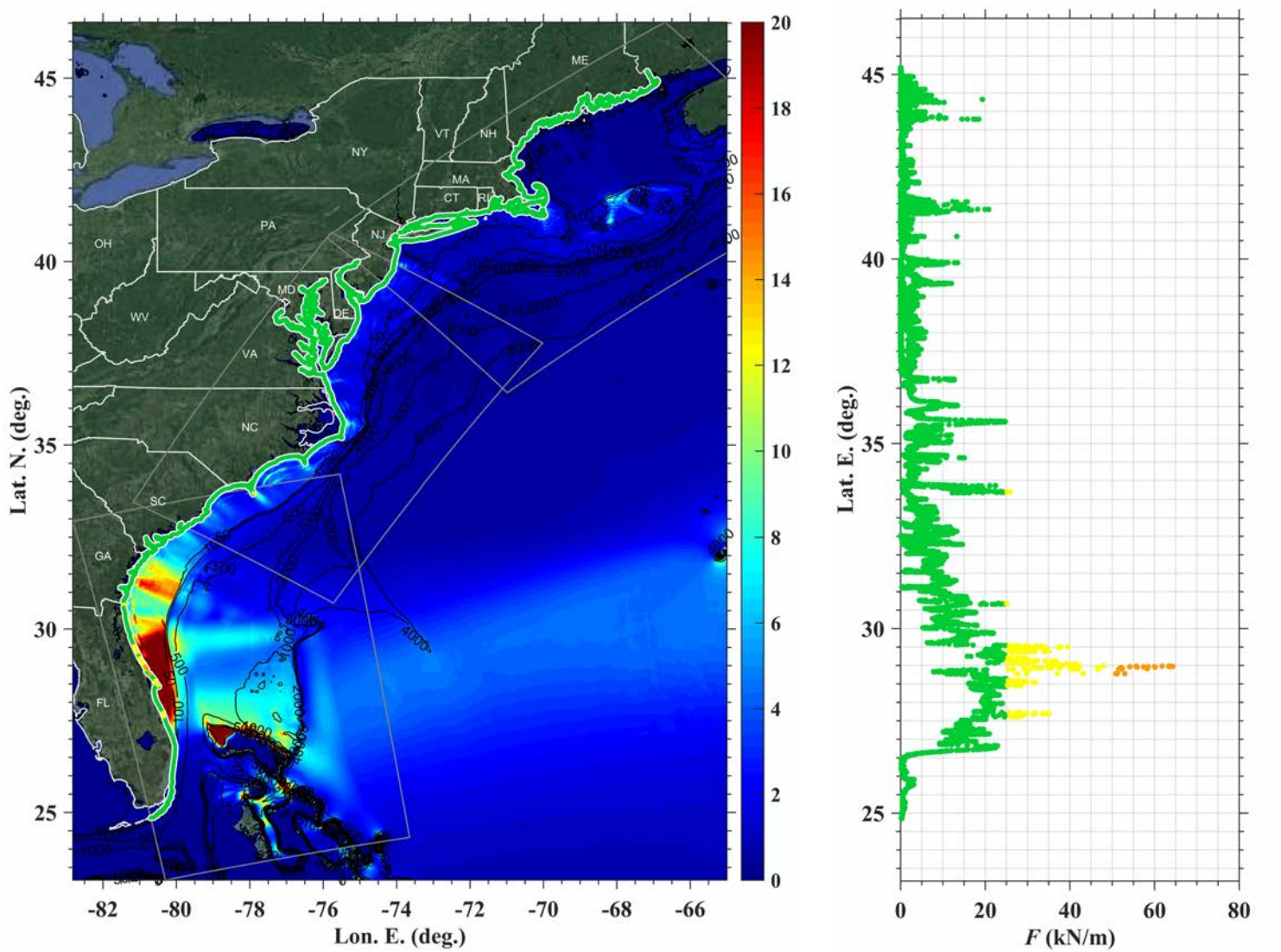

Figure 20: Maximum impulse force for LSB Mw 9.0 15° strike coseismic source in grid G1, G2, G3 with color-coded hazard along the 5m isobath contour. Color-coding reflects impulse force classes: below 25 kN/m (green); 25-50 kN/m (yellow); 50-100 kN/m (orange); 100-200 kN/m (red); over 200 kN/m (purple).

Azores Convergence Zone 345° Strike Mw 9.0 Coseismic Source

Maximum Surface Elevation, Velocity, and Impulse Force

Figure 21 shows an overview of the maximum surface elevation in grids Large G0, G1, G2, and G3 computed with FUNWAVE-TVD for a LSB Mw 9.0 345° strike coseismic source (Figure 5, Table 4) with a simulation time of t = 86400 s (24 h).

Figure 22 shows the surface elevation time series at the grid save points (Table 2).

Figure 23, Figure 24, and Figure 25 show the maximum surface elevation, velocity, and impulse force respectively in grids Large G0, G1, G2, and G3 with values along the 5 m isobath contour (calculated in G1-G3) plotted as a function of latitude.

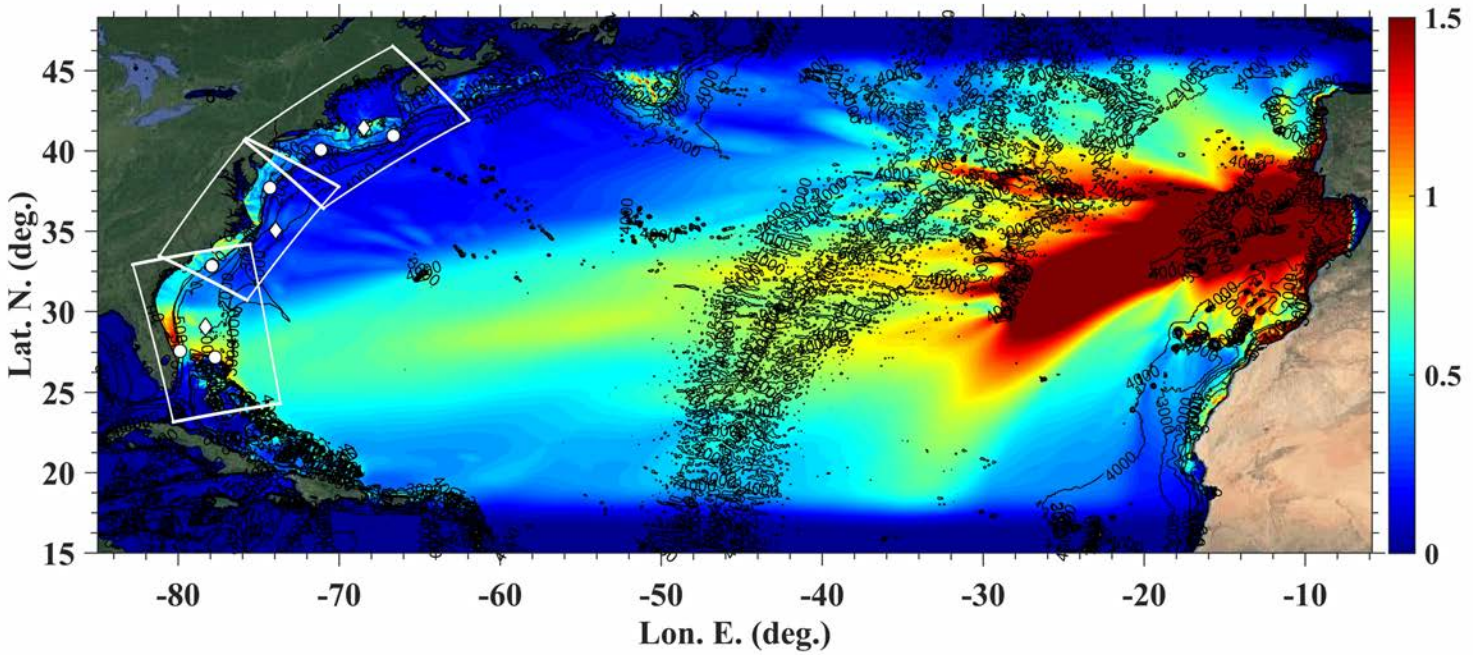

Figure 21: Maximum surface elevation for LSB Mw 9.0 345° strike coseismic source

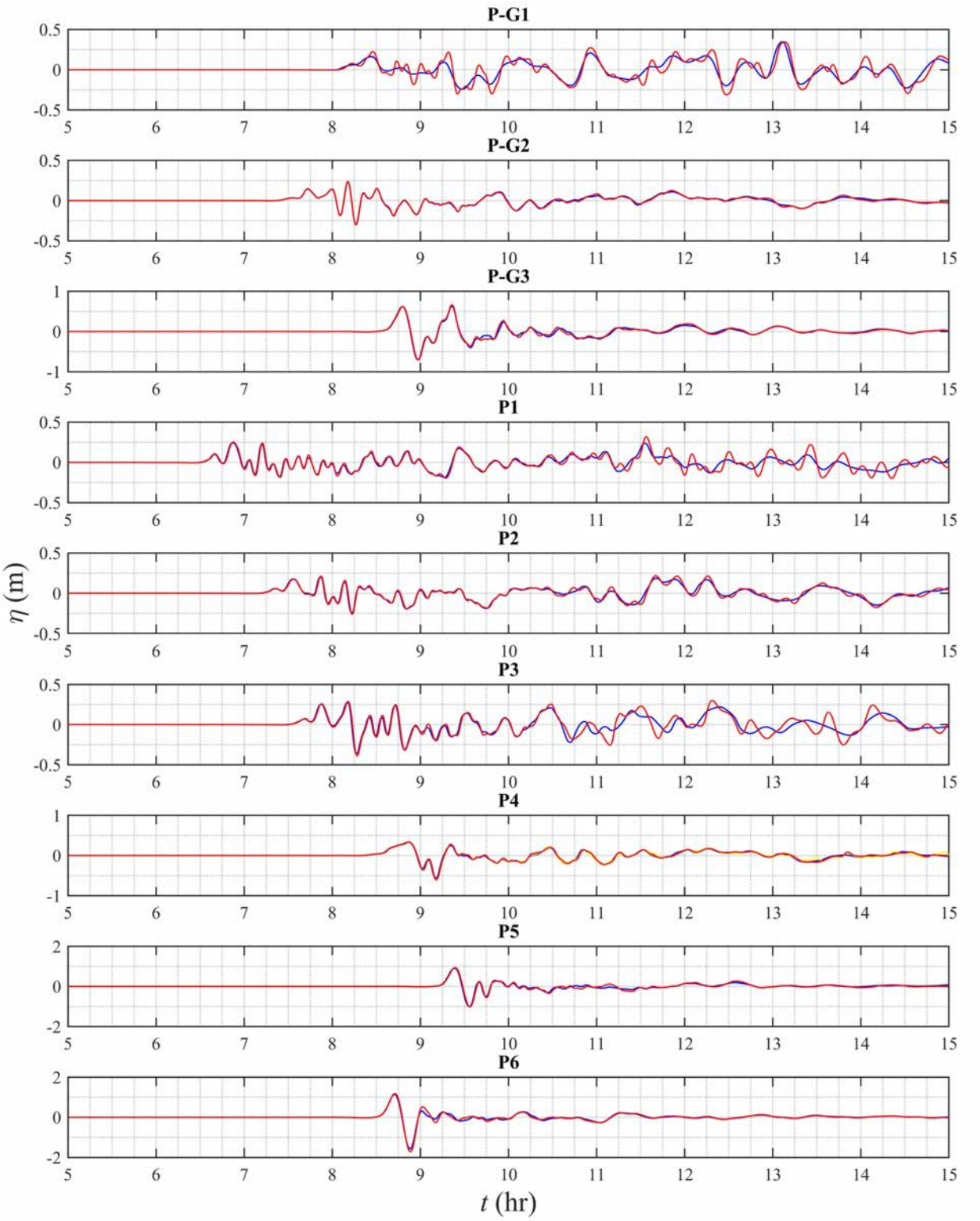

Figure 22: Tsunami wave time series at grid save points. Blue indicates surface elevation computed in grid Large G0, red indicates surface elevation computed in nested grids G1-G3. For point P4, yellow indicates surface elevation computed in G2, red indicates surface elevation computed in G3

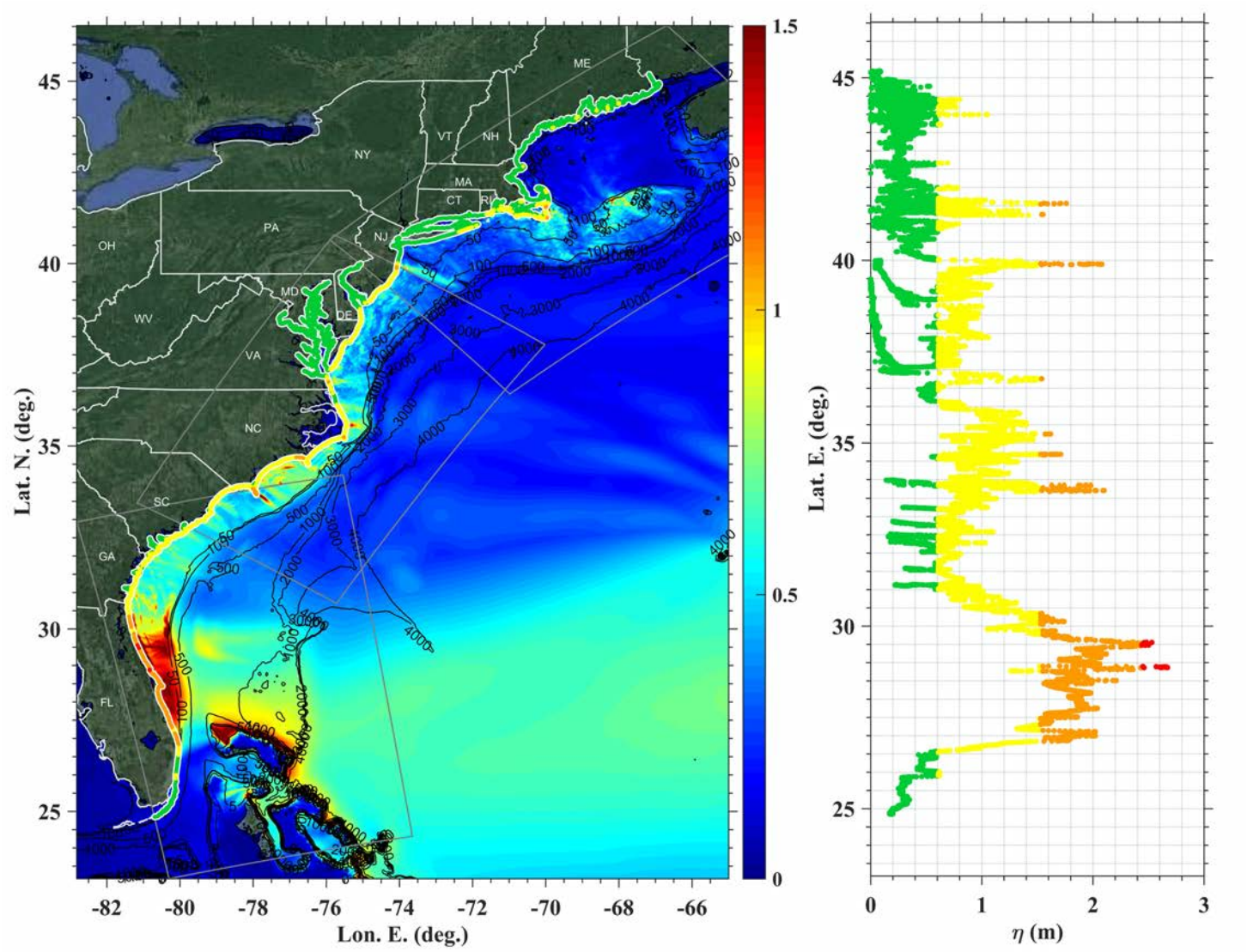

Figure 23: Maximum surface elevation for LSB Mw 9.0 345° strike coseismic source in grid G1, G2, G3 with color-coded hazard along the 5m isobath contour. Color-coding reflects elevation classes: below 2 ft (green); 2-5 ft (yellow); 5-8 ft (orange); 8-11 ft (red); over 11 ft (purple).

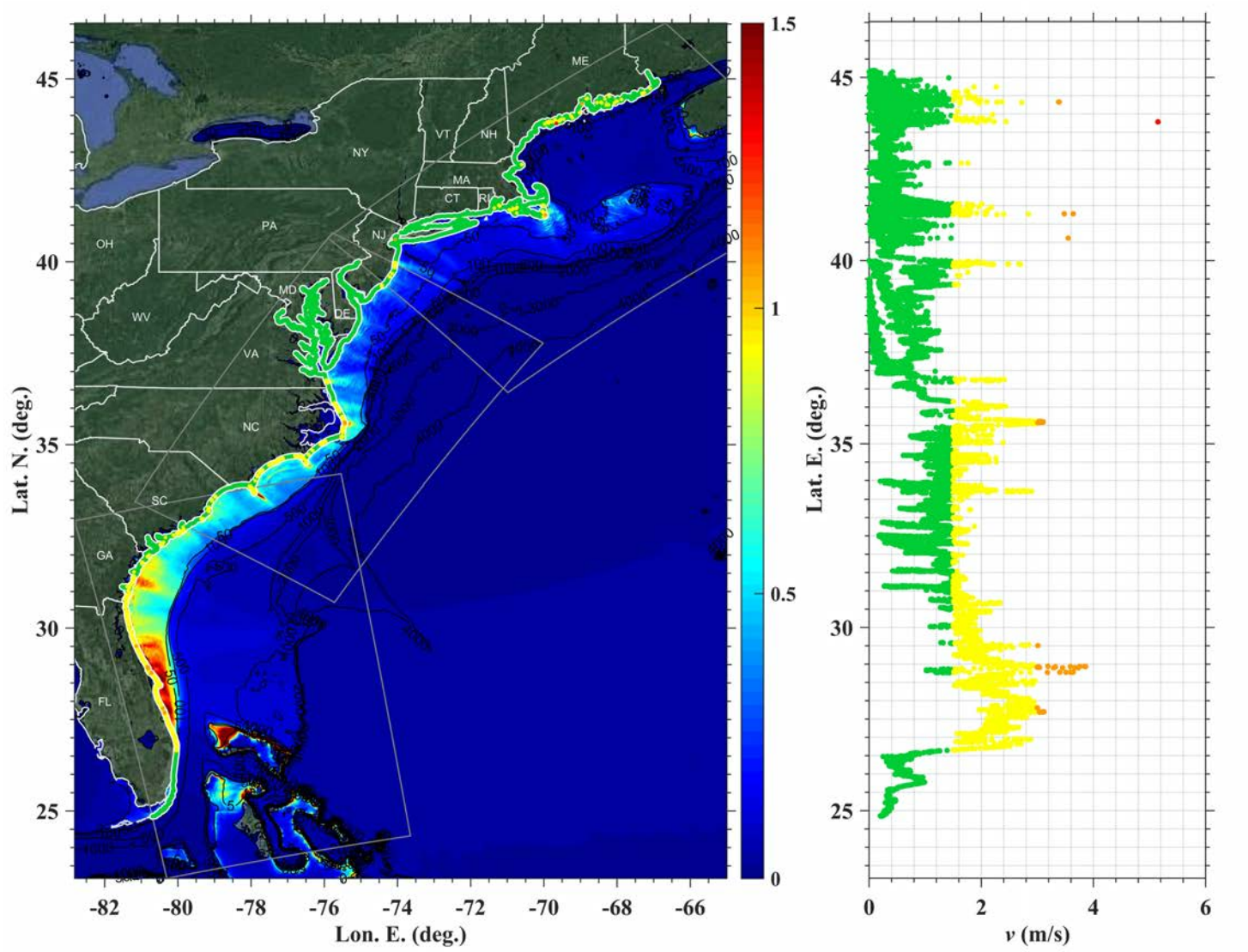

Figure 24: Maximum velocity for LSB Mw 9.0 345° strike coseismic source in grid G1, G2, G3 with color-coded hazard along the 5m isobath contour. Color-coding reflects velocity classes: below 1.5 m/s (green); 1.5-3 m/s (yellow); 3-4.5 m/s (orange); 4.5-6 m/s (red); over 6 m/s (purple).

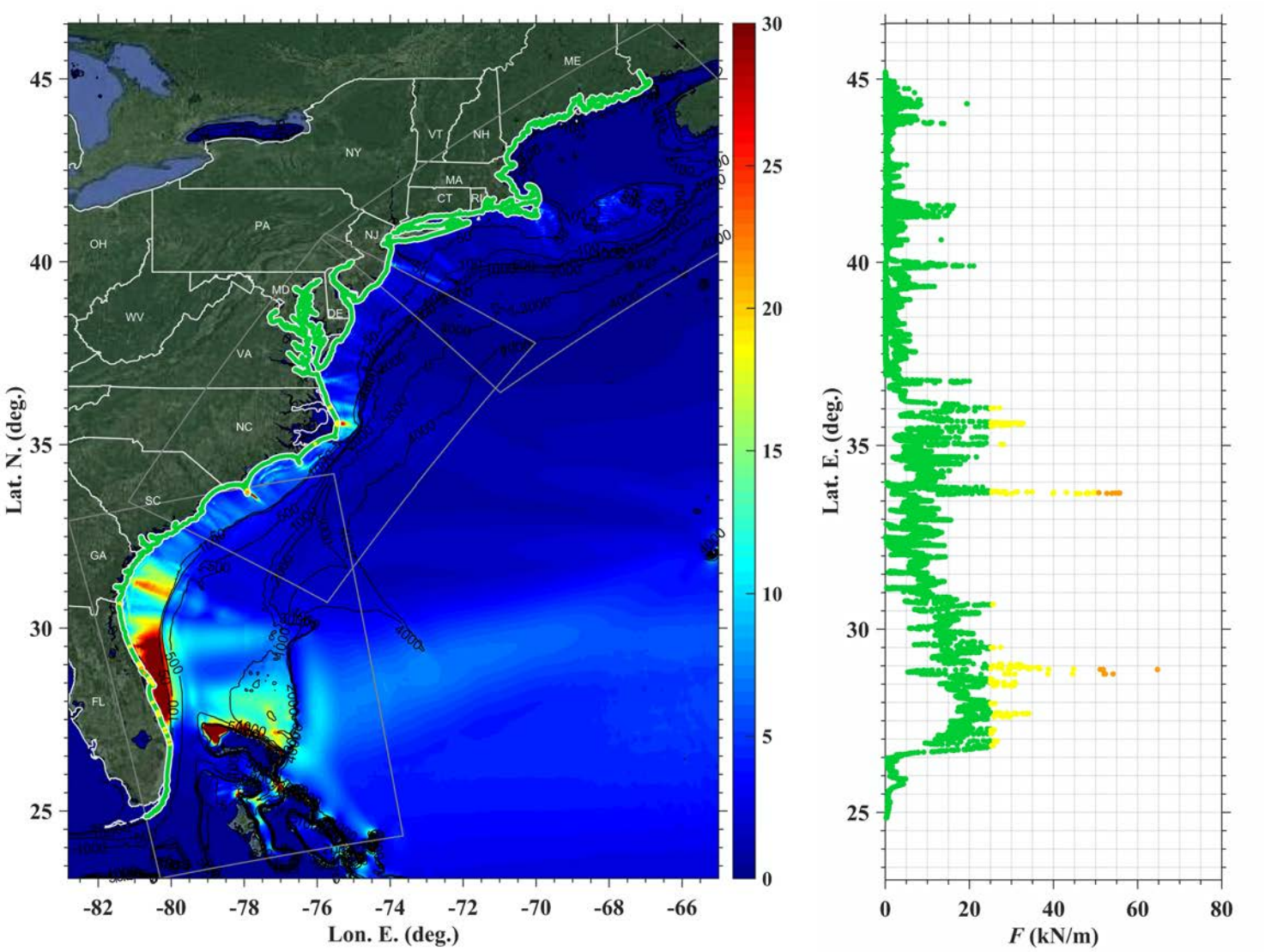

Figure 25: Maximum impulse force for LSB Mw 9.0 345° strike coseismic source in grid G1, G2, G3 with color-coded hazard along the 5m isobath contour. Color-coding reflects impulse force classes: below 25 kN/m (green); 25-50 kN/m (yellow); 50-100 kN/m (orange); 100-200 kN/m (red); over 200 kN/m (purple).

Study Area 1 Rigid Slump Submarine Mass Failure

Maximum Surface Elevation, Velocity, and Impulse Force

Figure 26 shows an overview of the maximum surface elevation in grids Local G0, G1, G2, and G3 computed with FUNWAVE-TVD for the Study Area 1 SMF source (Figure 6, Table 1) with a simulation time of t = 86400 s (24 h).

Figure 27 shows the surface elevation time series at the grid save points (Table 2).

Figure 28, Figure 29, and Figure 30 show the maximum surface elevation, velocity, and impulse force respectively in grids Local G0, G1, G2, and G3 with values along the 5 m isobath contour (calculated in G1-G3) plotted as a function of latitude.

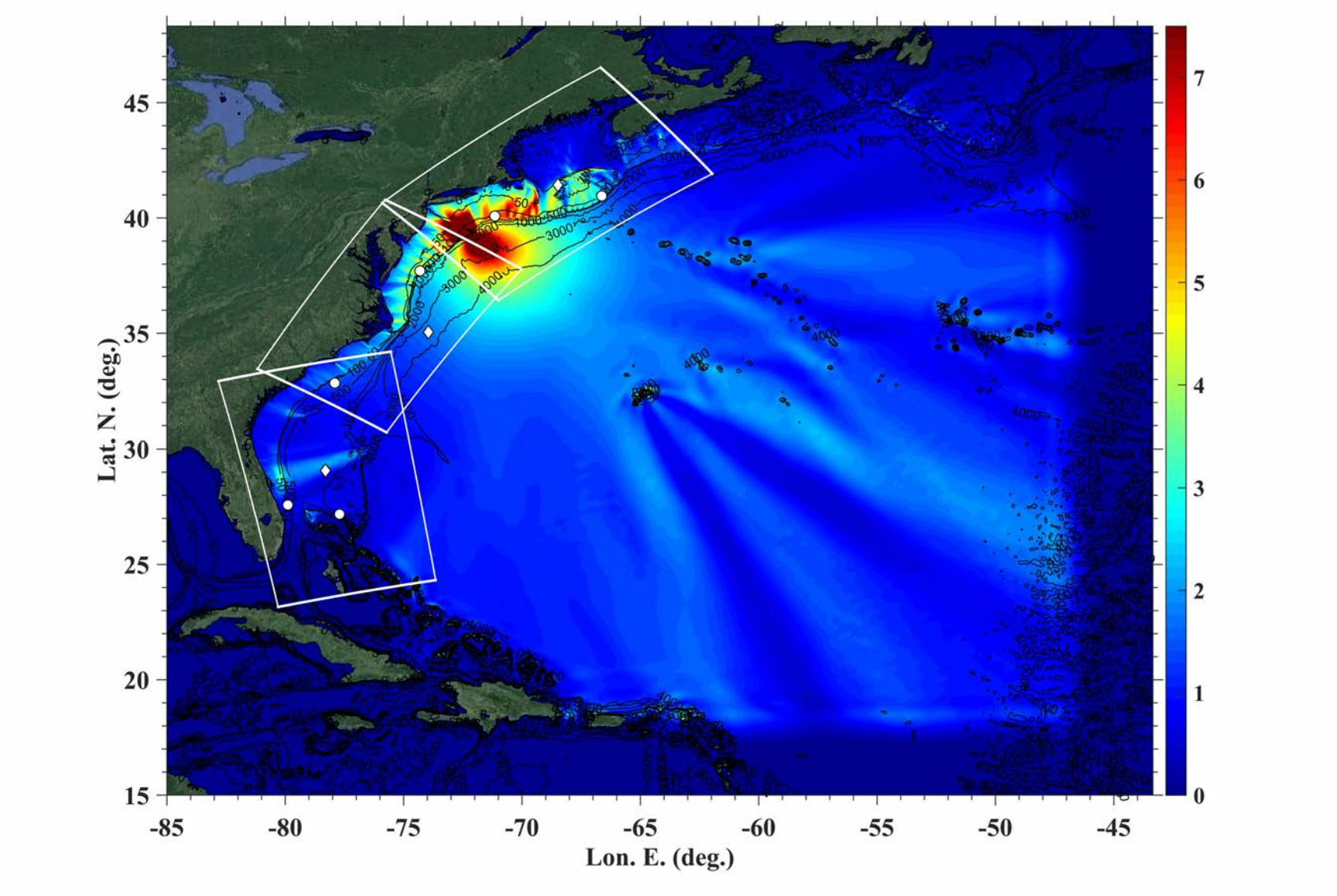

Figure 26: Maximum surface elevation for Study Area 1 SMF source

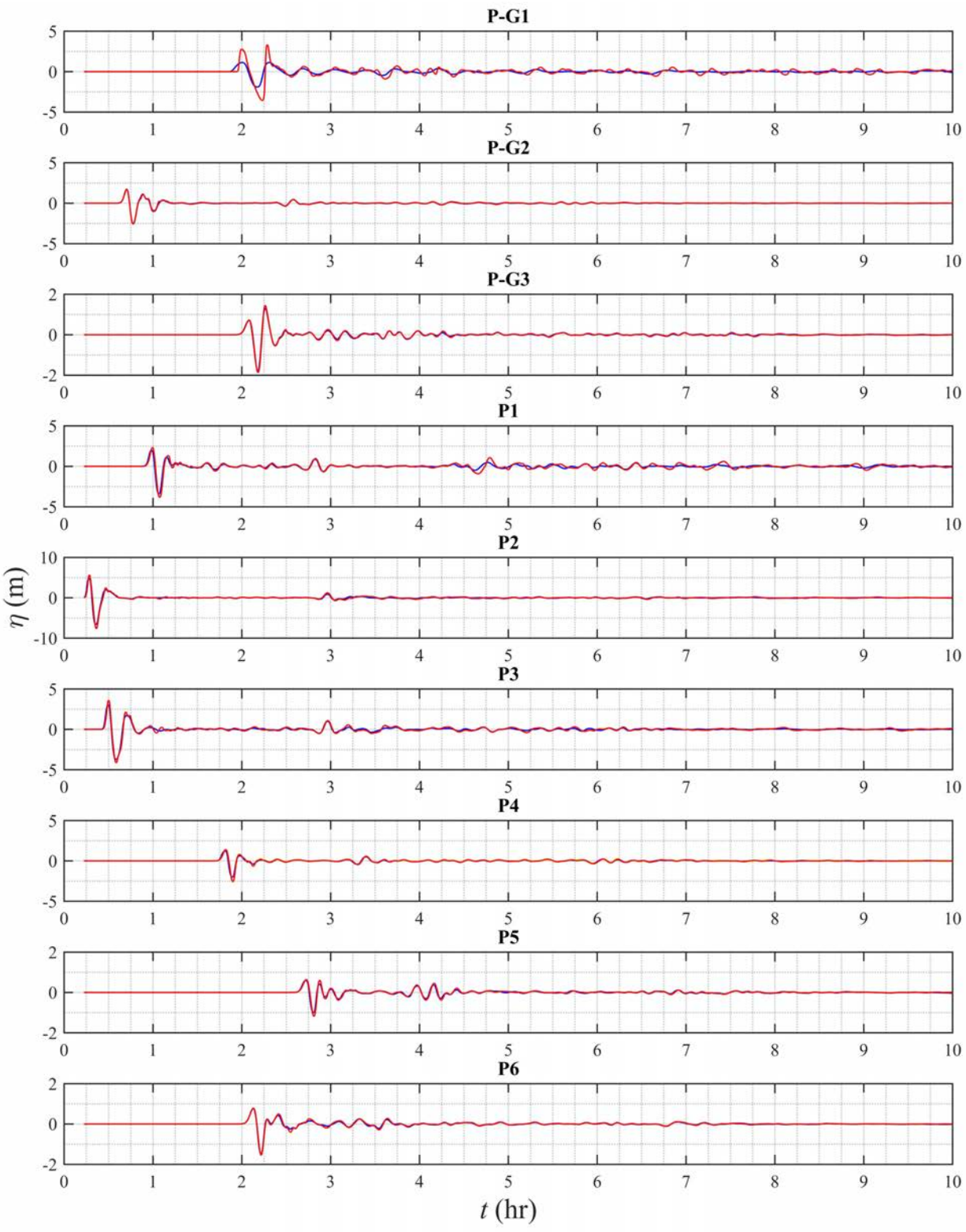

Figure 27: Tsunami wave time series at grid save points. Blue indicates surface elevation computed in grid Local G0, red indicates surface elevation computed in nested grids G1-G3. For point P4, yellow indicates surface elevation computed in G2, red indicates surface elevation computed in G3

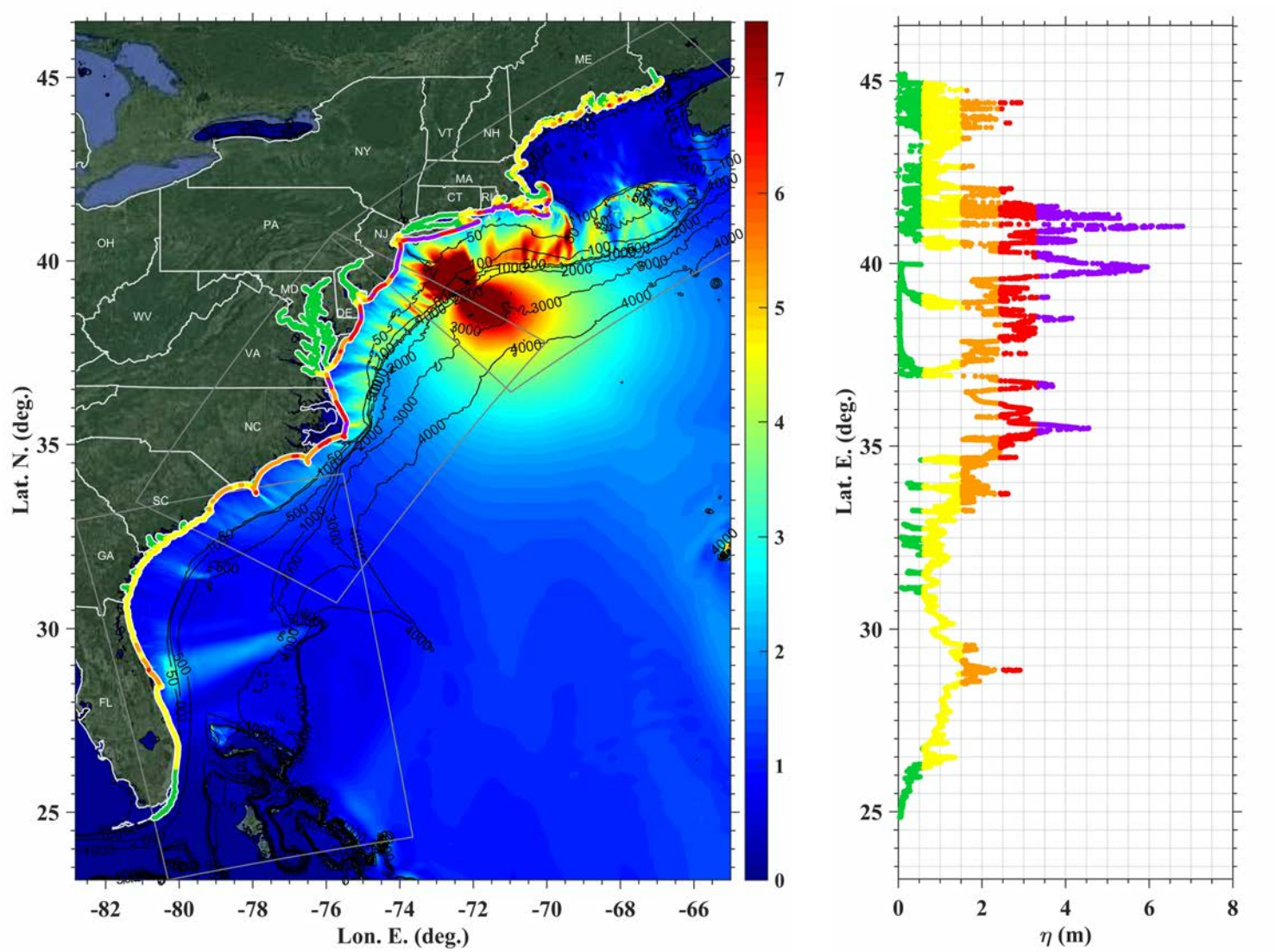

Figure 28: Maximum surface elevation for the Study Area 1 SMF source in grid G1, G2, G3 with color-coded hazard along the 5m isobath contour. Color-coding reflects elevation classes: below 2 ft (green); 2-5 ft (yellow); 5-8 ft (orange); 8-11 ft (red); over 11 ft (purple).

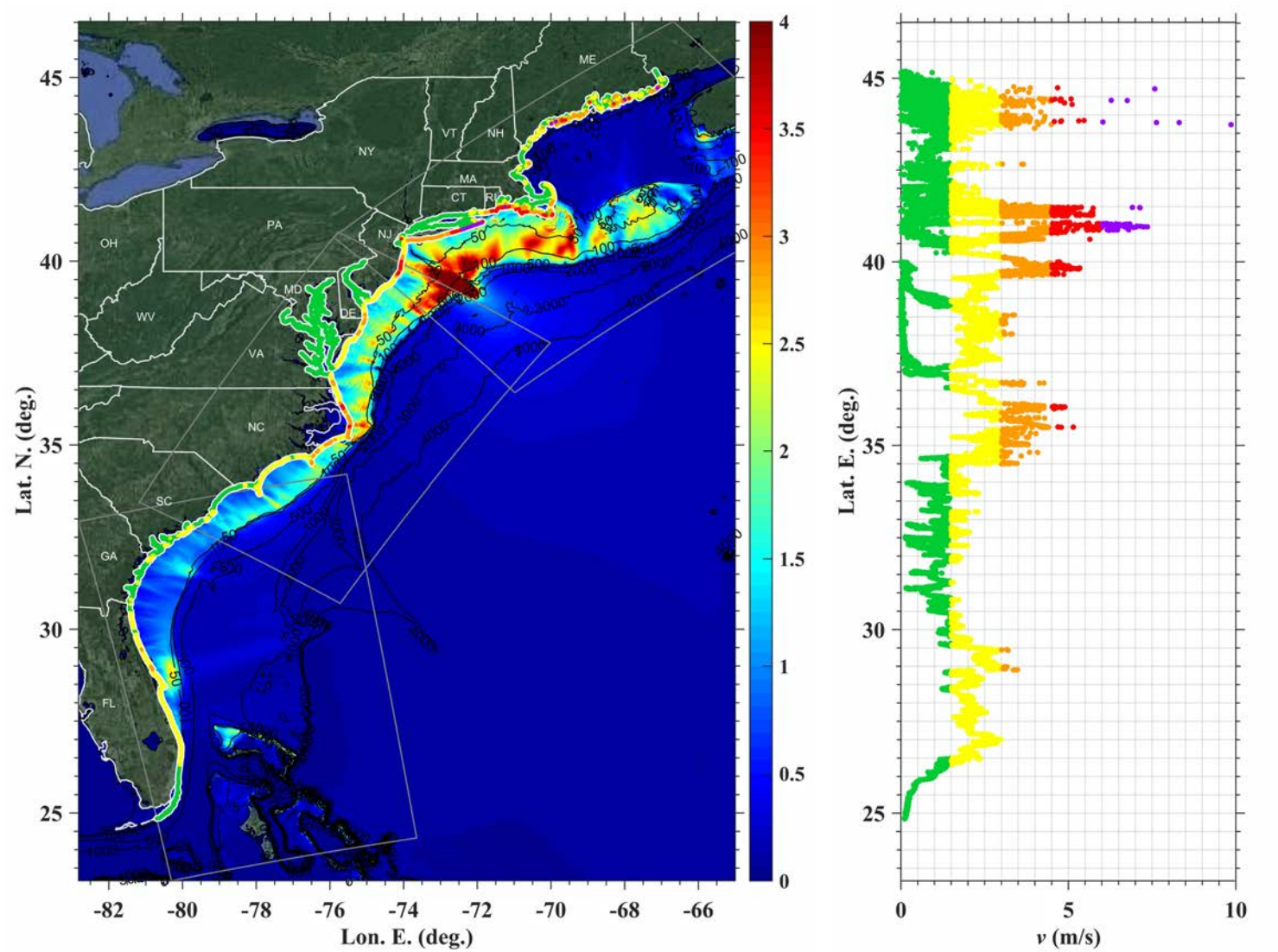

Figure 29: Maximum velocity for the Study Area 1 SMF source in grid G1, G2, G3 with color-coded hazard along the 5m isobath contour. Color-coding reflects velocity classes: below 1.5 m/s (green); 1.5-3 m/s (yellow); 3-4.5 m/s (orange); 4.5-6 m/s (red); over 6 m/s (purple).

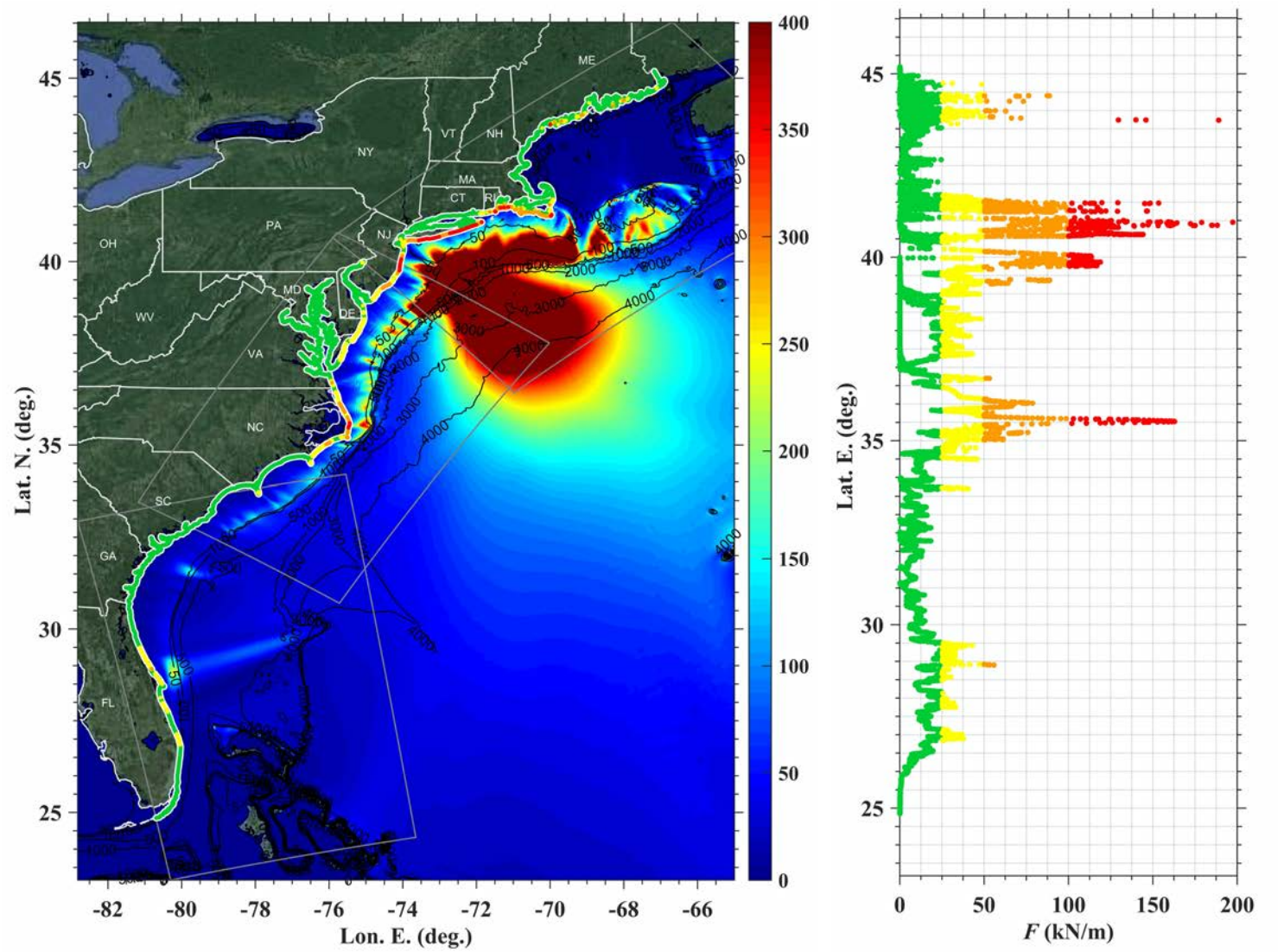

Figure 30: Maximum impulse force for Study Area 1 SMF source in grid G1, G2, G3 with color-coded hazard along the 5m isobath contour. Color-coding reflects impulse force classes: below 25 kN/m (green); 25-50 kN/m (yellow); 50-100 kN/m (orange); 100-200 kN/m (red); over 200 kN/m (purple).

Study Area 2 Rigid Slump Submarine Mass Failure

Maximum Surface Elevation, Velocity, and Impulse Force

Figure 31 shows an overview of the maximum surface elevation in grids Local G0, G1, G2, and G3 computed with FUNWAVE-TVD for the Study Area 2 SMF source (Figure 6, Table 1) with a simulation time of t = 86400 s (24 h).

Figure 32 shows the surface elevation time series at the grid save points (Table 2).

Figure 33, Figure 34, and Figure 35 show the maximum surface elevation, velocity, and impulse force respectively in grids Local G0, G1, G2, and G3 with values along the 5 m isobath contour (calculated in G1-G3) plotted as a function of latitude.

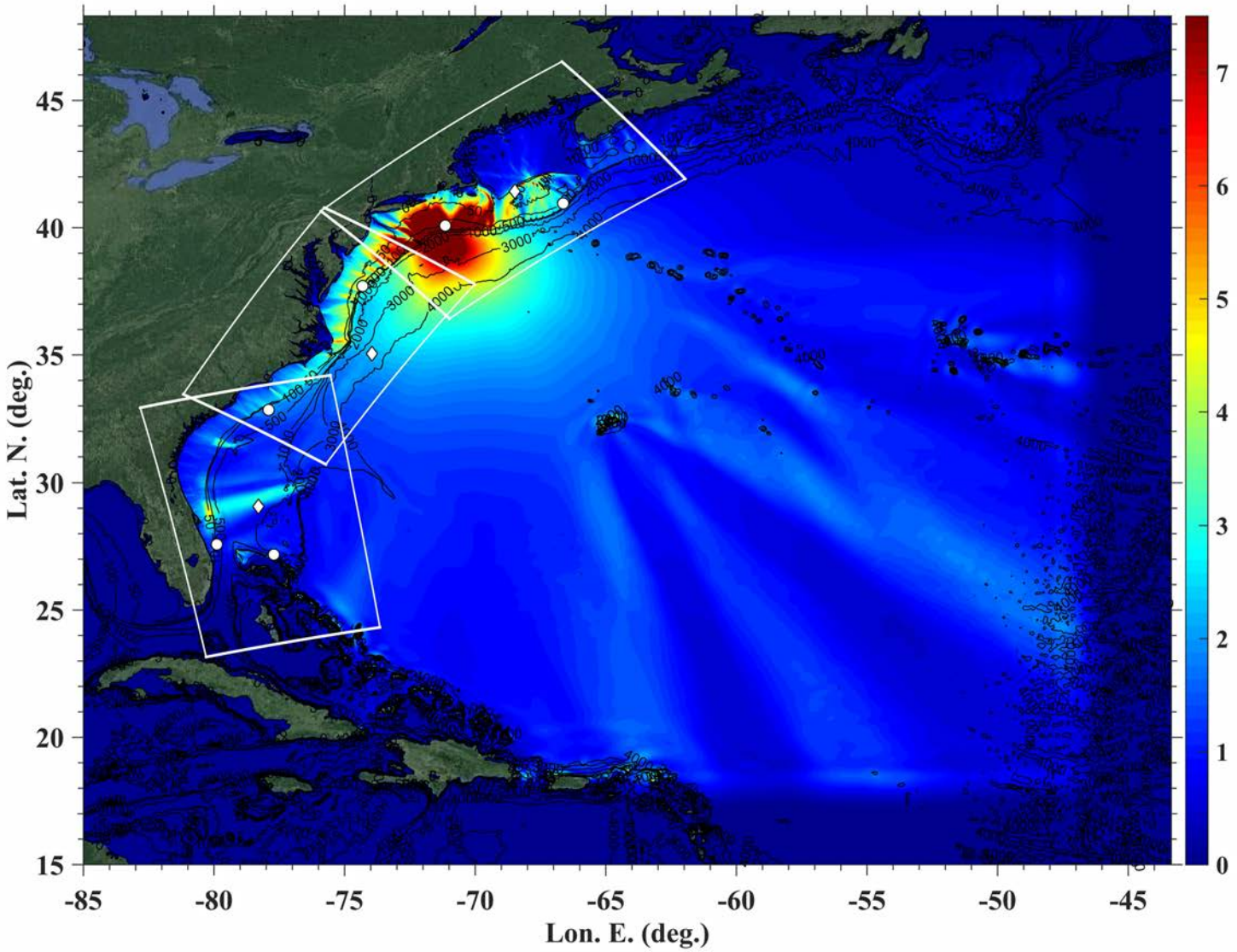

Figure 31: Maximum surface elevation for Study Area 2 SMF source

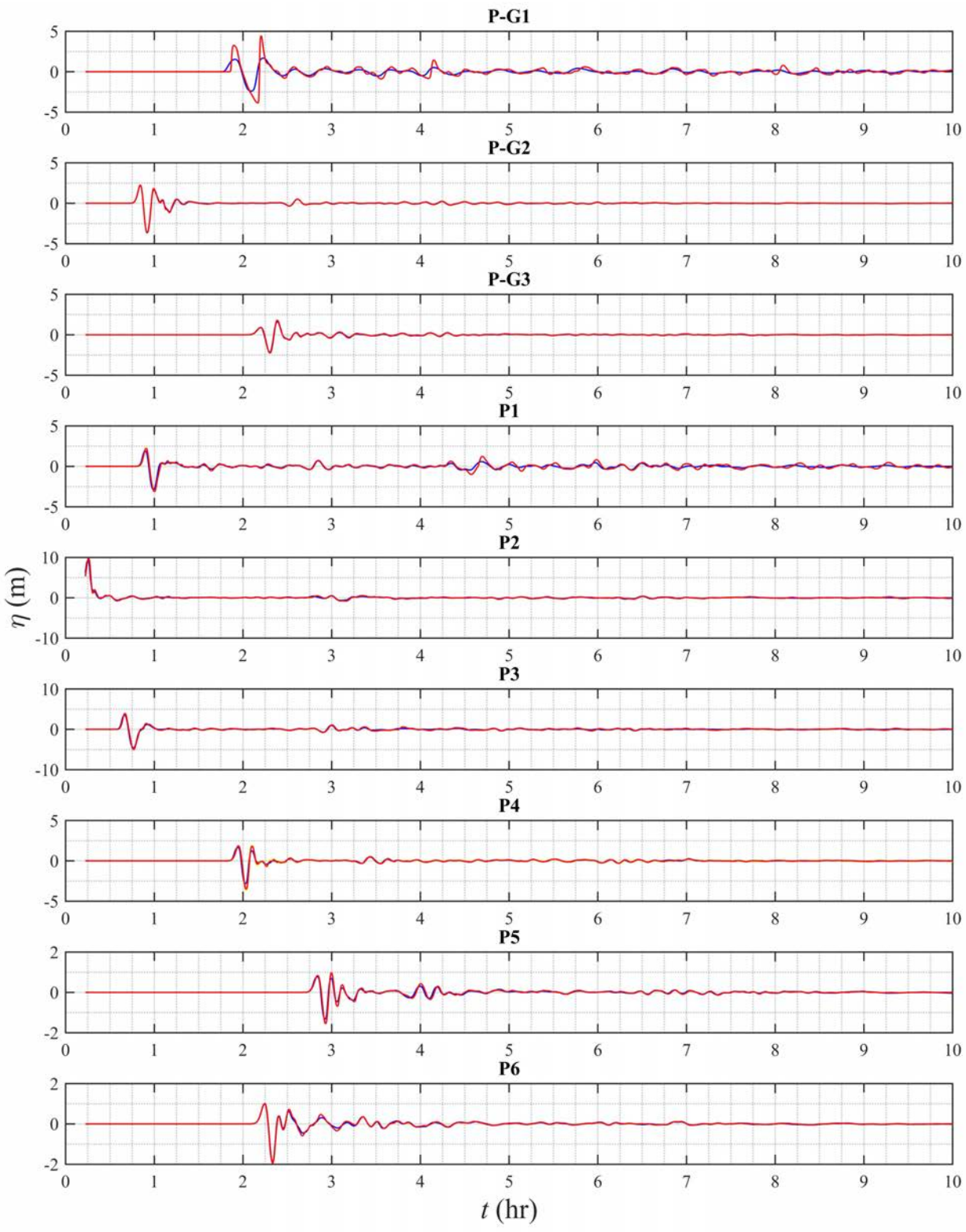

Figure 32: Tsunami wave time series at grid save points. Blue indicates surface elevation computed in grid Local G0, red indicates surface elevation computed in nested grids G1-G3. For point P4, yellow indicates surface elevation computed in G2, red indicates surface elevation computed in G3

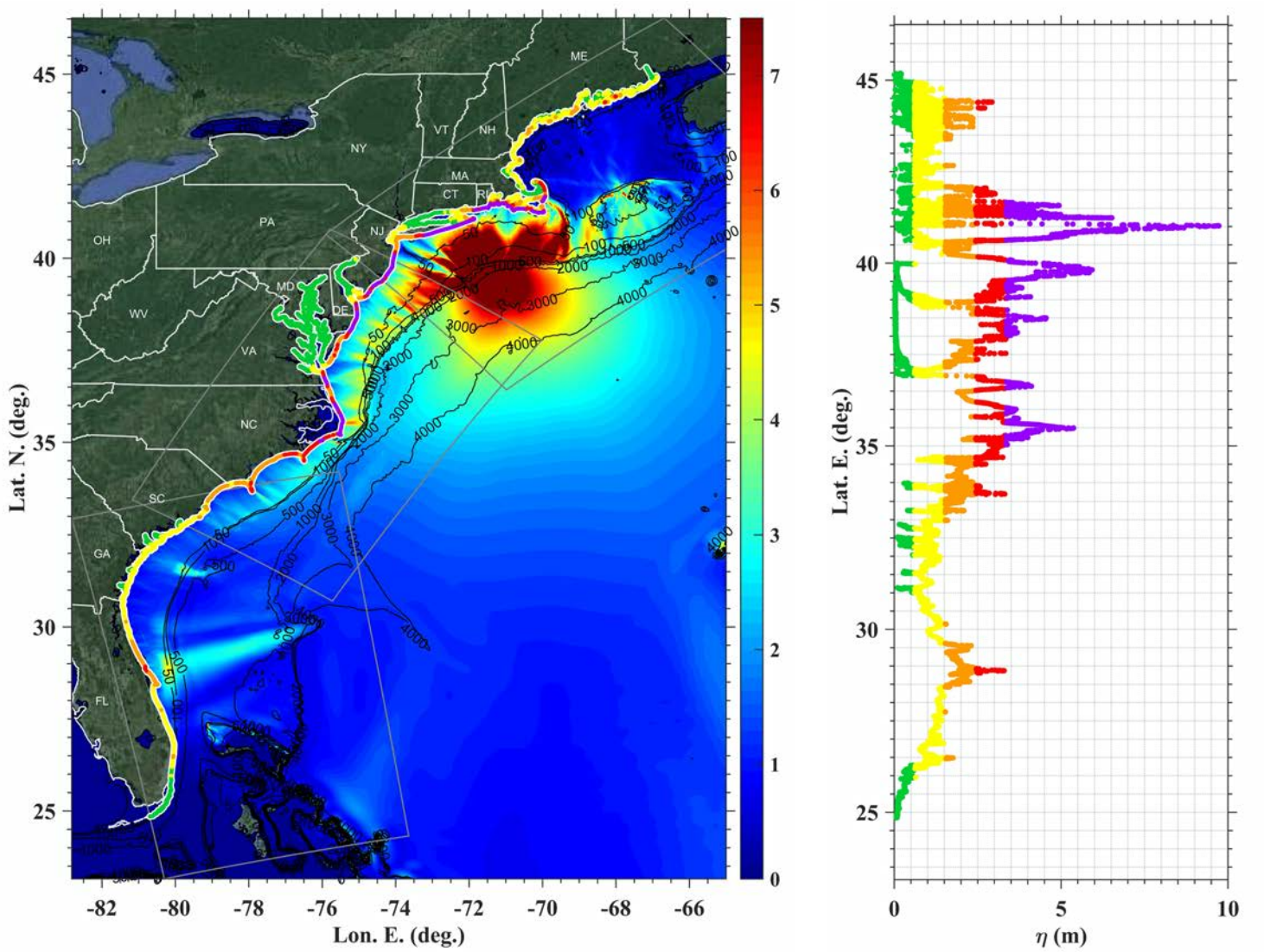

Figure 33: Maximum surface elevation for the Study Area 2 SMF source in grid G1, G2, G3 with color-coded hazard along the 5m isobath contour. Color-coding reflects elevation classes: below 2 ft (green); 2-5 ft (yellow); 5-8 ft (orange); 8-11 ft (red); over 11 ft (purple).

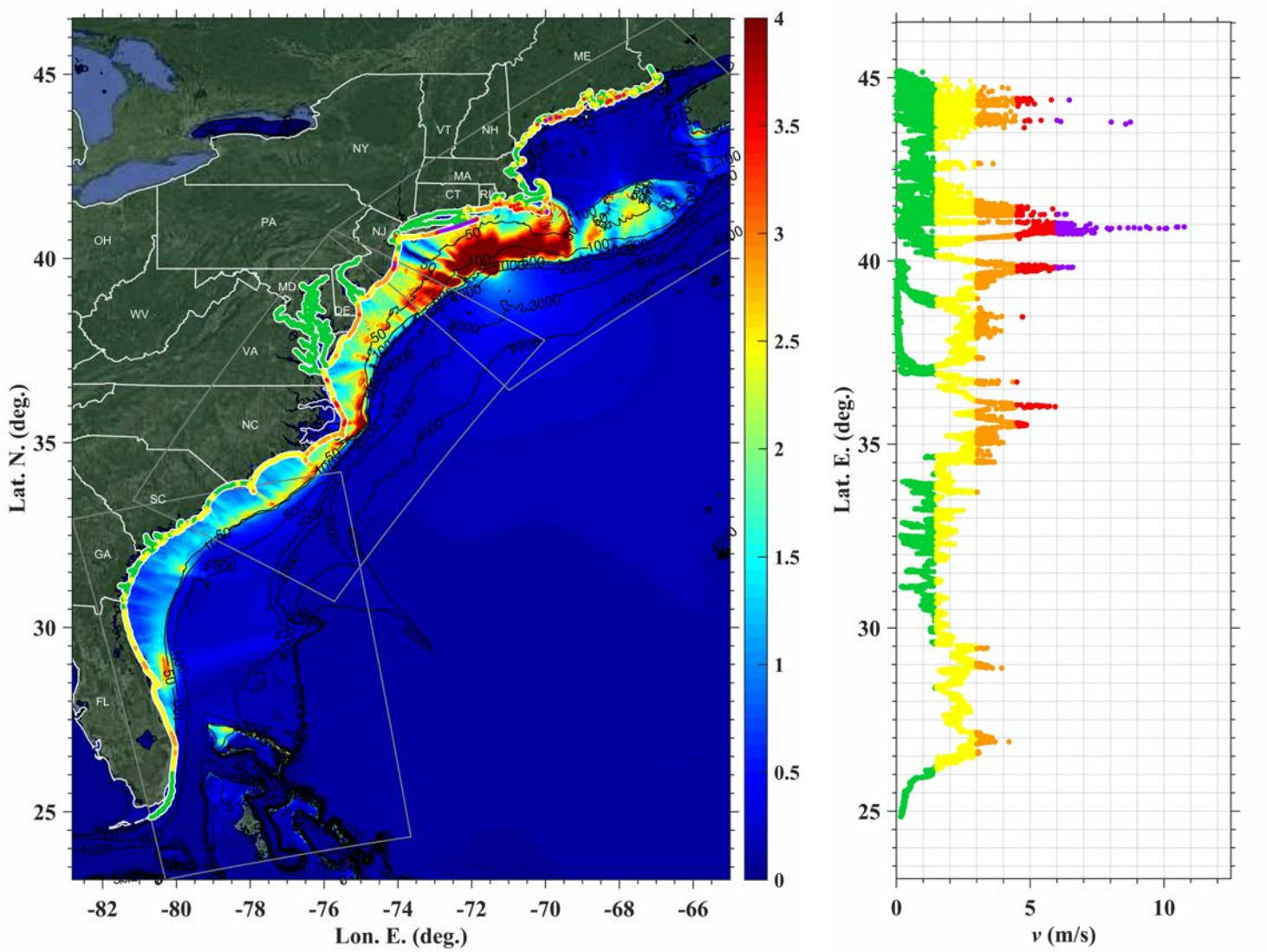

Figure 34: Maximum velocity for the Study Area 2 SMF source in grid G1, G2, G3 with color-coded hazard along the 5m isobath contour. Color-coding reflects velocity classes: below 1.5 m/s (green); 1.5-3 m/s (yellow); 3-4.5 m/s (orange); 4.5-6 m/s (red); over 6 m/s (purple).

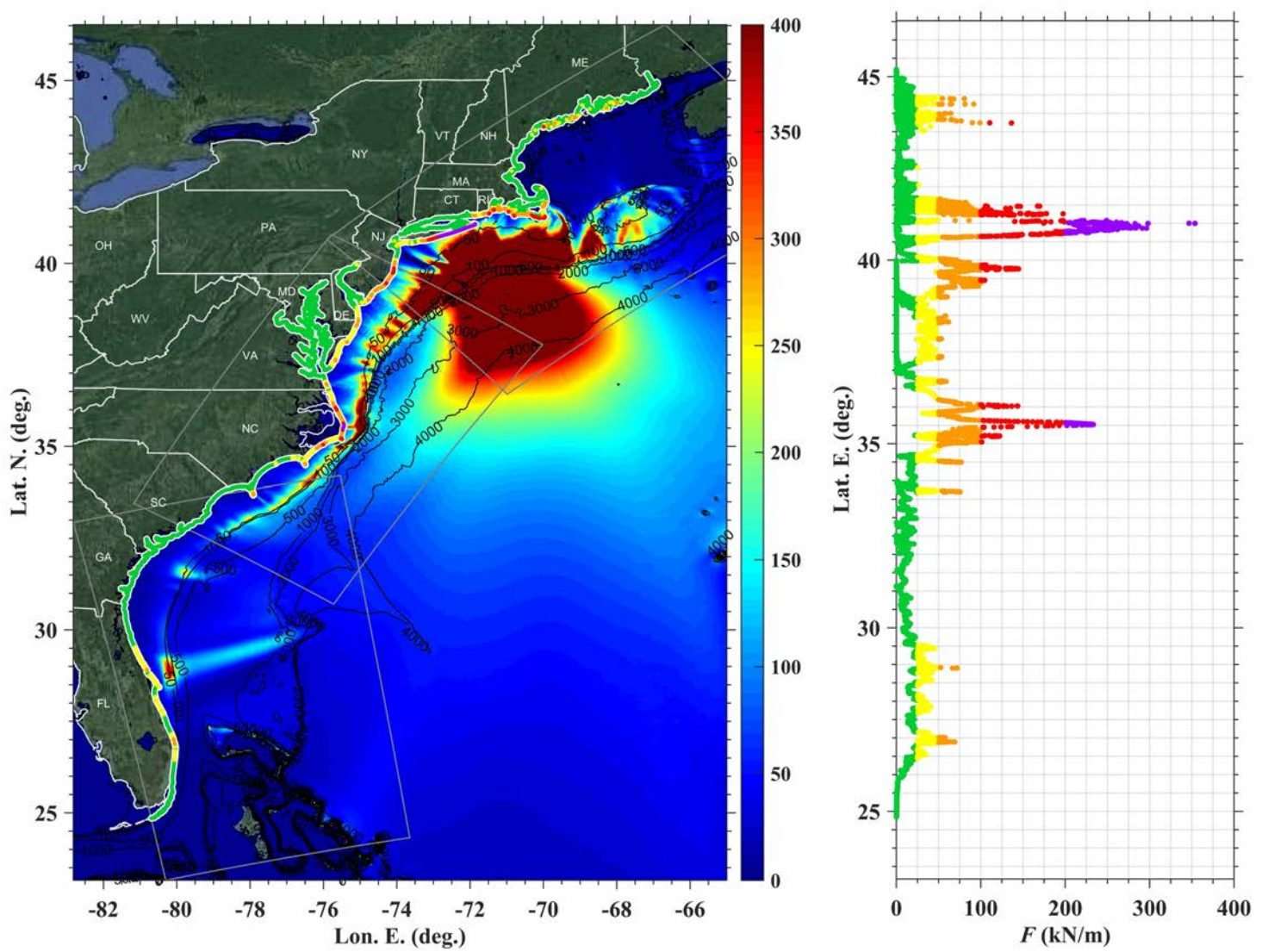

Figure 35: Maximum impulse force for Study Area 2 SMF source in grid G1, G2, G3 with color-coded hazard along the 5m isobath contour. Color-coding reflects impulse force classes: below 25 kN/m (green); 25-50 kN/m (yellow); 50-100 kN/m (orange); 100-200 kN/m (red); over 200 kN/m (purple).

Study Area 3 Rigid Slump Submarine Mass Failure

Maximum Surface Elevation, Velocity, and Impulse Force

Figure 36 shows an overview of the maximum surface elevation in grids Local G0, G1, G2, and G3 computed with FUNWAVE-TVD for the Study Area 3 SMF source (Figure 6, Table 1) with a simulation time of t = 86400 s (24 h).

Figure 37 shows the surface elevation time series at the grid save points (Table 2).

Figure 38, Figure 39, and Figure 40 show the maximum surface elevation, velocity, and impulse force respectively in grids Local G0, G1, G2, and G3 with values along the 5 m isobath contour (calculated in G1-G3) plotted as a function of latitude.

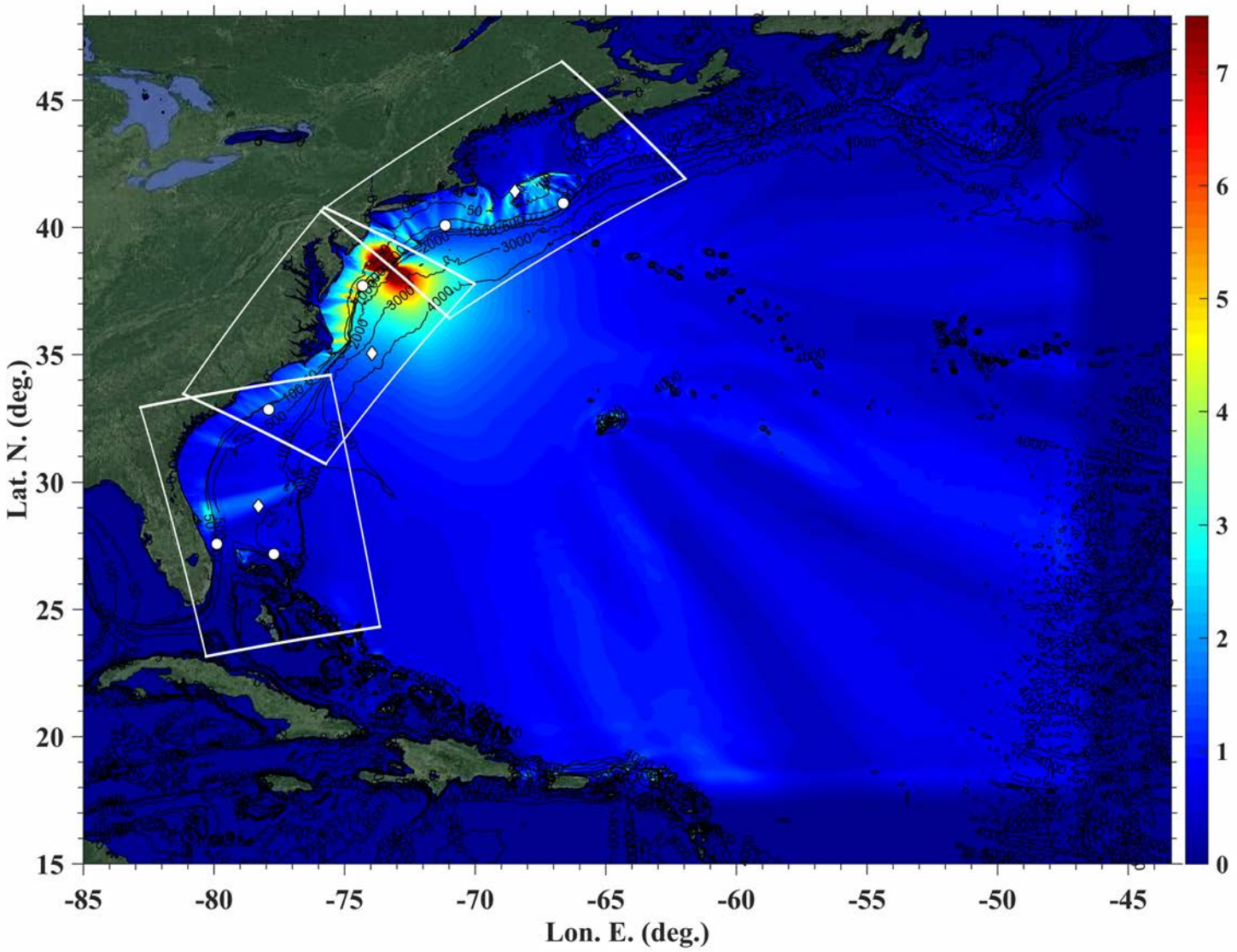

Figure 36: Maximum surface elevation for Study Area 3 SMF source

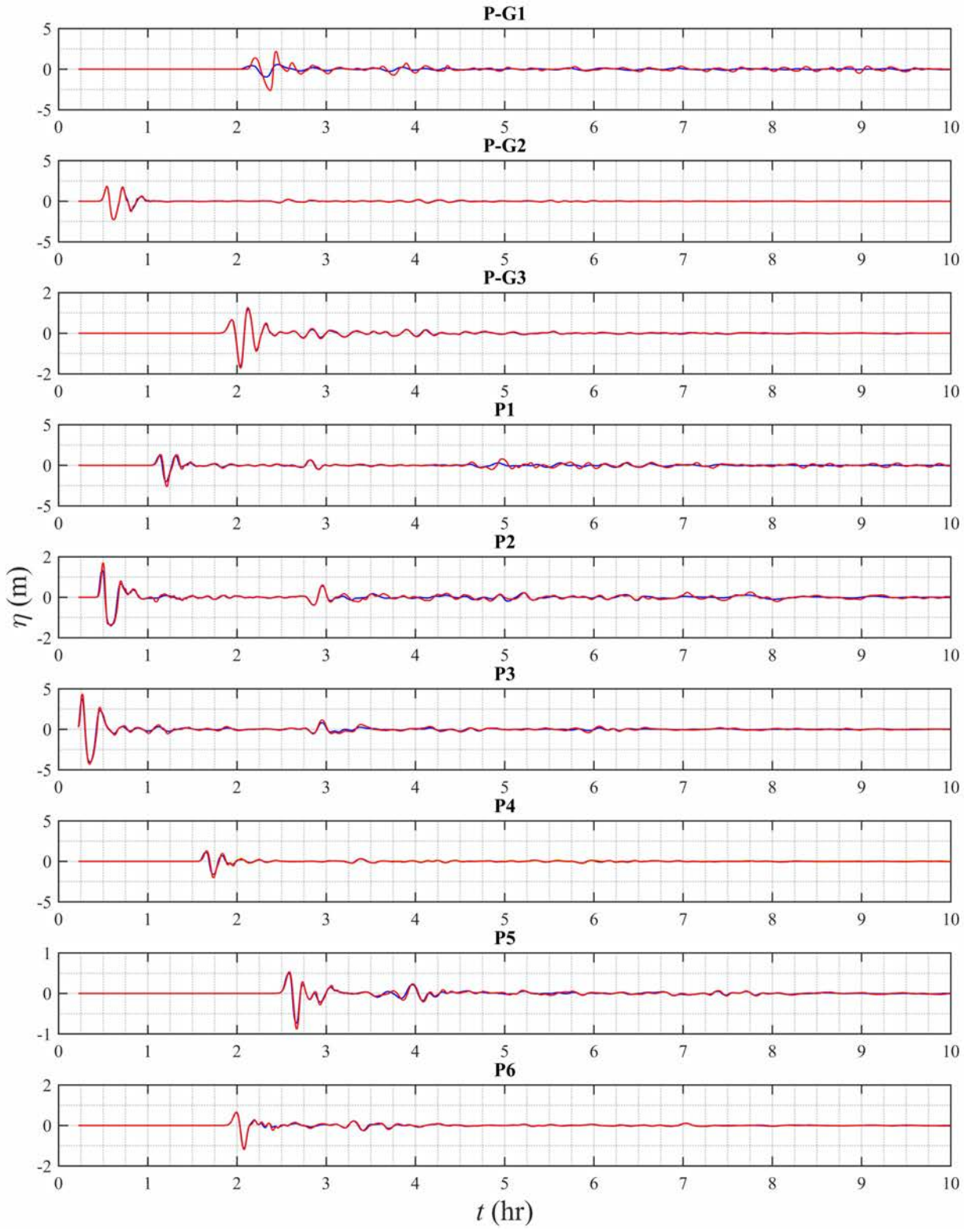

Figure 37: Tsunami wave time series at grid save points. Blue indicates surface elevation computed in grid Local G0, red indicates surface elevation computed in nested grids G1-G3. For point P4, yellow indicates surface elevation computed in G2, red indicates surface elevation computed in G3.

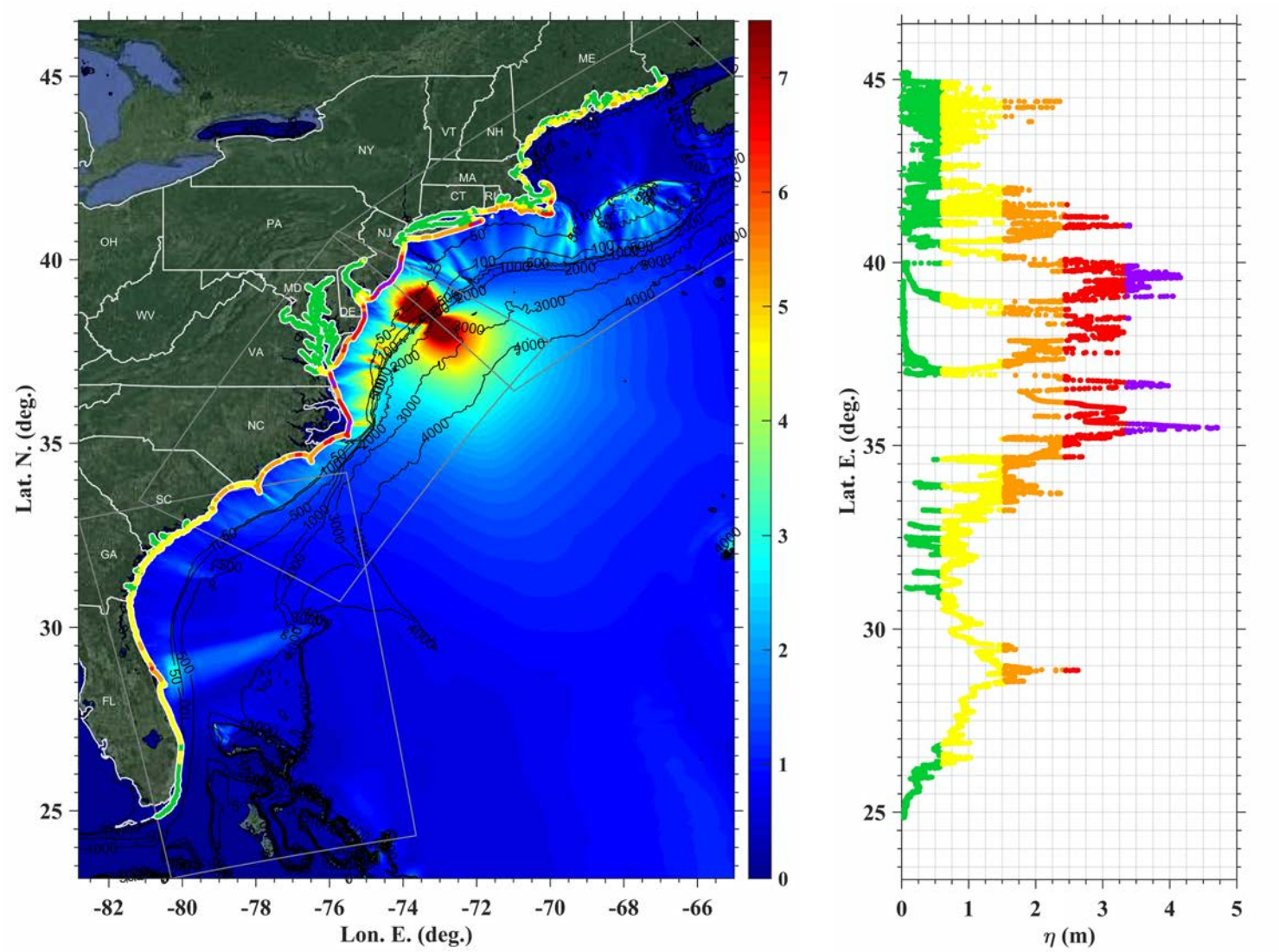

Figure 38: Maximum surface elevation for the Study Area 3 SMF source in grid G1, G2, G3 with color-coded hazard along the 5m isobath contour. Color-coding reflects elevation classes: below 2 ft (green); 2-5 ft (yellow); 5-8 ft (orange); 8-11 ft (red); over 11 ft (purple).

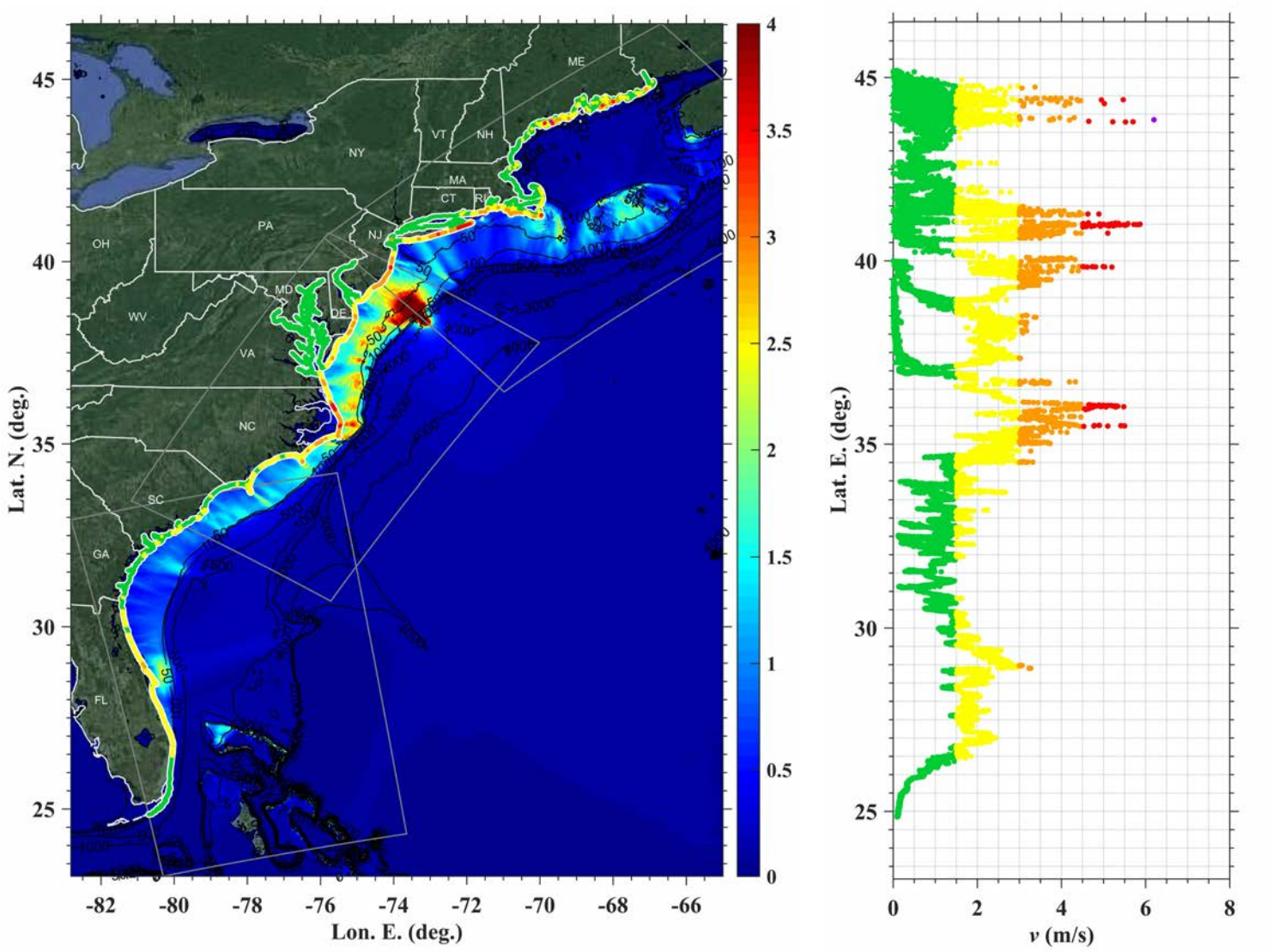

Figure 39: Maximum velocity for the Study Area 3 SMF source in grid G1, G2, G3 with color-coded hazard along the 5m isobath contour. Color-coding reflects velocity classes: below 1.5 m/s (green); 1.5-3 m/s (yellow); 3-4.5 m/s (orange); 4.5-6 m/s (red); over 6 m/s (purple).

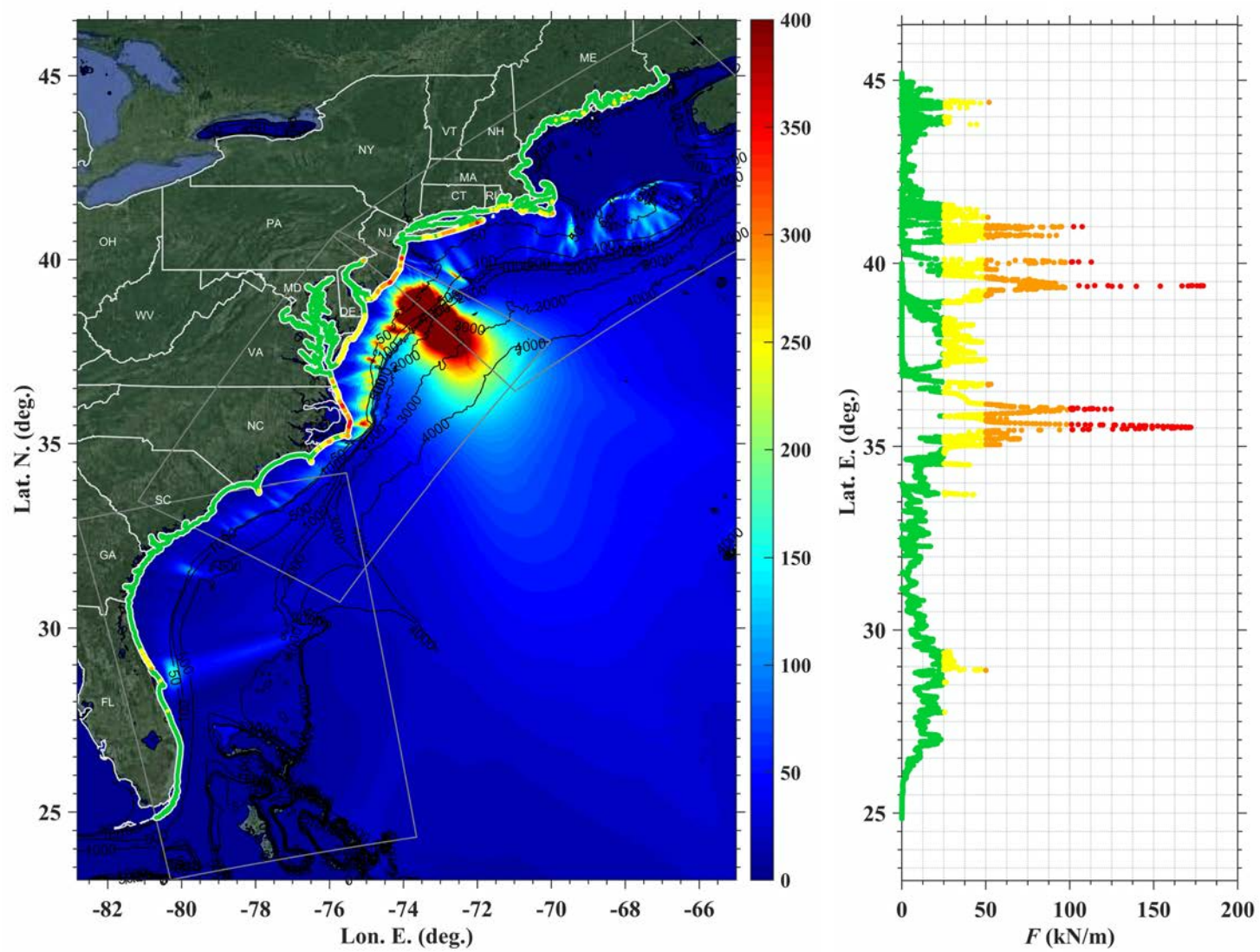

Figure 40: Maximum impulse force for Study Area 3 SMF source in grid G1, G2, G3 with color-coded hazard along the 5m isobath contour. Color-coding reflects impulse force classes: below 25 kN/m (green); 25-50 kN/m (yellow); 50-100 kN/m (orange); 100-200 kN/m (red); over 200 kN/m (purple).

Study Area 4 Rigid Slump Submarine Mass Failure

Maximum Surface Elevation, Velocity, and Impulse Force

Figure 41 shows an overview of the maximum surface elevation in grids Local G0, G1, G2, and G3 computed with FUNWAVE-TVD for the Study Area 4 SMF source (Figure 6, Table 1) with a simulation time of t = 86400 s (24 h).

Figure 42 shows the surface elevation time series at the grid save points (Table 2).

Figure 43, Figure 44, and Figure 45 show the maximum surface elevation, velocity, and impulse force respectively in grids Local G0, G1, G2, and G3 with values along the 5 m isobath contour (calculated in G1-G3) plotted as a function of latitude.

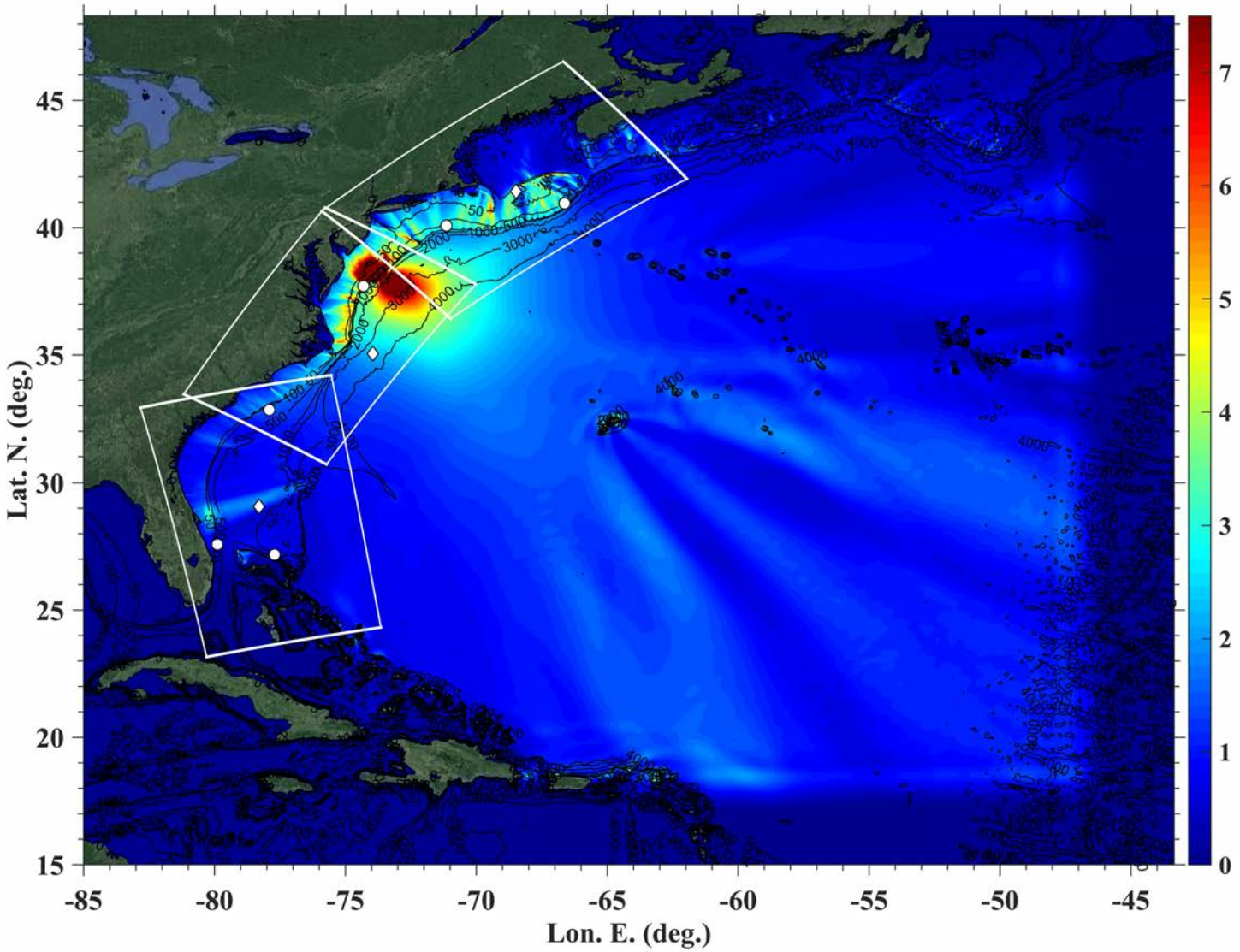

Figure 41: Maximum surface elevation for Study Area 4 SMF source

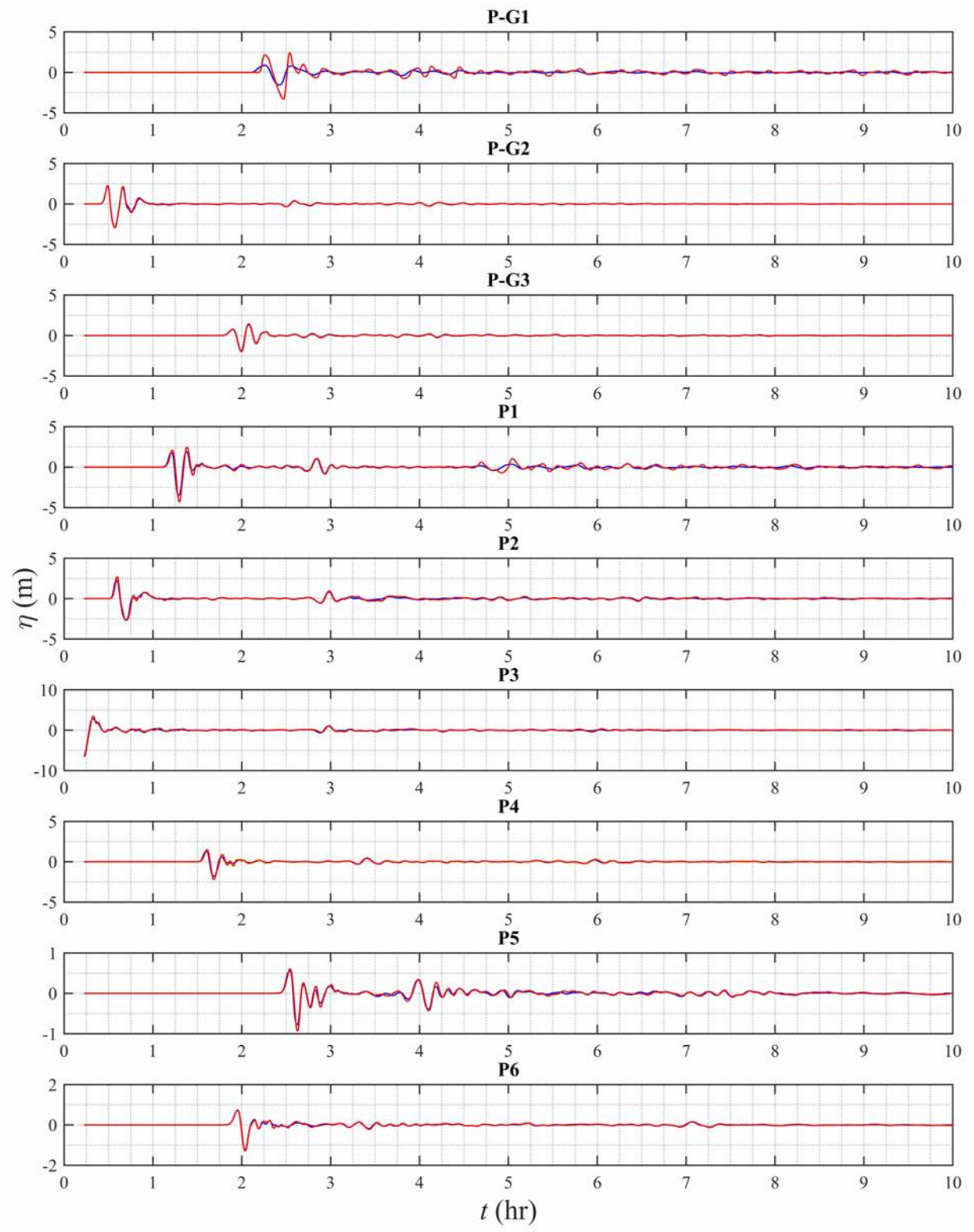

Figure 42: Tsunami wave time series at grid save points. Blue indicates surface elevation computed in grid Local G0, red indicates surface elevation computed in nested grids G1-G3. For point P4, yellow indicates surface elevation computed in G2, red indicates surface elevation computed in G3.

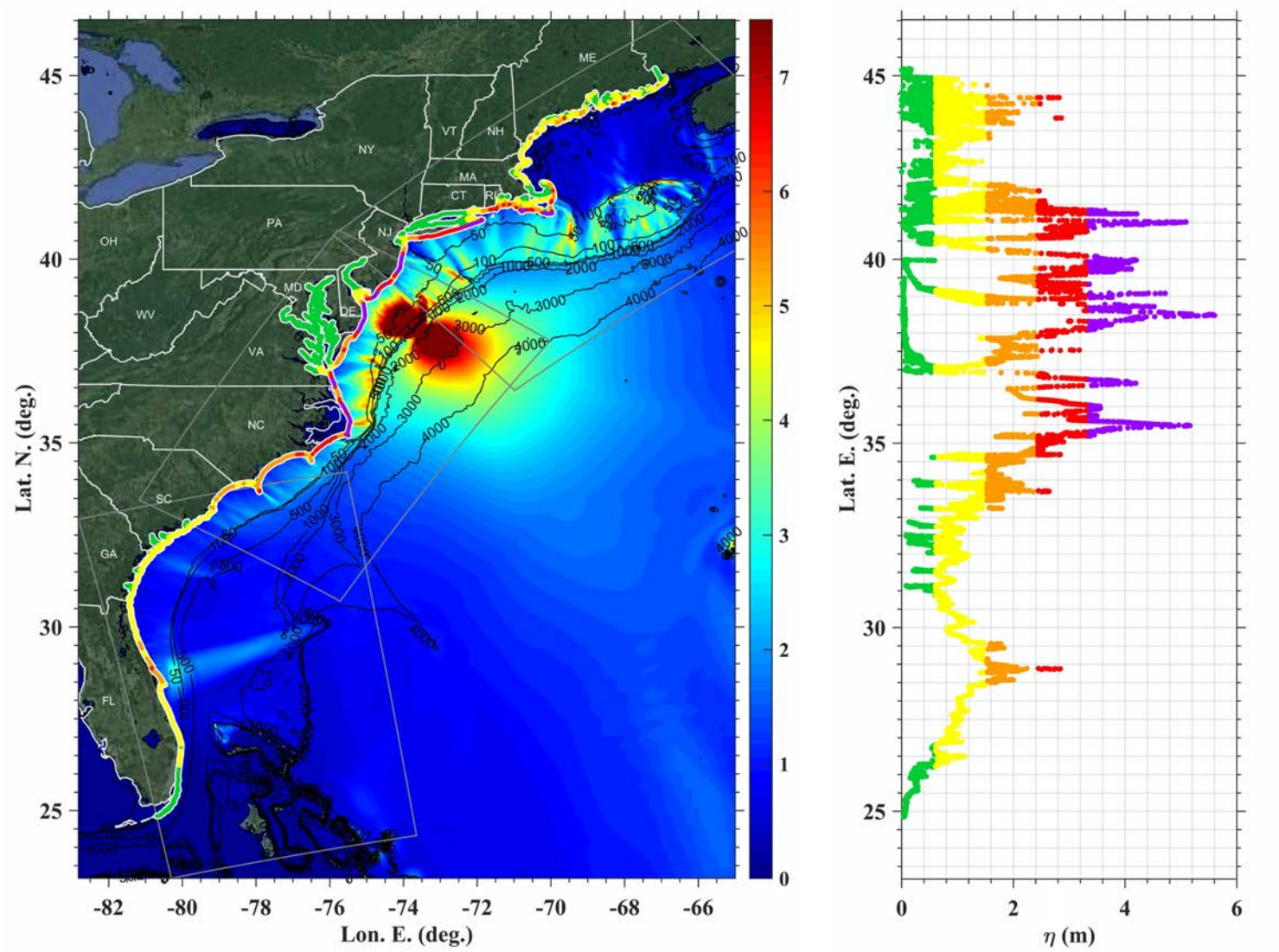

Figure 43: Maximum surface elevation for the Study Area 4 SMF source in grid G1, G2, G3 with color-coded hazard along the 5m isobath contour. Color-coding reflects elevation classes: below 2 ft (green); 2-5 ft (yellow); 5-8 ft (orange); 8-11 ft (red); over 11 ft (purple).

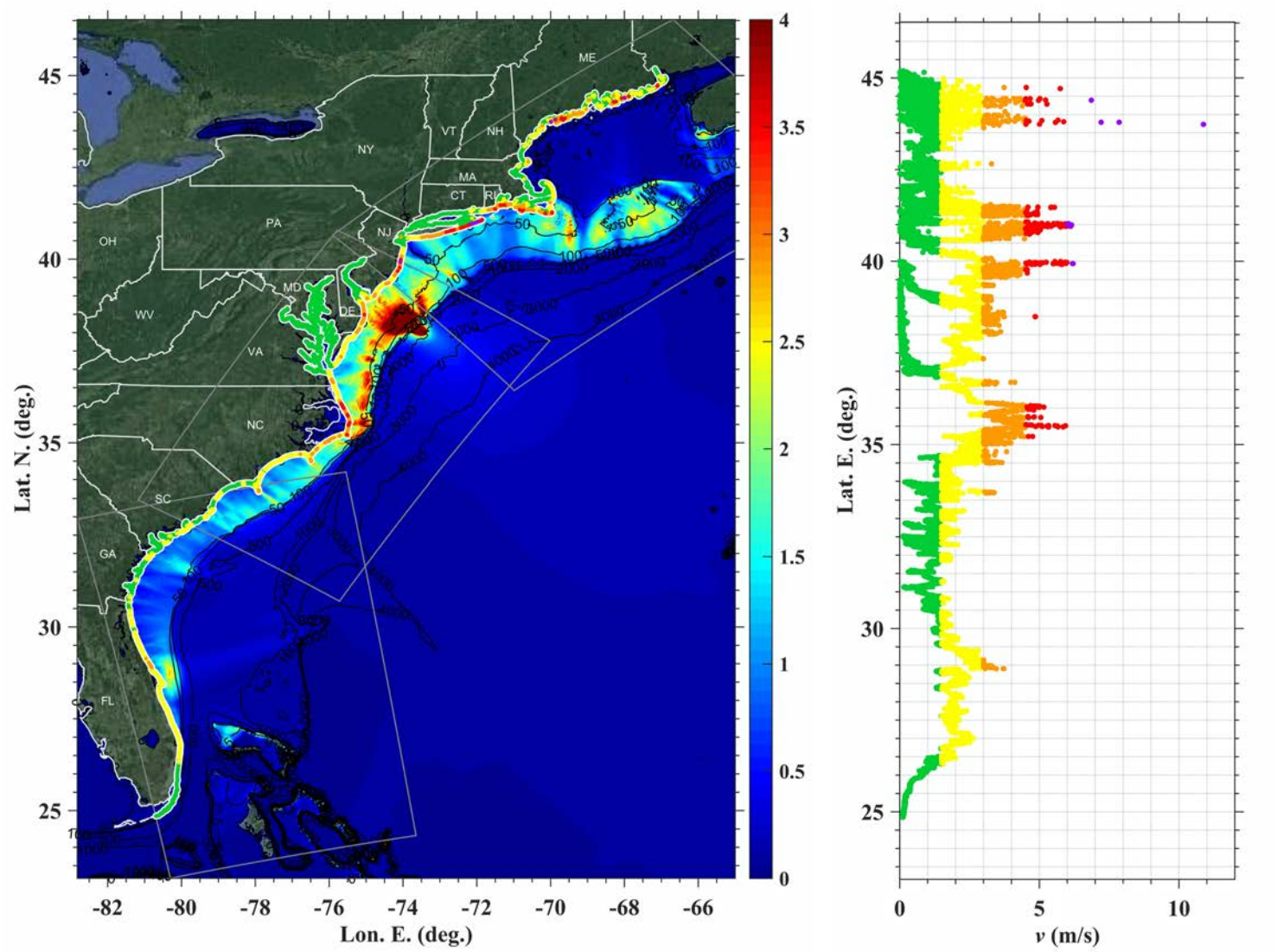

Figure 44: Maximum velocity for the Study Area 4 SMF source in grid G1, G2, G3 with color-coded hazard along the 5m isobath contour. Color-coding reflects velocity classes: below 1.5 m/s (green); 1.5-3 m/s (yellow); 3-4.5 m/s (orange); 4.5-6 m/s (red); over 6 m/s (purple).

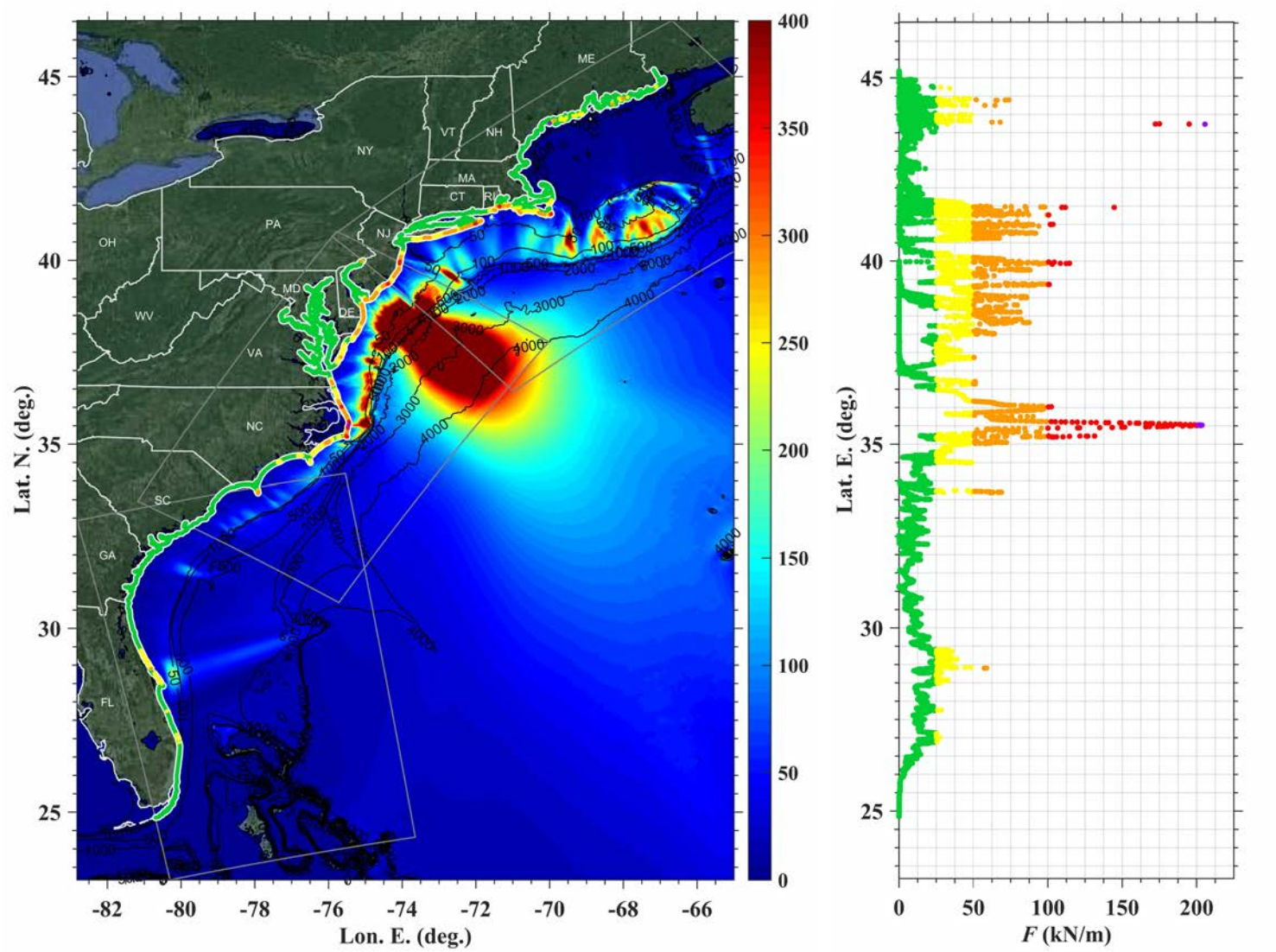

Figure 45: Maximum impulse force for Study Area 4 SMF source in grid G1, G2, G3 with color-coded hazard along the 5m isobath contour. Color-coding reflects impulse force classes: below 25 kN/m (green); 25-50 kN/m (yellow); 50-100 kN/m (orange); 100-200 kN/m (red); over 200 kN/m (purple).

Cape Fear Rigid Slump Submarine Mass Failure

Maximum Surface Elevation, Velocity, and Impulse Force

Figure 46 shows an overview of the maximum surface elevation in grids Local G0, G1, G2, and G3 computed with FUNWAVE-TVD for the Cape Fear SMF source (Figure 7) with a simulation time of t = 86400 s (24 h).

Figure 47 shows the surface elevation time series at the grid save points (Table 2).

Figure 48, Figure 49, and Figure 50 show the maximum surface elevation, velocity, and impulse force respectively in grids Local G0, G1, G2, and G3 with values along the 5 m isobath contour (calculated in G1-G3) plotted as a function of latitude.

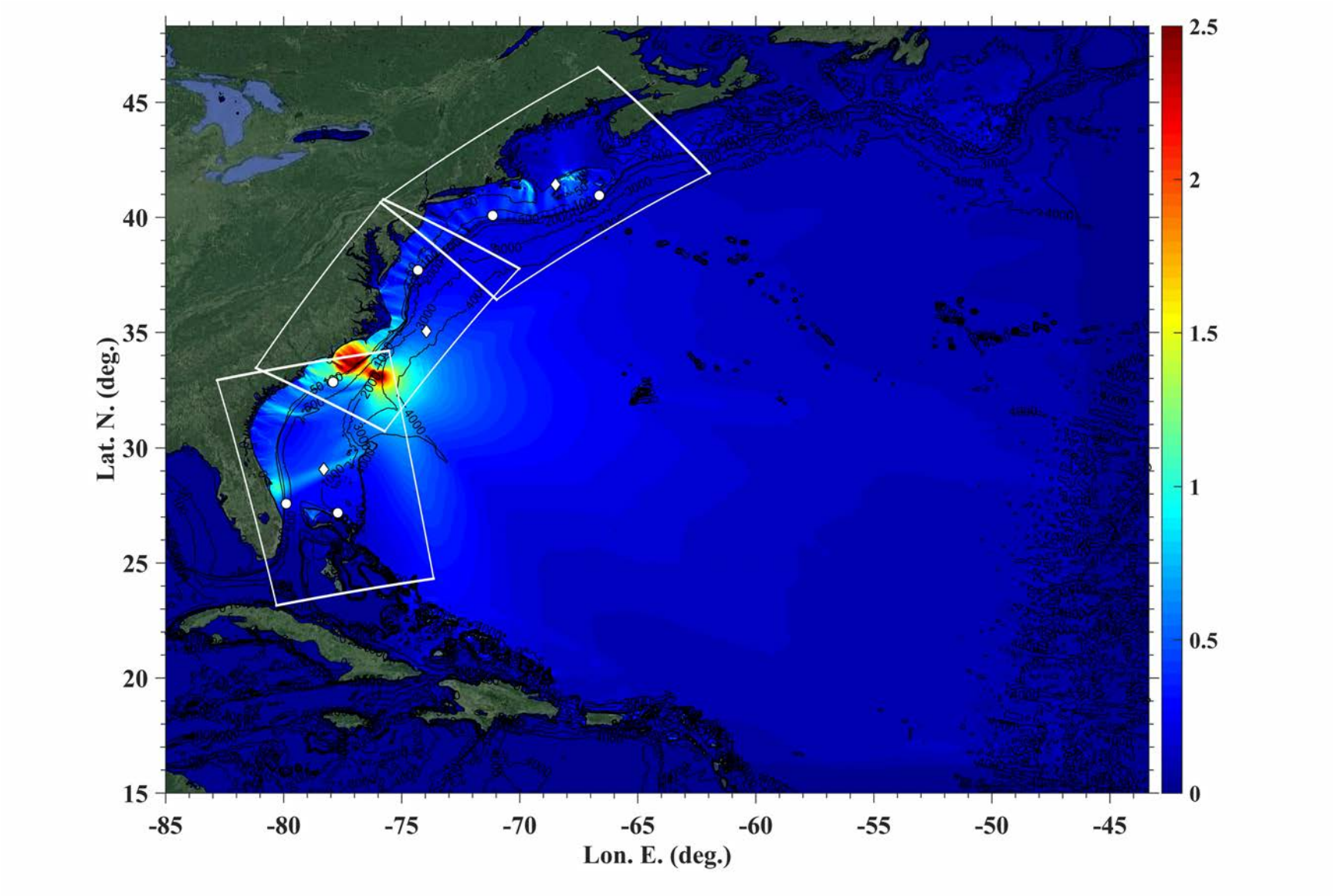

Figure 46: Maximum surface elevation for the Cape Fear SMF source

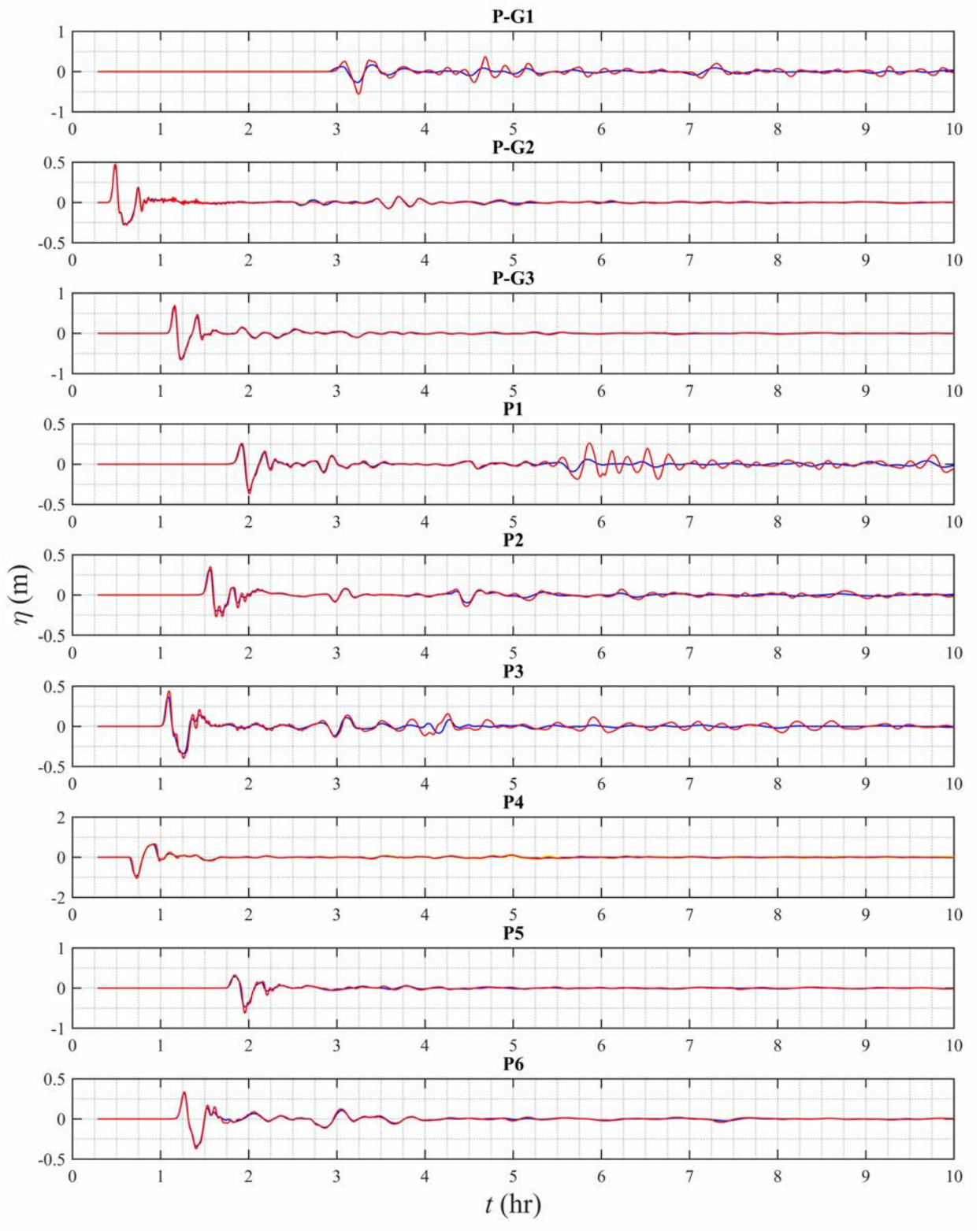

Figure 47: Tsunami wave time series at grid save points. Blue indicates surface elevation computed in grid Local G0, red indicates surface elevation computed in nested grids G1-G3. For point P4, yellow indicates surface elevation computed in G2, red indicates surface elevation computed in G3.

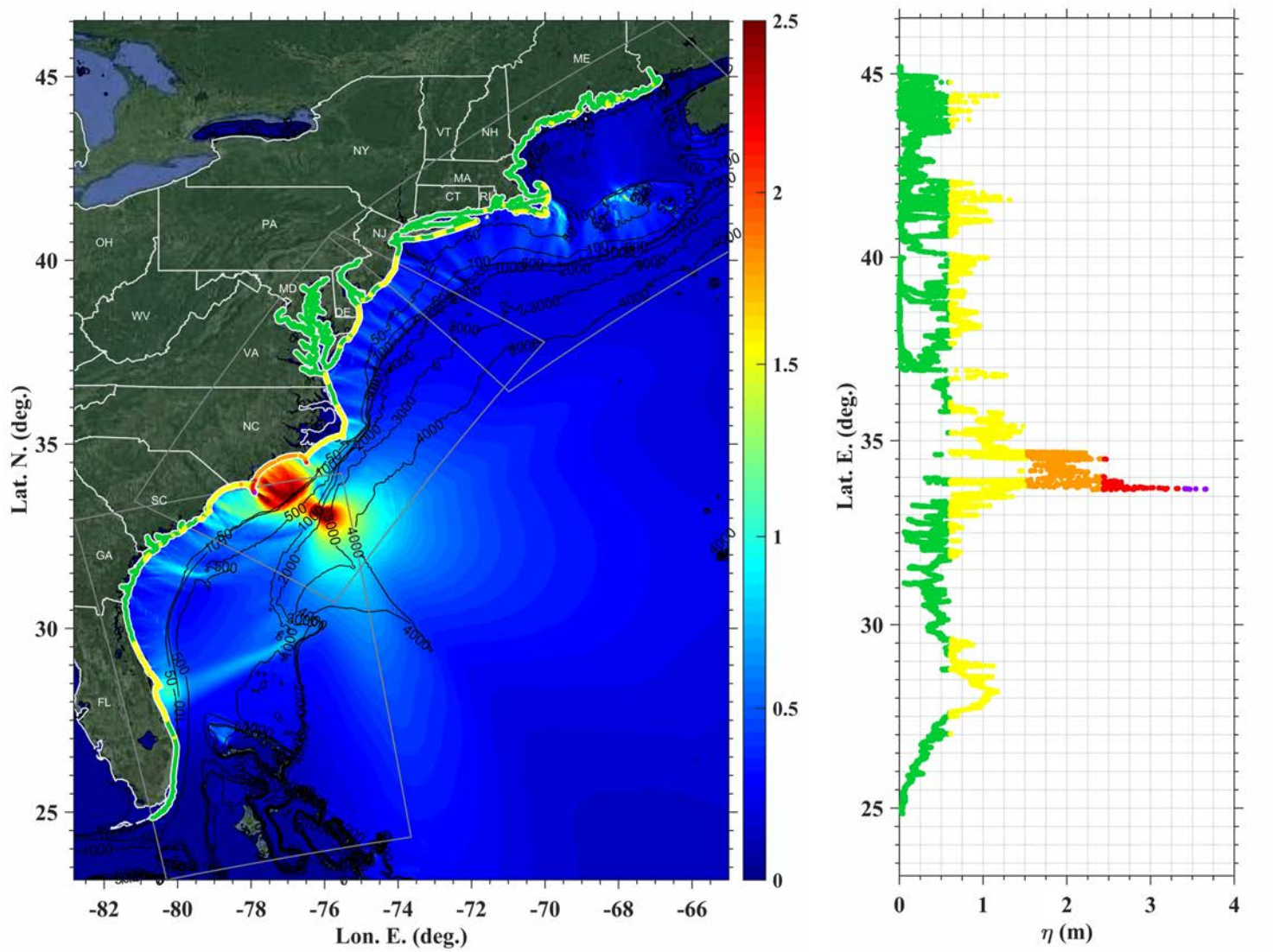

Figure 48: Maximum surface elevation for the Cape Fear SMF source in grid G1, G2, G3 with color-coded hazard along the 5m isobath contour. Color-coding reflects elevation classes: below 2 ft (green); 2-5 ft (yellow); 5-8 ft (orange); 8-11 ft (red); over 11 ft (purple).

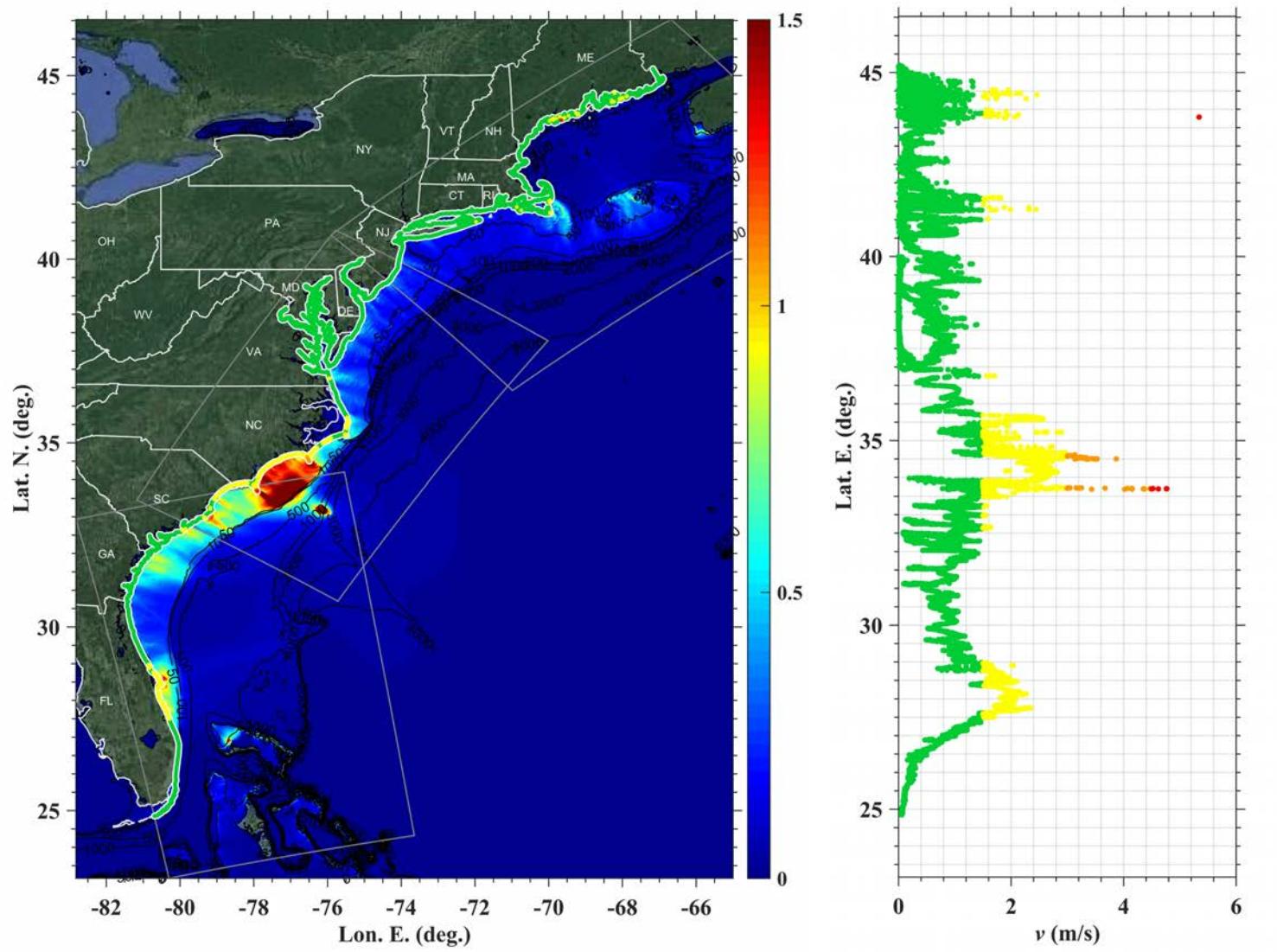

Figure 49: Maximum velocity for the Cape Fear SMF source in grid G1, G2, G3 with color-coded hazard along the 5m isobath contour. Color-coding reflects velocity classes: below 1.5 m/s (green); 1.5-3 m/s (yellow); 3-4.5 m/s (orange); 4.5-6 m/s (red); over 6 m/s (purple).

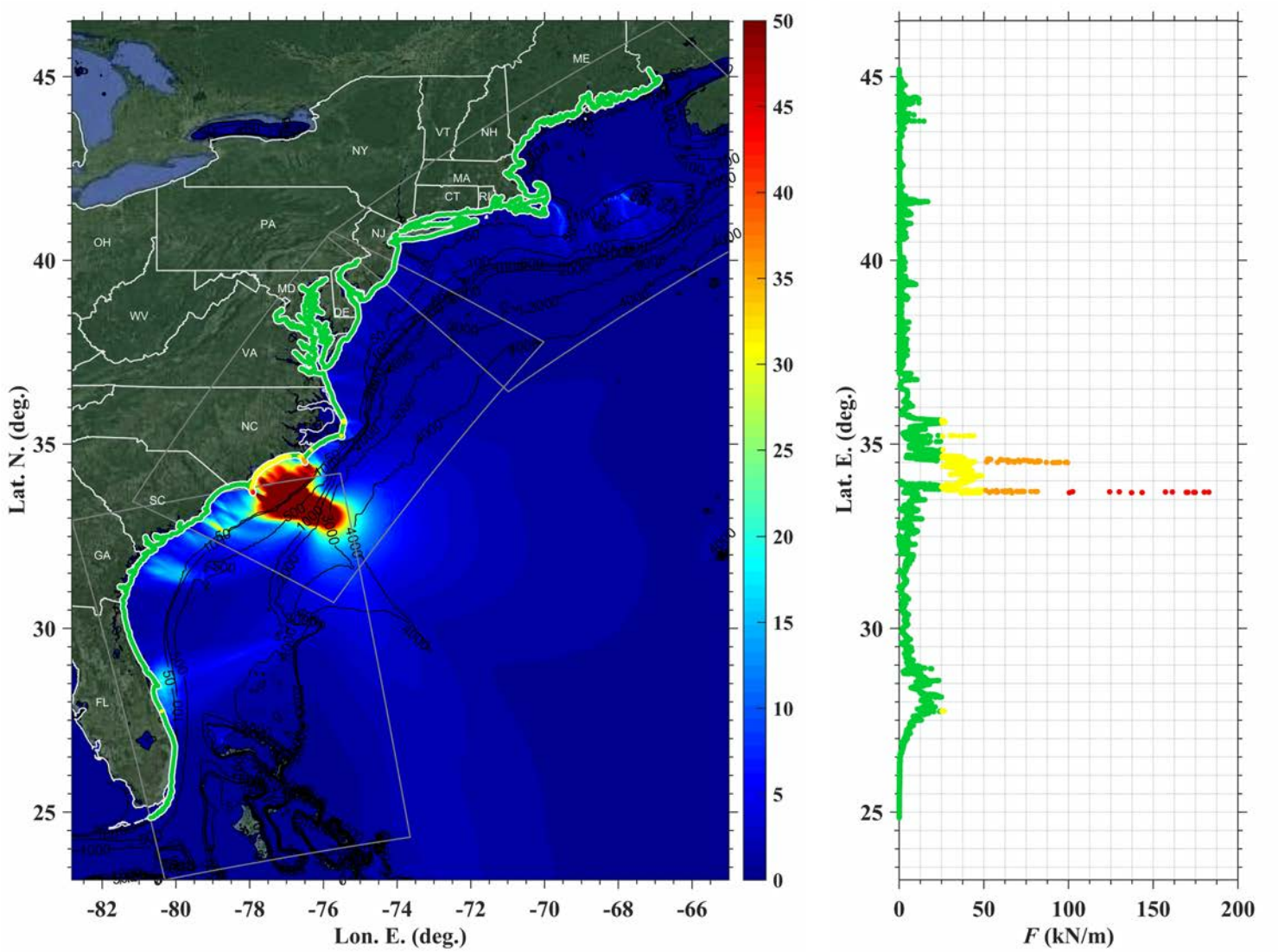

Figure 50: Maximum impulse force for Cape Fear SMF source in grid G1, G2, G3 with color-coded hazard along the 5m isobath contour. Color-coding reflects impulse force classes: below 25 kN/m (green); 25-50 kN/m (yellow); 50-100 kN/m (orange); 100-200 kN/m (red); over 200 kN/m (purple).

Great Bahama Bank 1.6 km^3 Deforming Submarine Mass Failure

Maximum Surface Elevation, Velocity, and Impulse Force

Figure 51 shows an overview of the maximum surface elevation in grid G3 computed with FUNWAVE-TVD for the Great Bahama Bank 1.6 km^3 SMF source (Figure 8a) with a simulation time of t = 30000 s (8.3 h).

The surface elevation time series at grid save points (Table 2) for this case are on the order of 0.5 mm and not included.

Figure 52, Figure 53, and Figure 54 show the maximum surface elevation, velocity, and impulse force respectively in grid G3 with values along the 5 m isobath contour plotted as a function of latitude.

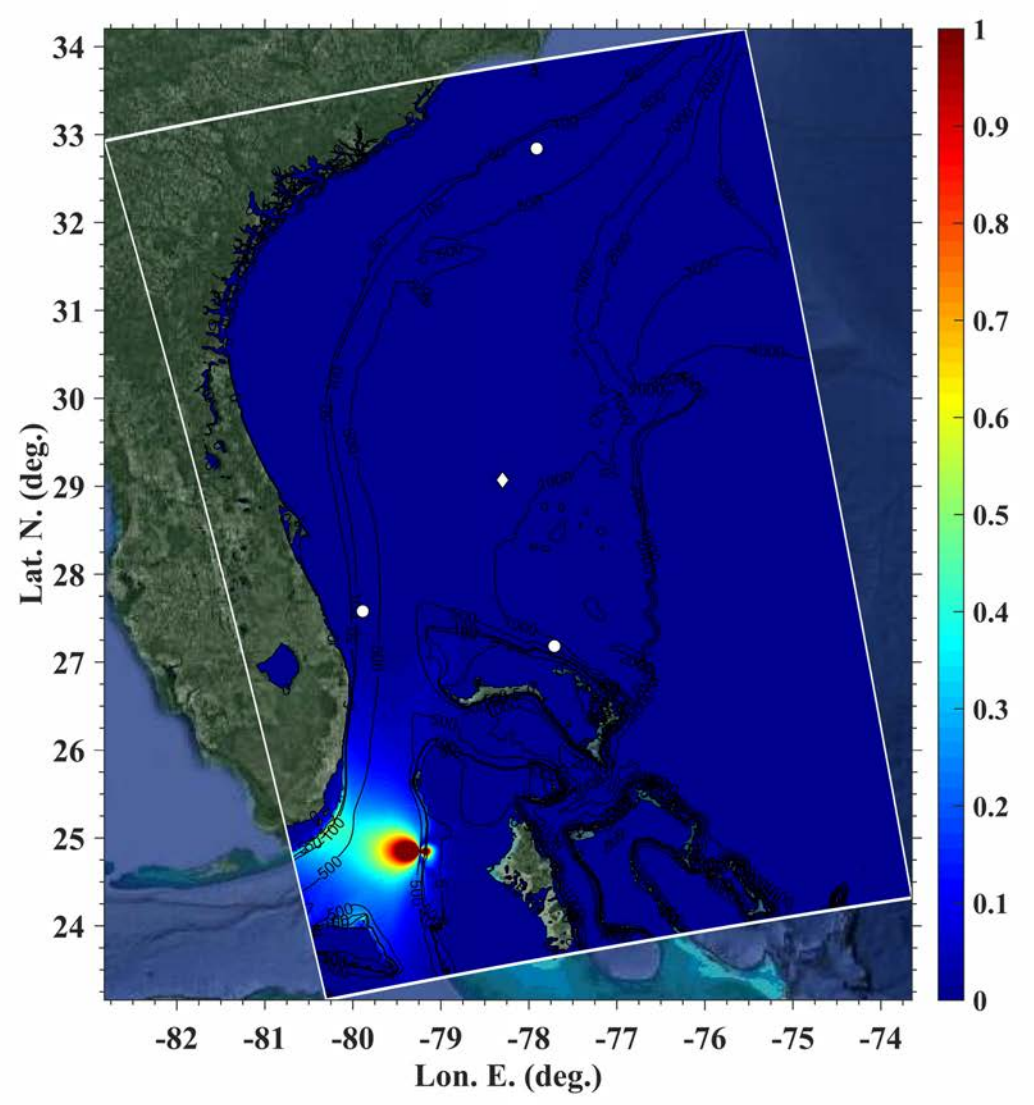

Figure 51: Maximum surface elevation for the Great Bahama Bank 1.6 km^3 SMF source

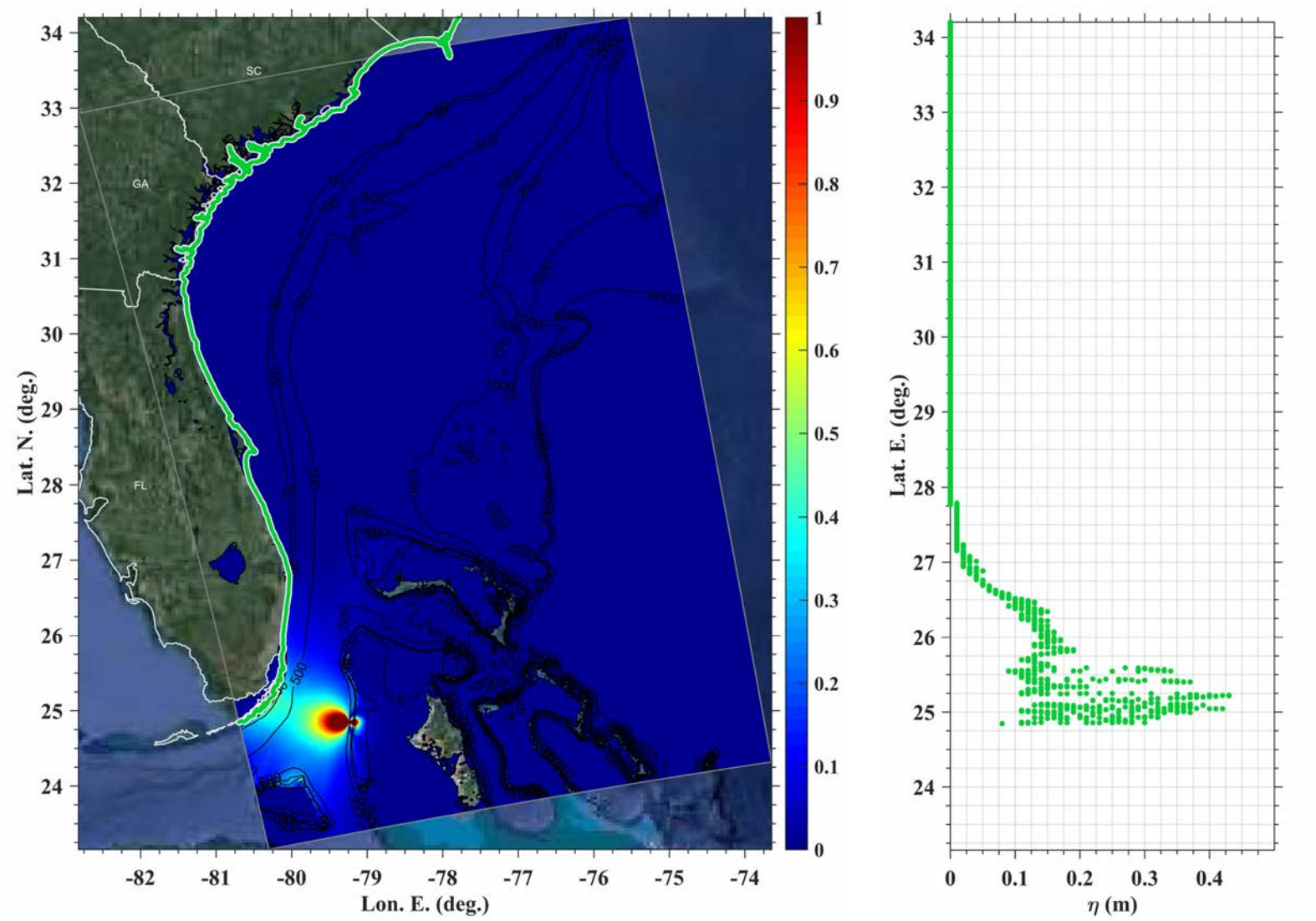

Figure 52: Maximum surface elevation for the Great Bahama Bank 1.6 km^3 SMF source in grid G1, G2, G3 with color-coded hazard along the 5m isobath contour. Color-coding reflects elevation classes: below 2 ft (green); 2-5 ft (yellow); 5-8 ft (orange); 8-11 ft (red); over 11 ft (purple).

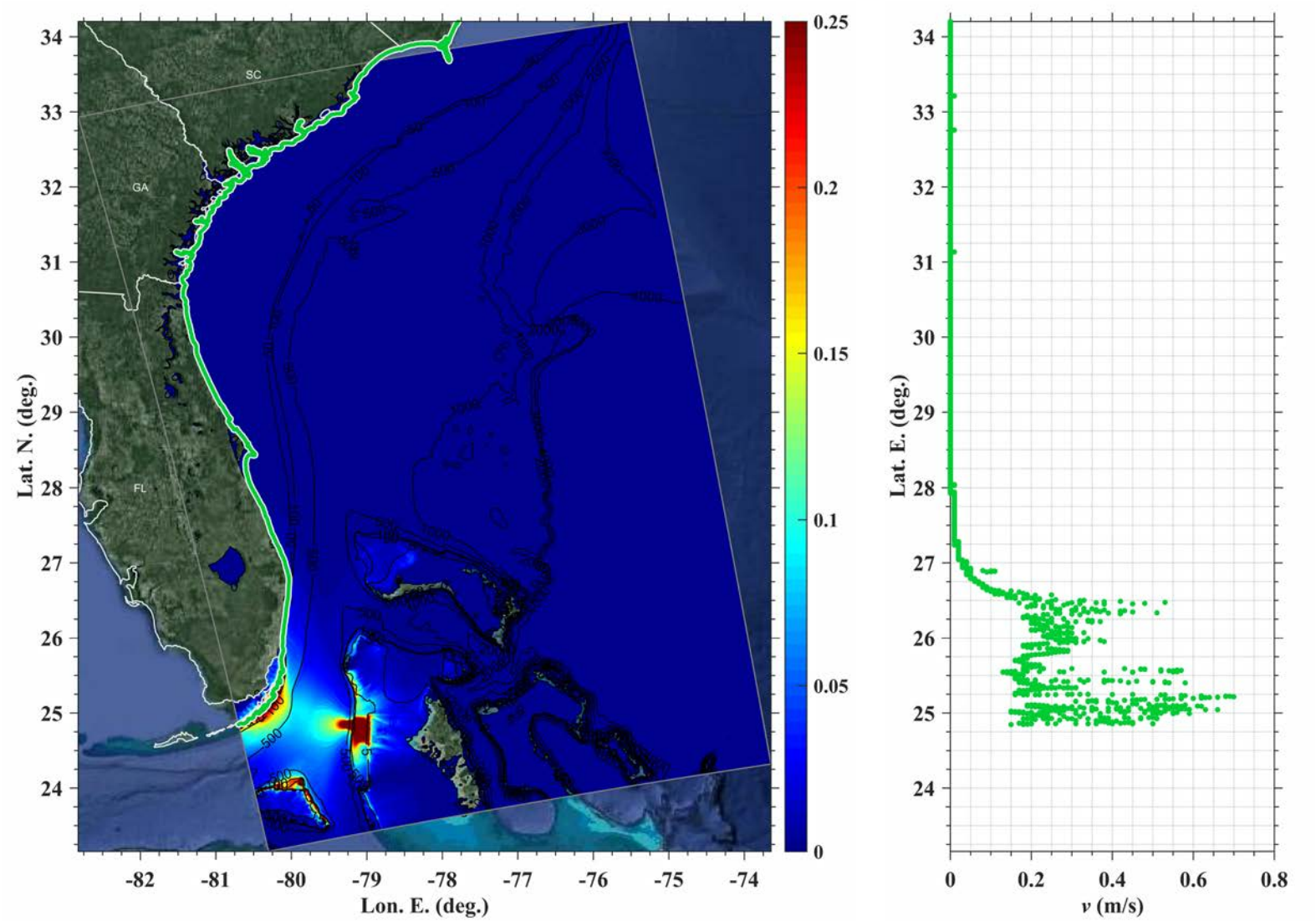

Figure 53: Maximum velocity for the Great Bahama Bank 1.6 km^3 SMF source in grid G1, G2, G3 with color-coded hazard along the 5m isobath contour. Color-coding reflects velocity classes: below 1.5 m/s (green); 1.5-3 m/s (yellow); 3-4.5 m/s (orange); 4.5-6 m/s (red); over 6 m/s (purple).

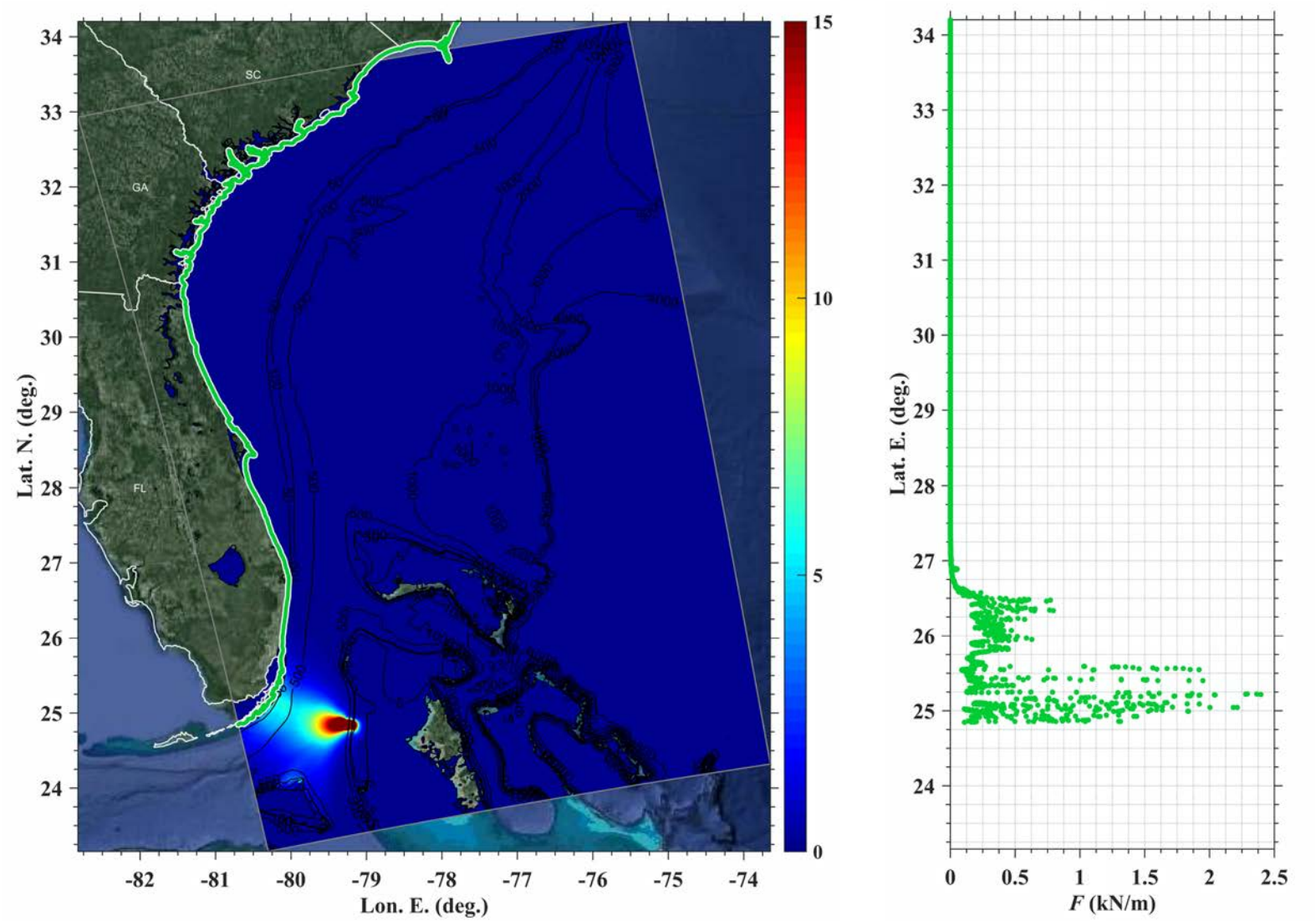

Figure 54: Maximum impulse force for Great Bahama Bank 1.6 km^3 SMF source in grid G1, G2, G3 with color-coded hazard along the 5m isobath contour. Color-coding reflects impulse force classes: below 25 kN/m (green); 25-50 kN/m (yellow); 50-100 kN/m (orange); 100-200 kN/m (red); over 200 kN/m (purple).

Great Bahama Bank 6.7 km^3 Deforming Submarine Mass Failure

Maximum Surface Elevation, Velocity, and Impulse Force

Figure 55 shows an overview of the maximum surface elevation in grid G3 computed with FUNWAVE-TVD for the Great Bahama Bank 6.7 km^3 SMF source (Figure 8b) with a simulation time of t = 30000 s (8.3 h).

The surface elevation time series at grid save points (Table 2) for this case are on the order of 0.5 mm and not included.

Figure 56, Figure 57, and Figure 58 show the maximum surface elevation, velocity, and impulse force respectively in grid G3 with values along the 5 m isobath contour plotted as a function of latitude.

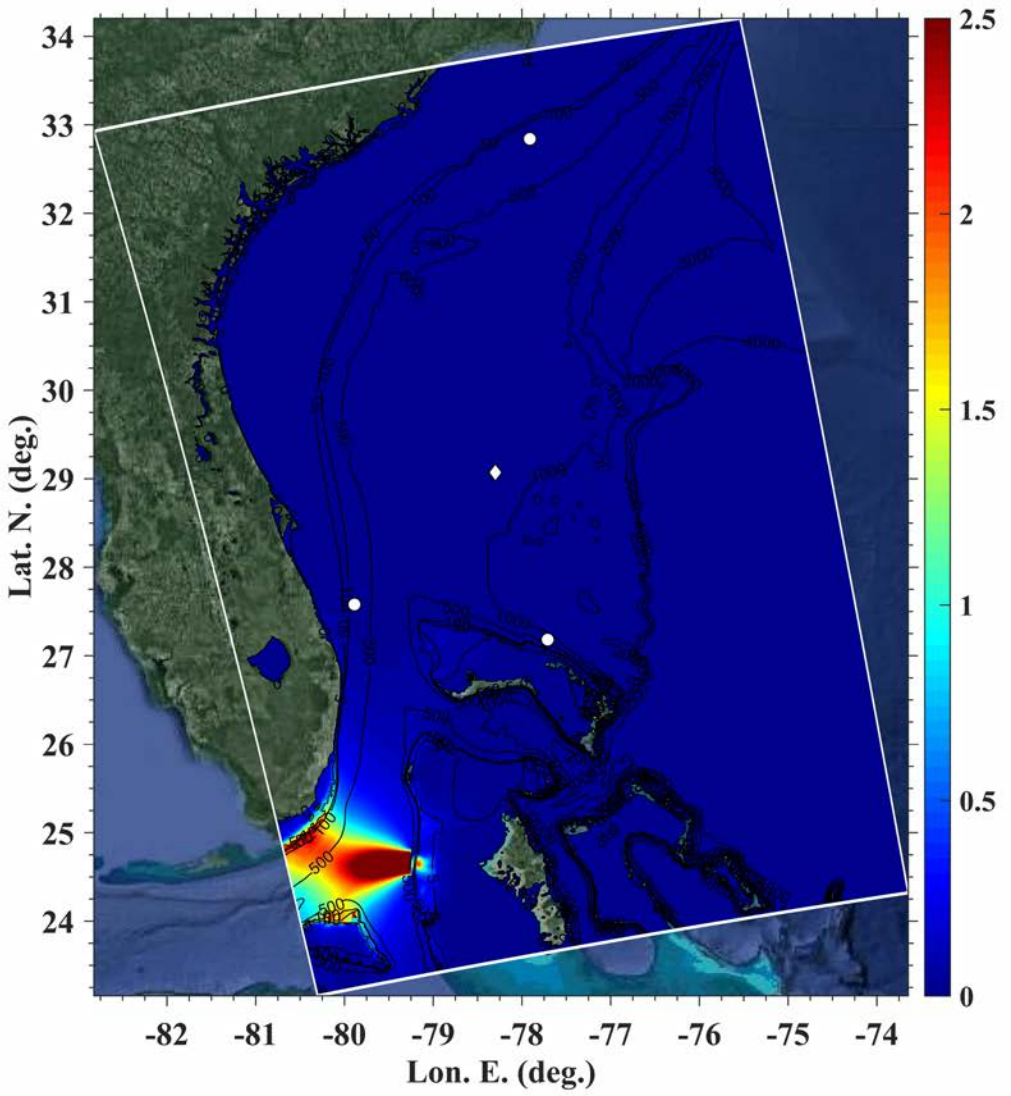

Figure 55: Maximum surface elevation for the Great Bahama Bank 6.7 km^3 SMF source

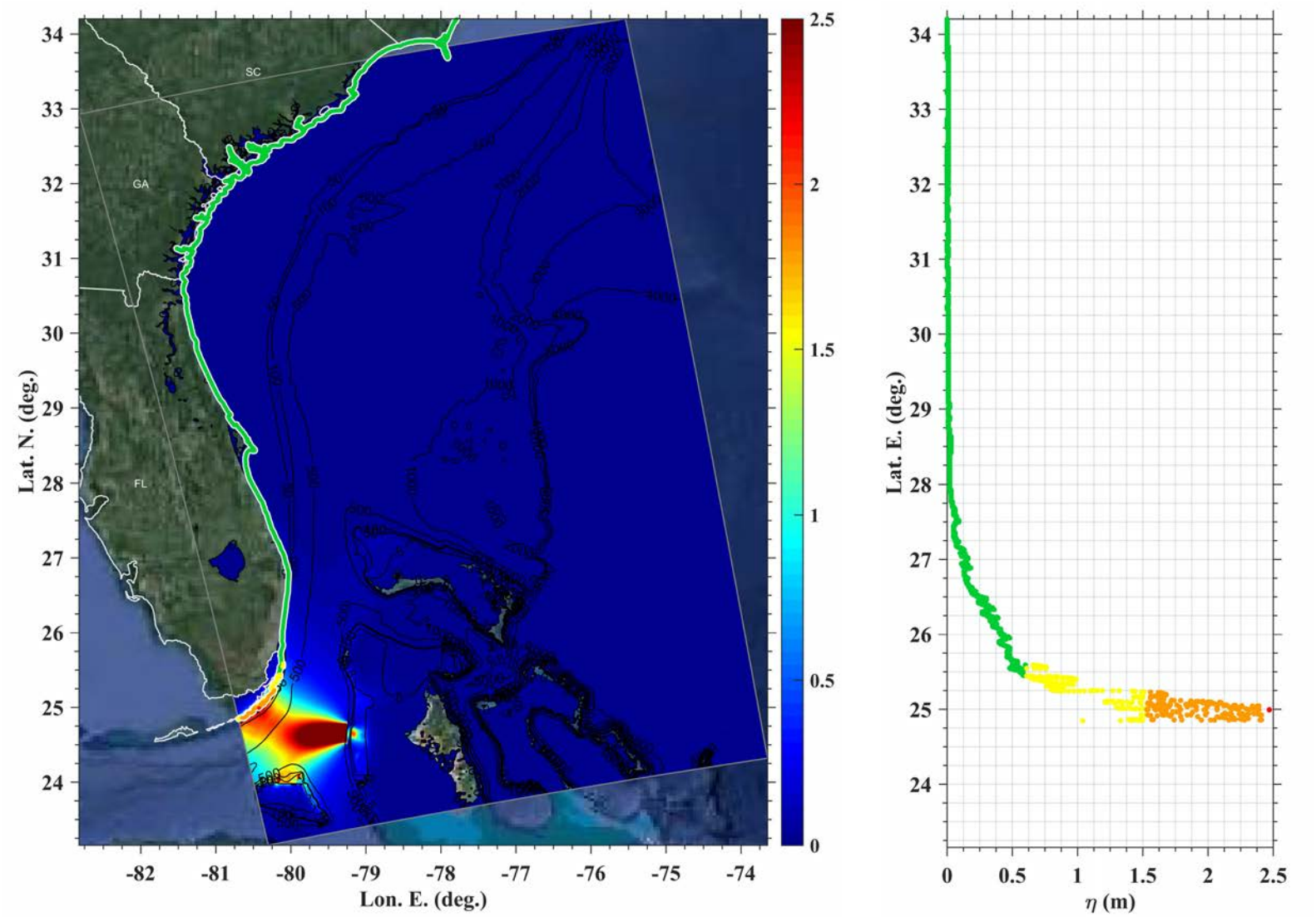

Figure 56: Maximum surface elevation for the Great Bahama Bank 6.7 km^3 SMF source in grid G1, G2, G3 with color-coded hazard along the 5m isobath contour. Color-coding reflects elevation classes: below 2 ft (green); 2-5 ft (yellow); 5-8 ft (orange); 8-11 ft (red); over 11 ft (purple).

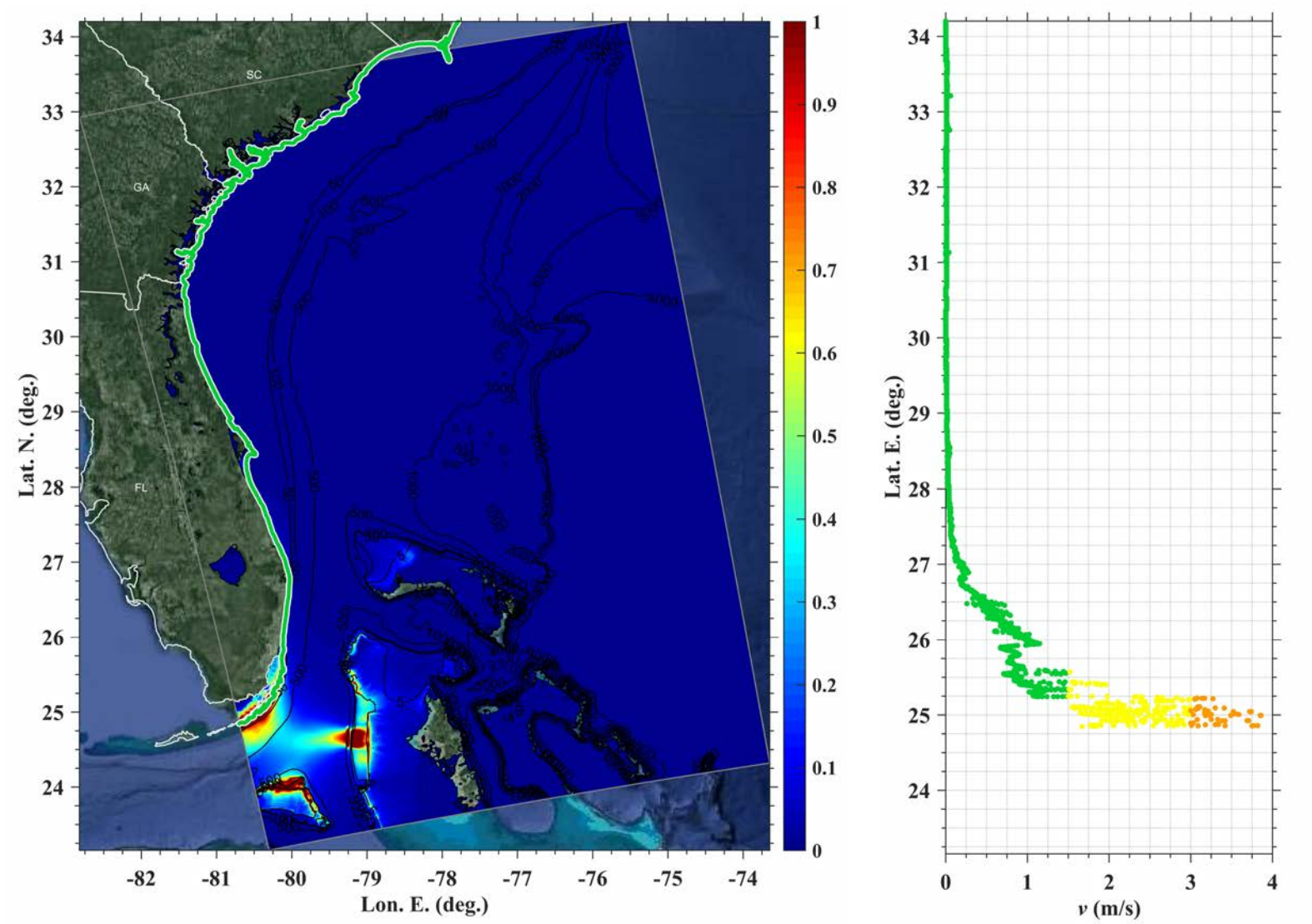

Figure 57: Maximum velocity for the Great Bahama Bank 6.7 km^3 SMF source in grid G1, G2, G3 with color-coded hazard along the 5m isobath contour. Color-coding reflects velocity classes: below 1.5 m/s (green); 1.5-3 m/s (yellow); 3-4.5 m/s (orange); 4.5-6 m/s (red); over 6 m/s (purple).

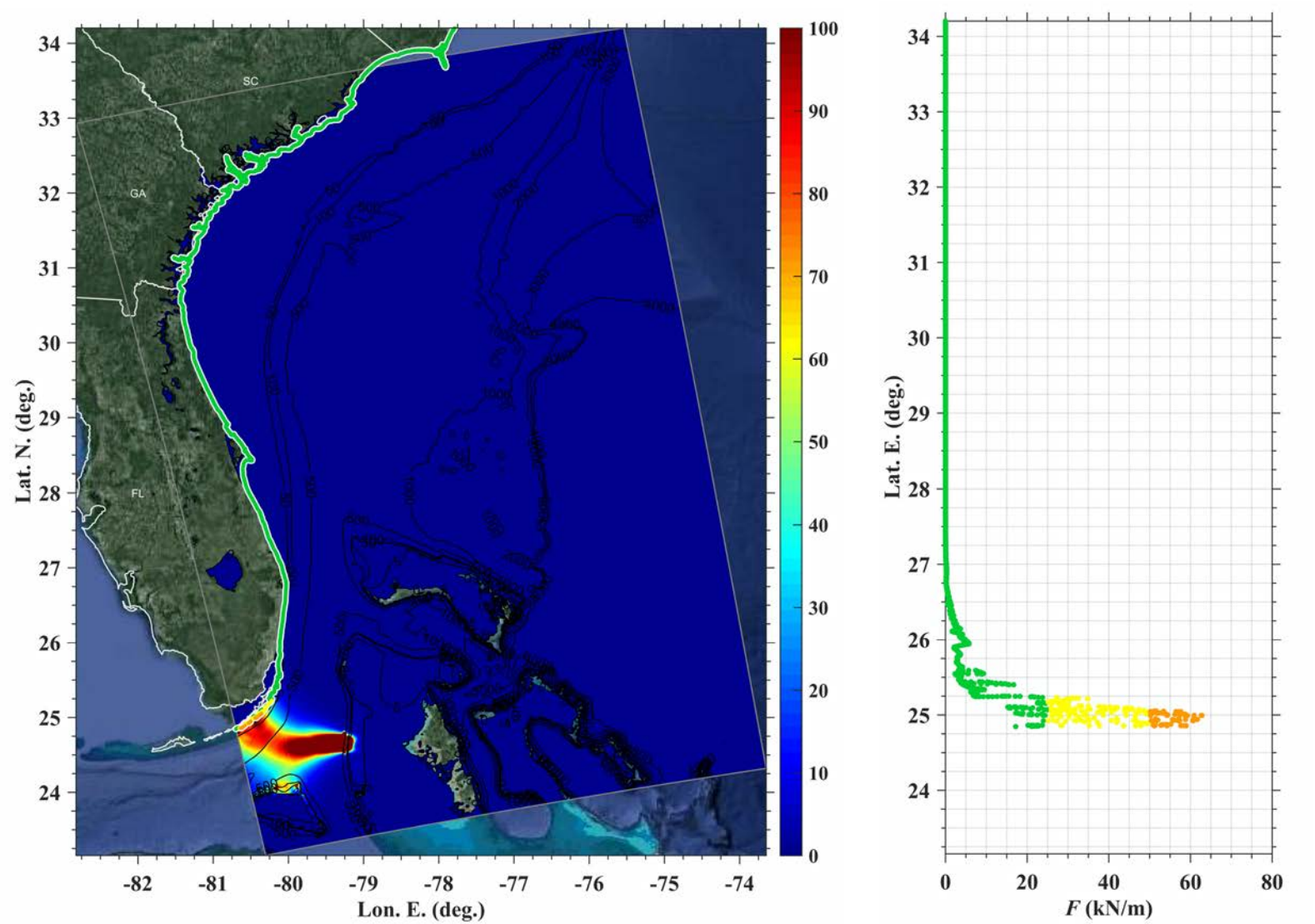

Figure 58: Maximum impulse force for Great Bahama Bank 6.7 km^3 SMF source in grid G1, G2, G3 with color-coded hazard along the 5m isobath contour. Color-coding reflects impulse force classes: below 25 kN/m (green); 25-50 kN/m (yellow); 50-100 kN/m (orange); 100-200 kN/m (red); over 200 kN/m (purple).

Cumbre Vieja 80 km^3 Volcanic Flank Collapse

Maximum Surface Elevation, Velocity, and Impulse Force

Figure 59 shows an overview of the maximum surface elevation in grids Local G0, G1, G2, and G3 computed with FUNWAVE-TVD for the Cumbre Vieja 80 km^3 volcanic flank collapse source (Figure 9a) with a simulation time of t = 86400 s (24 h).

Figure 60 shows the surface elevation time series at the grid save points (Table 2).

Figure 61, Figure 62, and Figure 63 show the maximum surface elevation, velocity, and impulse force respectively in grid G1, G2, and G3 with values along the 5 m isobath contour (calculated in G1-G3) plotted as a function of latitude.

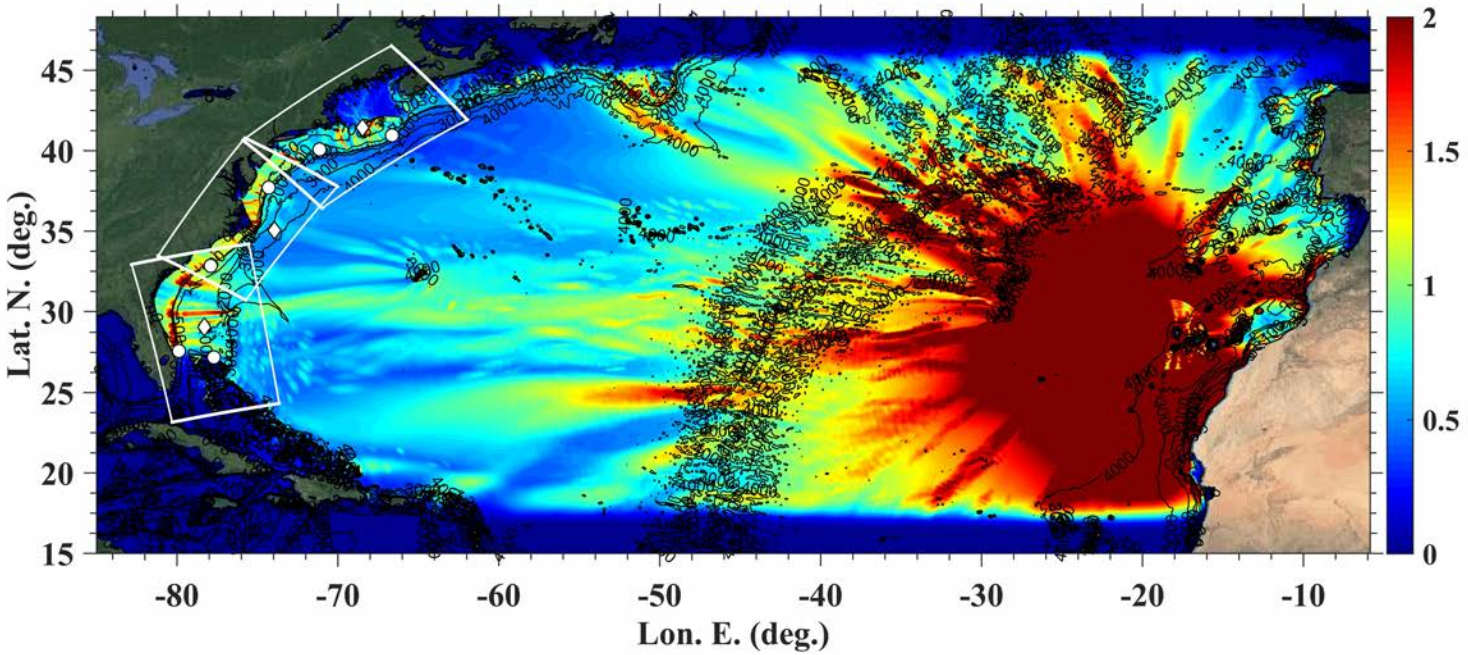

Figure 59: Maximum surface elevation for Cumbre Vieja 80 km^3 volcanic flank collapse source

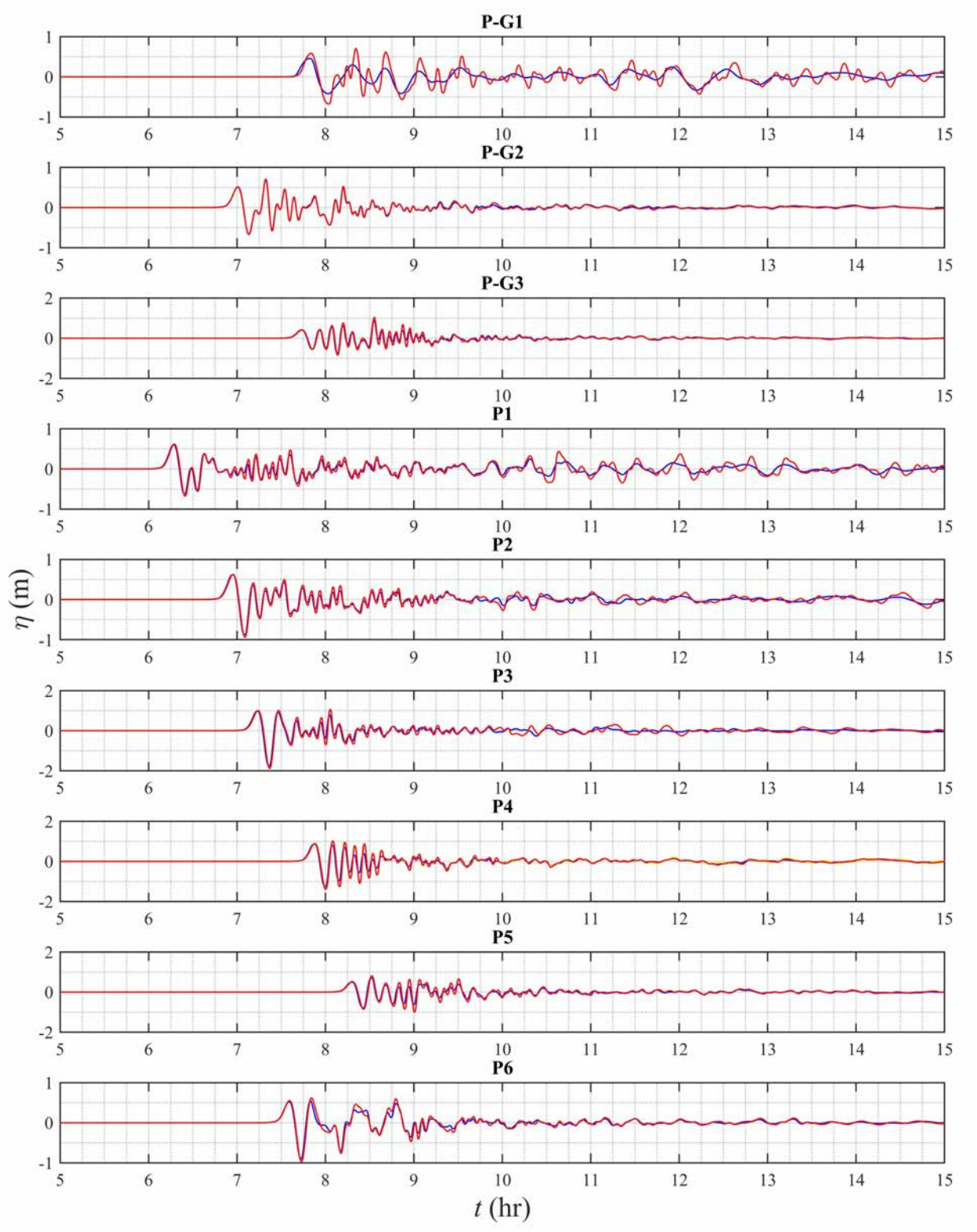

Figure 60: Tsunami wave time series at grid save points. Blue indicates surface elevation computed in grid Local G0, red indicates surface elevation computed in nested grids G1-G3. For point P4, yellow indicates surface elevation computed in G2, red indicates surface elevation computed in G3.

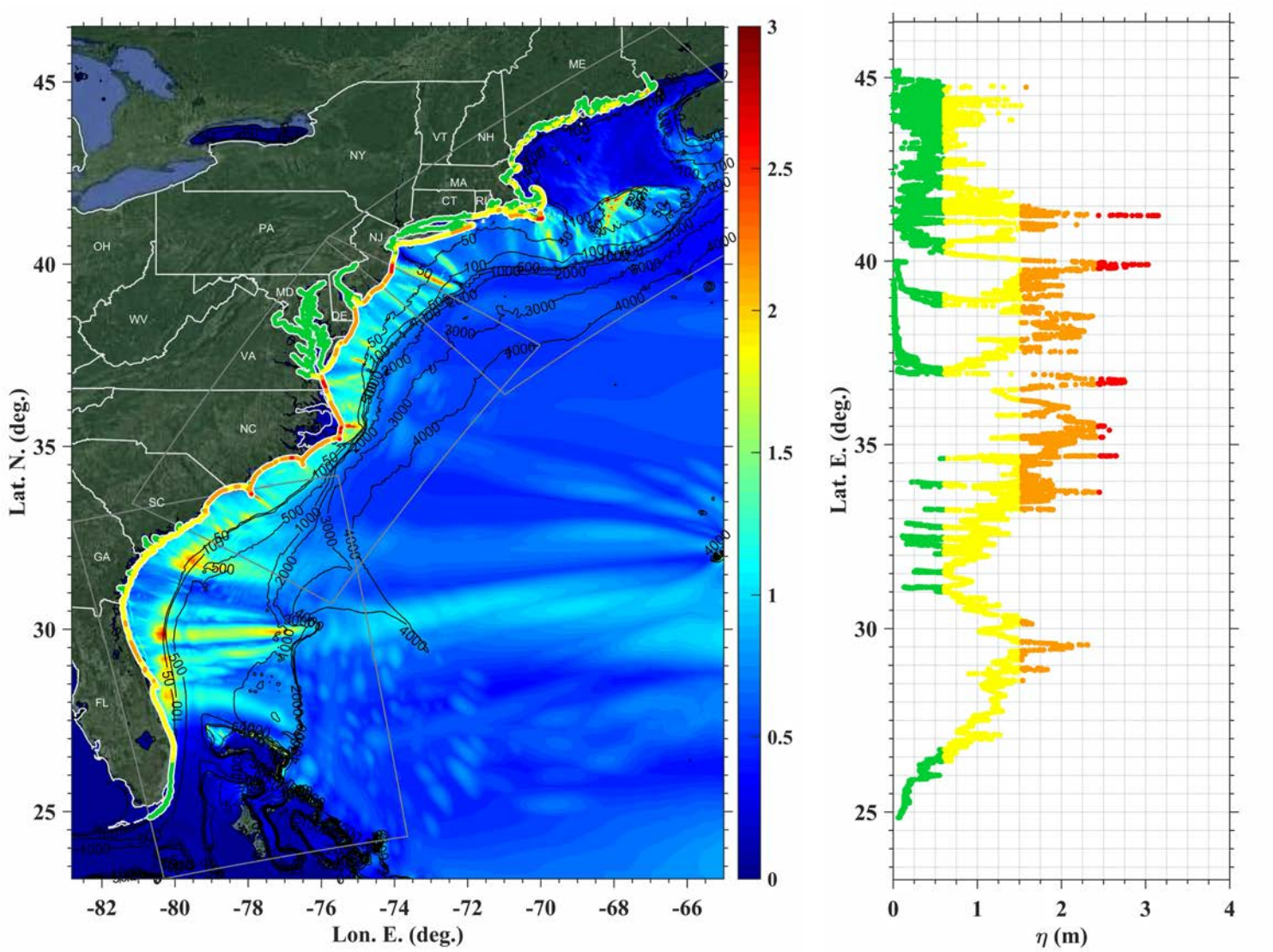

Figure 61: Maximum surface elevation for the Cumbre Vieja 80 km^3 volcanic flank collapse source in grid G1, G2, G3 with color-coded hazard along the 5m isobath contour. Color-coding reflects elevation classes: below 2 ft (green); 2-5 ft (yellow); 5-8 ft (orange); 8-11 ft (red); over 11 ft (purple).

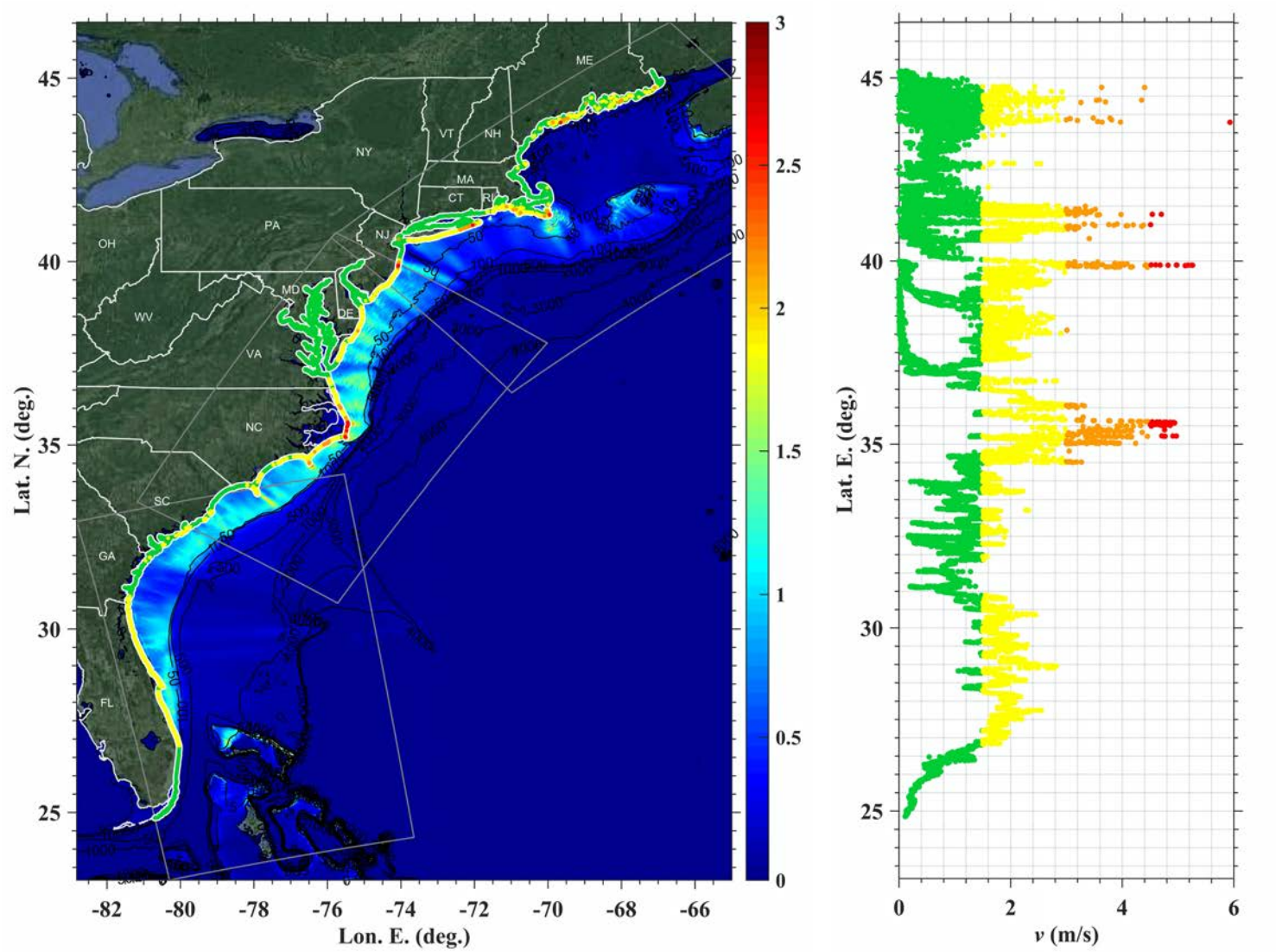

Figure 62: Maximum velocity for the Cumbre Vieja 80 km^3 volcanic flank collapse source in grid G1, G2, G3 with color-coded hazard along the 5m isobath contour. Color-coding reflects velocity classes: below 1.5 m/s (green); 1.5-3 m/s (yellow); 3-4.5 m/s (orange); 4.5-6 m/s (red); over 6 m/s (purple).

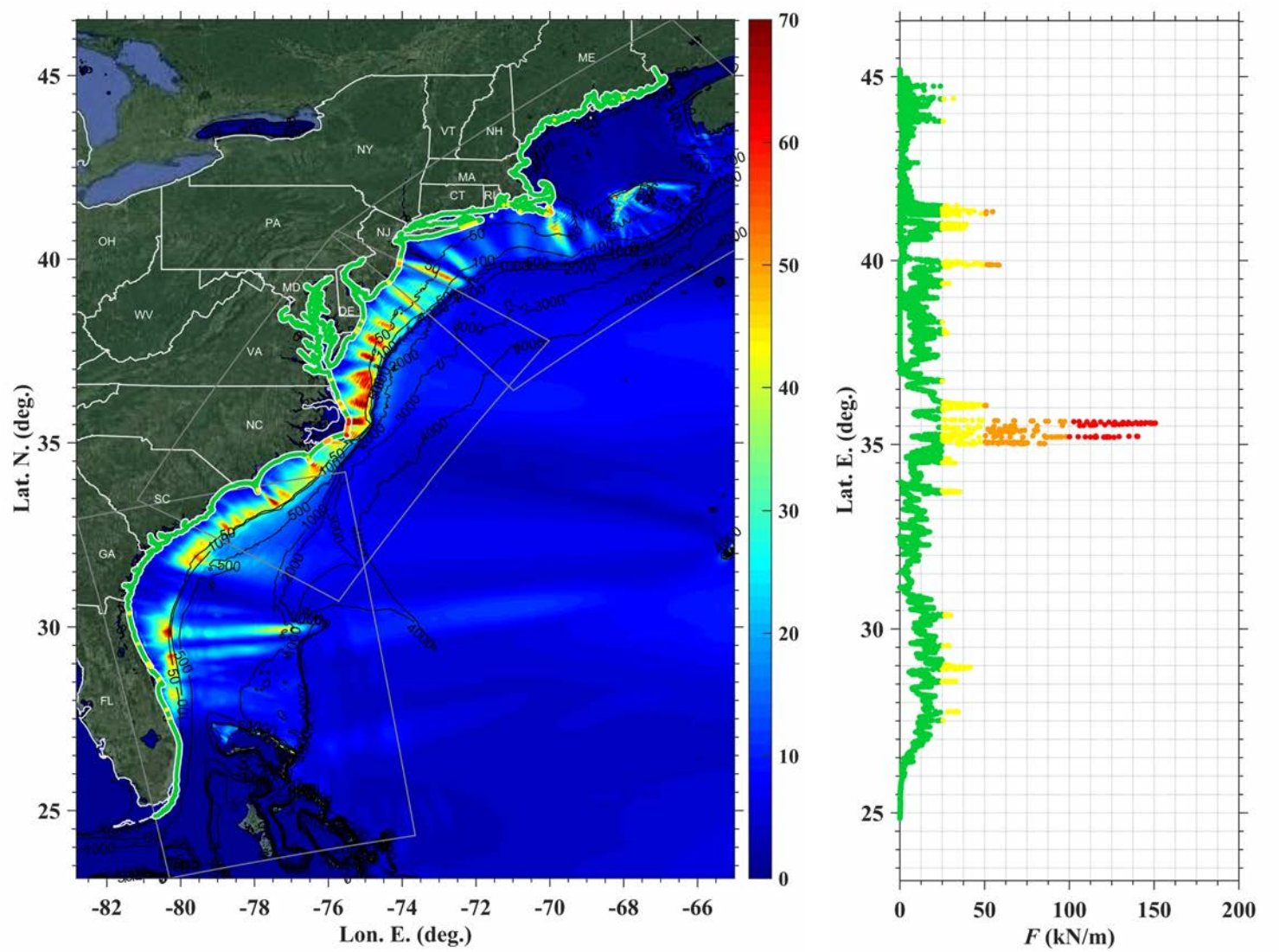

Figure 63: Maximum impulse force for the Cumbre Vieja 80 km^3 volcanic flank collapse source in grid G1, G2, G3 with color-coded hazard along the 5m isobath contour. Color-coding reflects impulse force classes: below 25 kN/m (green); 25-50 kN/m (yellow); 50-100 kN/m (orange); 100-200 kN/m (red); over 200 kN/m (purple).

Cumbre Vieja 450 km^3 Volcanic Flank Collapse

Maximum Surface Elevation, Velocity, and Impulse Force

Figure 64 shows an overview of the maximum surface elevation in grids Local G0, G1, G2, and G3 computed with FUNWAVE-TVD for the Cumbre Vieja 80 km^3 volcanic flank collapse source (Figure 9b) with a simulation time of t = 86400 s (24 h).

Figure 65 shows the surface elevation time series at the grid save points (Table 2).

Figure 66, Figure 67, and Figure 68 show the maximum surface elevation, velocity, and impulse force respectively in grid G1, G2, and G3 with values along the 5 m isobath contour (calculated in G1-G3) plotted as a function of latitude.

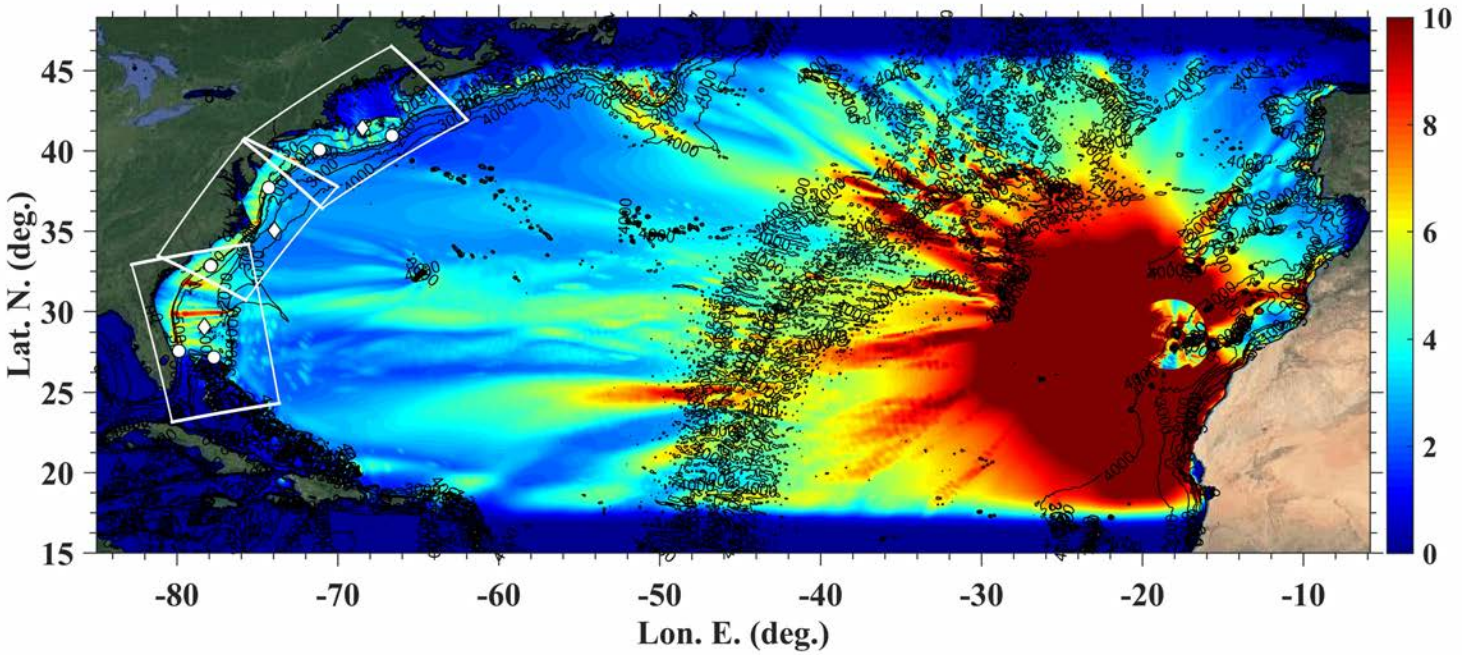

Figure 64: Maximum surface elevation for Cumbre Vieja 450 km^3 volcanic flank collapse source

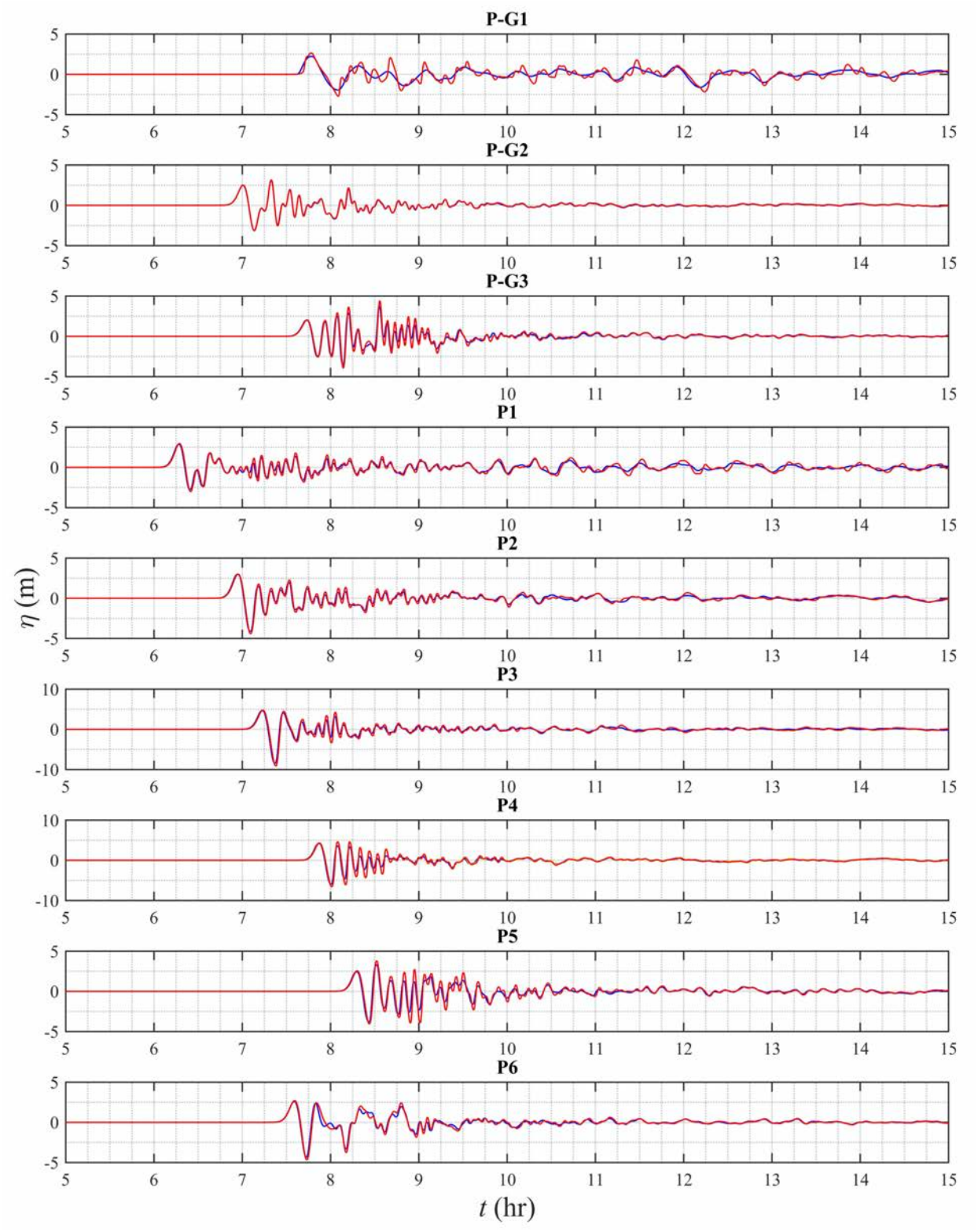

Figure 65: Tsunami wave time series at grid save points. Blue indicates surface elevation computed in grid Local G0, red indicates surface elevation computed in nested grids G1-G3. For point P4, yellow indicates surface elevation computed in G2, red indicates surface elevation computed in G3.

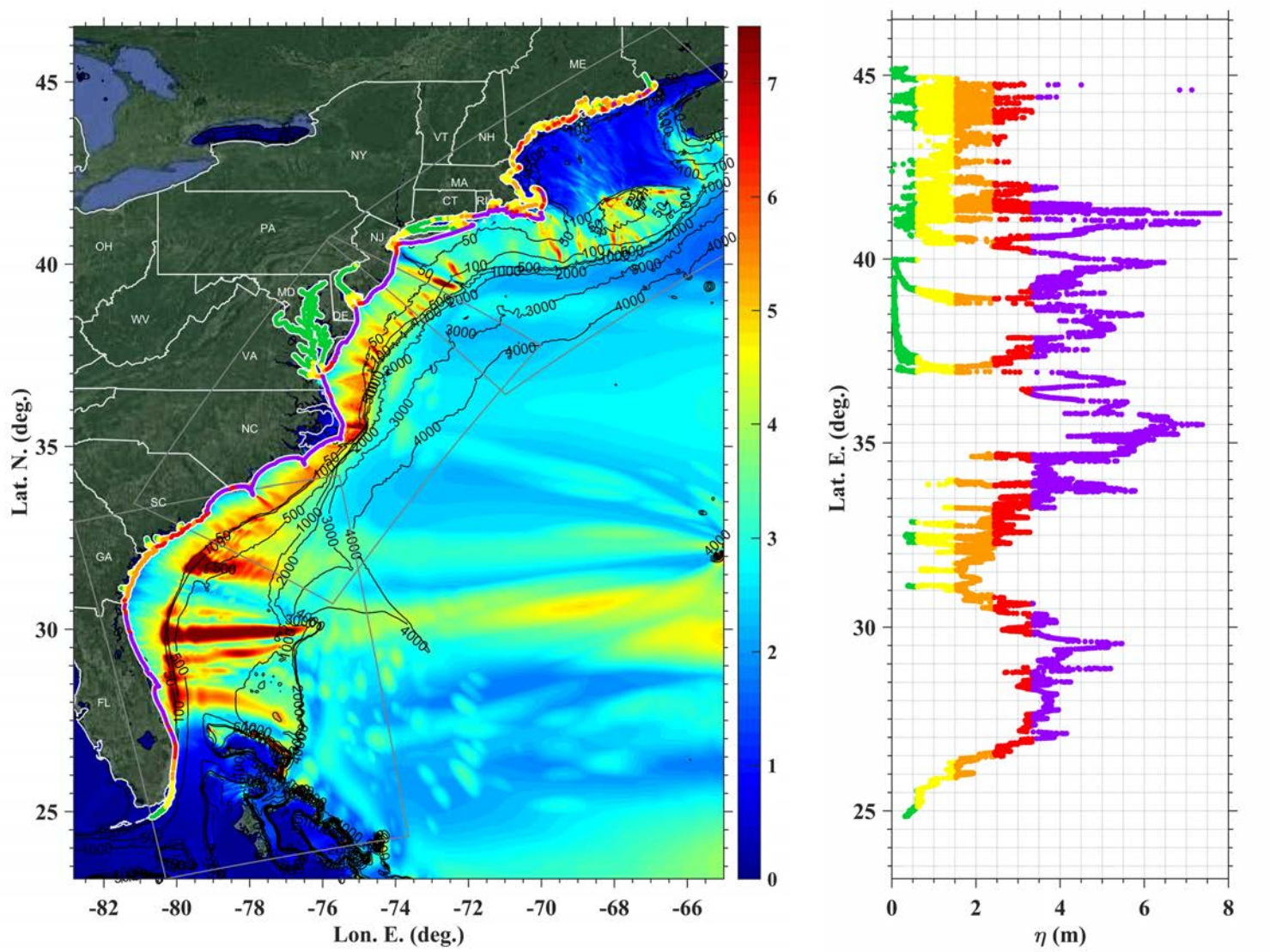

Figure 66: Maximum surface elevation for the Cumbre Vieja 450 km^3 volcanic flank collapse source in grid G1, G2, G3 with color-coded hazard along the 5m isobath contour. Color-coding reflects elevation classes: below 2 ft (green); 2-5 ft (yellow); 5-8 ft (orange); 8-11 ft (red); over 11 ft (purple).

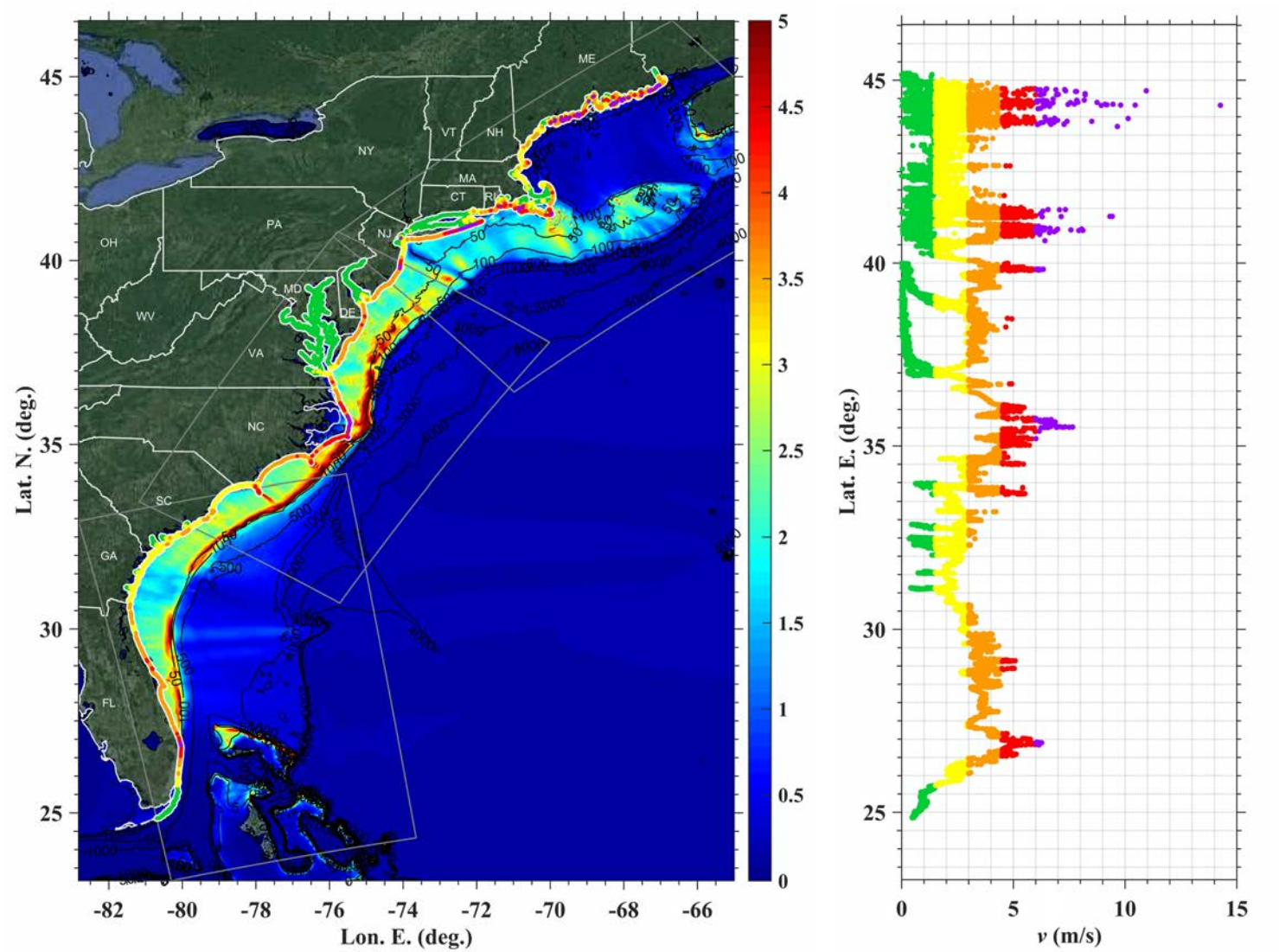

Figure 67: Maximum velocity for the Cumbre Vieja 450 km^3 volcanic flank collapse source in grid G1, G2, G3 with color-coded hazard along the 5m isobath contour. Color-coding reflects velocity classes: below 1.5 m/s (green); 1.5-3 m/s (yellow); 3-4.5 m/s (orange); 4.5-6 m/s (red); over 6 m/s (purple).

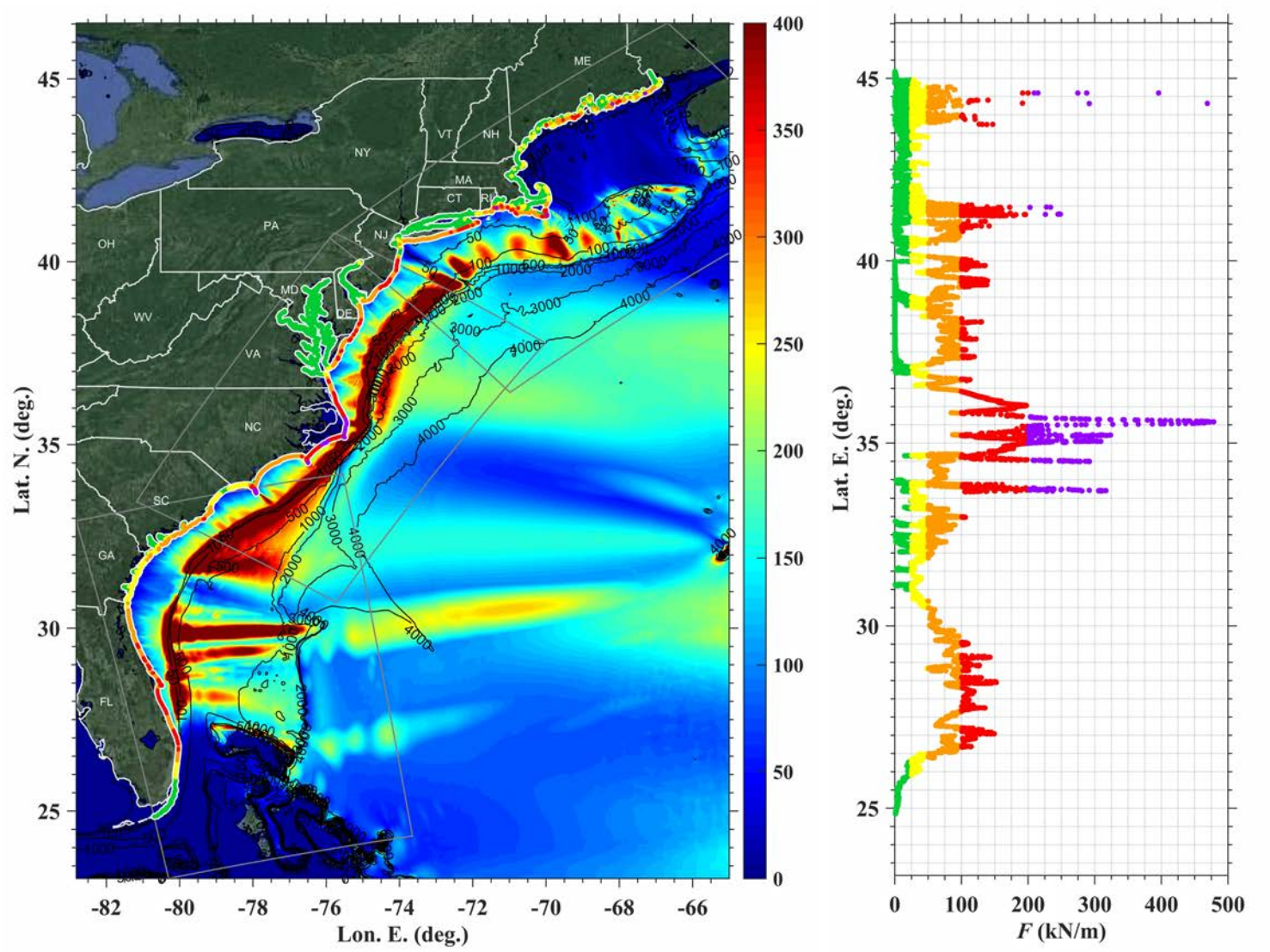

Figure 68: Maximum impulse force for the Cumbre Vieja 450 km^3 volcanic flank collapse source in grid G1, G2, G3 with color-coded hazard along the 5m isobath contour. Color-coding reflects impulse force classes: below 25 kN/m (green); 25-50 kN/m (yellow); 50-100 kN/m (orange); 100-200 kN/m (red); over 200 kN/m (purple).

Combined Tsunami Hazard to the USEC

Maximum Surface Elevation, Velocity, and Impulse Force

Figure 69, Figure 70, and Figure 71 show the combined maximum surface elevation, velocity, and impulse force respectively, for all tsunami sources except the extreme Cumbre Vieja 450 km^3 volcanic flank collapse case, in grids G0, G1, G2, and G3 with values along the 5 m isobath contour (calculated in G1-G3) plotted as a function of latitude.

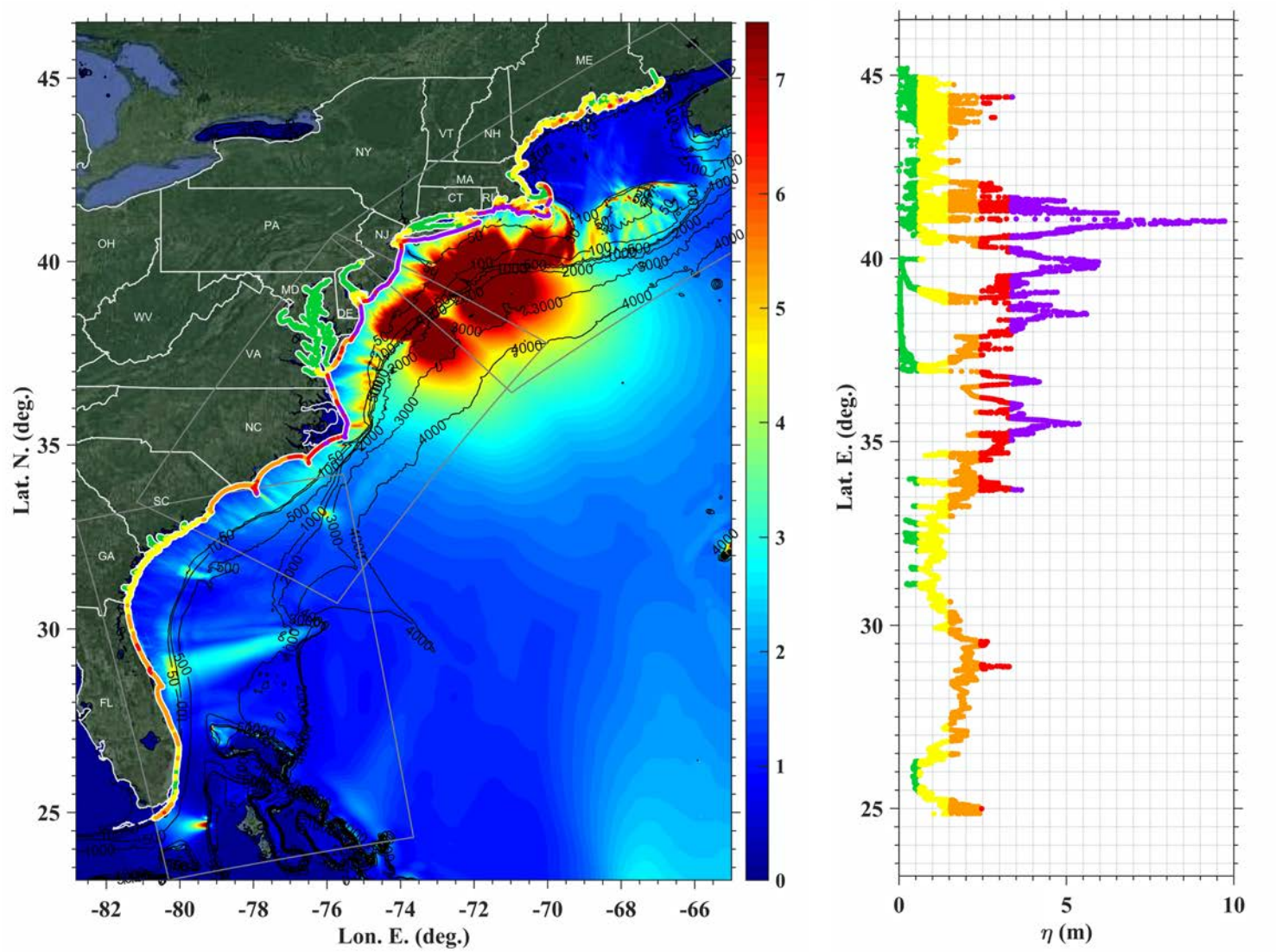

Figure 69: Maximum surface elevation for all sources in grid G1, G2, G3 with color-coded hazard along the 5m isobath contour. Color-coding reflects elevation classes: below 2 ft (green); 2-5 ft (yellow); 5-8 ft (orange); 8-11 ft (red); over 11 ft (purple).

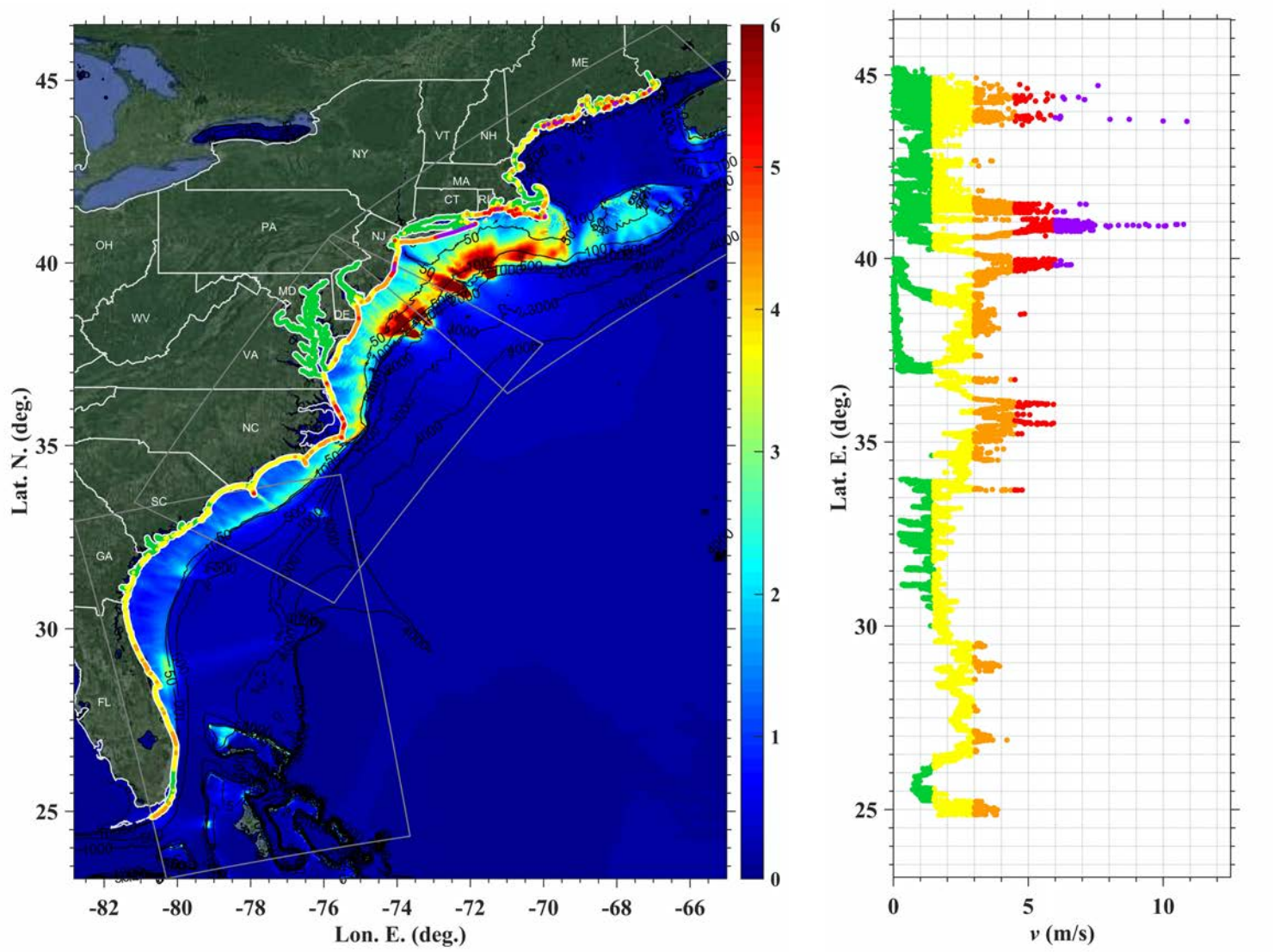

Figure 70: Maximum velocity for all sources in grid G1, G2, G3 with color-coded hazard along the 5m isobath contour. Color-coding reflects velocity classes: below 1.5 m/s (green); 1.5-3 m/s (yellow); 3-4.5 m/s (orange); 4.5-6 m/s (red); over 6 m/s (purple).

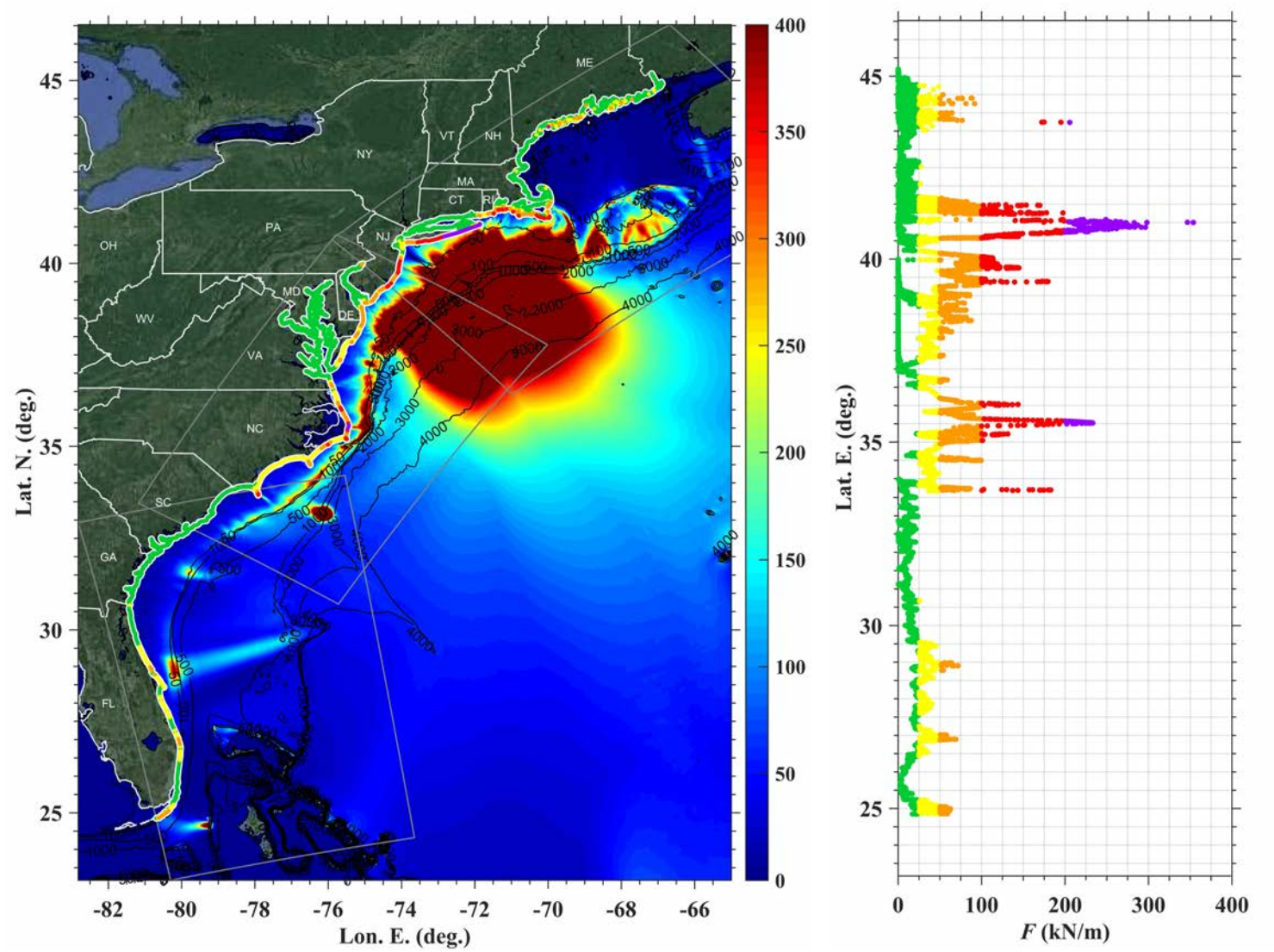

Figure 71: Maximum impulse force for the all sources in grid G1, G2, G3 with color-coded hazard along the 5m isobath contour. Color-coding reflects impulse force classes: below 25 kN/m (green); 25-50 kN/m (yellow); 50-100 kN/m (orange); 100-200 kN/m (red); over 200 kN/m (purple).

Supplementary Material

Result maps, contour points and values, and animations are provided in a Google drive that can be accessed at:

https://drive.google.com/drive/u/1/folders/0AG0VD9vWrfxBUk9PVA

Raw simulation files are provided in a Google drive that can be accessed at:

https://drive.google.com/drive/u/1/folders/0AGS8b6c6SHtZUk9PVA

References

Abadie, S., Gandon, C., Grilli, S.T., Fabre, R., Riss, J., Tric, E., Morichon, D., and S. Glockner 2009. 3D Numerical Simulations of Waves Generated by Subaerial Mass Failures. Application to La Palma Case. *Proc. 31st Intl. Coastal Engng. Conf.*, 1384-1395.

Abadie, S., Morichon, D., Grilli, S.T., and S. Glockner 2010. Numerical simulation of waves generated by landslides using a multiple-fluid Navier-Stokes model. *Coastal Engng.*, **57**, 779-794.

Abadie, S., J.C. Harris, S.T. Grilli and R. Fabre 2012. Numerical modeling of tsunami waves generated by the flank collapse of the Cumbre Vieja Volcano (La Palma, Canary Islands): tsunami source and near field effects. *J. Geophys. Res.*, **117**, C05030, doi:10.1029/2011JC007646

Barkan R., ten Brink U.S., and Lin J. 2009. Far Field tsunami simulations of the 1755 Lisbon earthquake: Implication for tsunami hazard to the U.S. East Coast and the Caribbean. *Marine Geology*, **264**, 109-122.

Chaytor, J. D., ten Brink, U. S., Solow, A. R. and Andrews, B. D. 2009. Size distribution of submarine landslides along the US Atlantic margin. *Marine Geology,* **264**(12), 16–27.

Enet F, and ST Grilli 2007. Experimental Study of Tsunami Generation by Three-Dimensional Rigid Underwater Landslides. *J. Waterway, Port, Coastal, Ocean Eng.,* **133**(6), 442-454. doi: 10.1061/(ASCE)0733-950X(2007)133:6(442).

Eggeling T 2012. *Analysis of earthquake triggered submarine landslides at gourd locations along the U.S. east coast*. Masters Thesis. University of Rhode Island.

Geist, E. L., Lynett, P. J., and Chaytor, J. D. 2009. Hydrodynamic modeling of tsunamis from the Currituck landslide. *Marine Geology*, **264**(1-2), 41-52.

Geist, E.L. and Lynett, P.J. 2014. Source processes for the probabilistic assessment of tsunami hazards. *Oceanography*, **27**(2), 86-93.

Geist, E.L., Uri, S. and Gove, M., 2014. A framework for the probabilistic analysis of meteotsunamis. In *Meteorological Tsunamis*: *The US East Coast and Other Coastal Regions* (pp. 123-142). Springer, Cham.

Gica, E., Spillane, M.C., Titov, V.V., Chamberlin, C.D., and J. Newman, 2008. Development of the forecast propagation database for NOAAs Short-Term Inundation Forecast for Tsunamis. NOAA Tech. Memo. OAR PMEL-139.

Grilli ST and P Watts 1999. Modeling of waves generated by a moving submerged body. Applications to underwater landslides. *Engng Analys Boundary Elements,* **23**, 645-656.

Grilli ST and P Watts 2005. Tsunami Generation by Submarine Mass Failure. I: Modeling, Experimental Validation, and Sensitivity Analyses. *J. Waterway, Port, Coastal, Ocean Eng.* **131**(6), 283-297. Doi:10.1061/(ASCE)0733-950X(2005)131:6(283).

Grilli A.R. and S.T. Grilli, 2013a. Modeling of tsunami generation, propagation and regional impact along the upper U.S east coast from the Puerto Rico trench. Research Report no. CACR-13-02. NTHMP Award, #NA10NWS4670010, National Weather Service Program Office, 18 pps. http://personal.egr.uri.edu/grilli/grilli-grilli-cacr-13-02

Grilli A.R. and S.T. Grilli, 2013b. Far-Field tsunami impact on the U.S. East Coast from an extreme flank collapse of the Cumbre Vieja Volcano (Canary Island). Research Report no. CACR-13-03. NTHMP Award, #NA10NWS4670010, National Weather Service Program Office, 13 pps. http://personal.egr.uri.edu/grilli/grilli-grilli-cacr-13-03

Grilli A.R. and S.T. Grilli, 2013c. Modeling of tsunami generation, propagation and regional impact along the U.S. East Coast from the Azores Convergence Zone. Research Report no. CACR-13-04. NTHMP Award, #NA10NWS4670010, National Weather Service Program Office, 20 pps. http://personal.egr.uri.edu/grilli/grilli-grilli-cacr-13-04

Grilli, S.T., Taylor, O.-D. S., Baxter, D.P. and S. Maretzki 2009. Probabilistic approach for determining submarine landslide tsunami hazard along the upper East Coast of the United States. *Marine Geology*, **264**(1-2), 74-97, doi:10.1016/j.margeo.2009.02.010.

Grilli, S.T., S. Dubosq, N. Pophet, Y. Pérignon, J.T. Kirby and F. Shi 2010. Numerical simulation and first-order hazard analysis of large co-seismic tsunamis generated in the Puerto Rico trench: near-field impact on the North shore of Puerto Rico and far-field impact on the US East Coast. *Natural Hazards and Earth System Sciences*, **10**, 2109-2125, doi:10.5194/nhess-2109-2010.

Grilli, S.T., O'Reilly, C., and T. Tajalli-Bakhsh 2013d. Modeling of SMF tsunami generation and regional impact along the Upper U.S. East Coast. Research Report no. CACR-13-05. NTHMP Award, #NA10NWS4670010, National Weather Service Program Office, 46 pps. http://personal.egr.uri.edu/grilli/grilli-grilli-cacr-13-05°.

Grilli S.T., O'Reilly C., Harris J.C., Tajalli-Bakhsh T., Tehranirad B., Banihashemi S., Kirby J.T., Baxter C.D.P., Eggeling T., Ma G. and F. Shi 2015. Modeling of SMF tsunami hazard along the upper US East Coast: Detailed impact around Ocean City, MD. *Natural Hazards*, **76**(2), 705-746, doi: 10.1007/s11069-014-1522-8

Grilli, S.T., Grilli A.R., David, E. and C. Coulet 2016. Tsunami Hazard Assessment along the North Shore of Hispaniola from far- and near-field Atlantic sources. *Natural Hazards*, **82**(2), 777-810, doi: 10.1007/s11069-016-2218-z

Grilli, S.T., Shelby, M., Kimmoun, O., Dupont, G., Nicolsky, D., Ma, G., Kirby, J. and F. Shi 2017a. Modeling coastal tsunami hazard from submarine mass failures: effect of slide rheology, experimental validation, and case studies off the US East coast. *Natural Hazards*, **86**(1), 353-391, doi:10.1007/s11069-016-2692-3

Grilli, S.T., Grilli, A.R., Tehranirad, B. and J.T. Kirby 2017b. Modeling tsunami sources and their propagation in the Atlantic Ocean for coastal tsunami hazard assessment and inundation mapping along the US East Coast. In *Proc. Coastal Structures and Solutions to Coastal Disasters* 2015 : Tsunamis(Boston, USA. September 9-11, 2015), American Soc. Civil Eng., pps. 1-12

Grilli, S.T., J.T. Kirby and I. Woodruff 2018. Recent progress in the modeling and detection of meteotsunamis and storm surges. Abstract OS54B-01 (invited presentation), AGU conference, Washington DC, December, 2018. http://personal.egr.uri.edu/grilli/COPRI15_sgrilli.pdf

Hornbach, M.J., Lavier, L.L., and C.D. Ruppel 2007. Triggering mechanism and tsunamigenic potential of the Cape Fear Slide complex, U.S. Atlantic margin. *Geochemistry Geophysics Geosystems*, **8**(12), 1-16, doi: 10.1029/2007/GC001722

Kirby, J.T., Shi, F., Tehranirad, B., Harris, J.C. and Grilli, S.T. 2013. Dispersive tsunami waves in the ocean: Model equations and sensitivity to dispersion and Coriolis effects. *Ocean Modeling*, **62**, 39-55, doi:10.1016/j.ocemod.2012.11.009

Kirby, J.T., Shi, F., Nicolsky, D., and S. Misra 2016. The 27 April 1975 Kitimat, British Columbia submarine landslide tsunami: A comparison of modeling approaches. *Landslides*, 13(6), 1421-1434, doi:10.1007/s10346-016-0682-x

Locat, J., Lee, H., ten Brink, U. S., Twitchell, D., Geist, E., and Sansoucy, M. 2009. Geomorphology, stability and mobility of the Currituck slide. *Marine Geology*, **264**, 28–40.

Ma, G., Shi, F., and J.T. Kirby 2012. Shock-capturing non-hydrostatic model for fully dispersive surface wave processes. *Ocean Modelling*, **43-44**, 22-35, doi: 10.1016/j.ocemod.2011.12.002

Okada Y 1985. Surface deformation due to shear and tensile faults in a half space. *Bull. Seismol. Soc. Am.*, **75**(4):1135–1154

Schambach L., Grilli S.T., Kirby J.T. and F. Shi 2018. Landslide tsunami hazard along the upper US East Coast: effects of slide rheology, bottom friction, and frequency dispersion. *Pure and Applied Geophys.*, pps. 1-40, doi.org/10.1007/s00024-018-1978-7

Schnyder, J.S.D., Eberli, G.P., Kirby, J.T., Shi, F., Tehranirad, B., Mulder, T., Ducassou, E., Hebbeln, D., and P. Wintersteller 2016. Tsunamis caused by submarine slope failures along western Great Bahama Bank. *Scientific Reports*, **6**, pp. 1-9, doi: 10.1038/srep35925

Shi, F., J.T. Kirby, J.C. Harris, J.D. Geiman and S.T. Grilli 2012. A High-Order Adaptive Time-Stepping TVD Solver for Boussinesq Modeling of Breaking Waves and Coastal Inundation. *Ocean Modeling*, **43-44**, 36-51, doi:10.1016/j.ocemod.2011.12.004

Tehranirad, B., Harris, J.C., Grilli, A.R., Grilli, S.T., Abadie, S., Kirby, J.T. and F. Shi 2015. Far-Field Tsunami Impact in the North Atlantic Basin from Large Scale Flank Collapses of the Cumbre Vieja Volcano, La Palma. *Pure and Applied Geophysics*, **172**(12), 3589–3616, doi:10.1007/s00024-015-1135-5.

Tehranirad, B., Kirby J. T., S. T. Grilli and F. Shi 2017. Does morphological adjustment during tsunami inundation increase levels of hazard ?. In *Proc. Coastal Structures and Solutions to Coastal Disasters 2015 : Tsunamis* (Boston, USA. September 9-11, 2015), American Soc. Civil Eng., pps. 145-153. http://personal.egr.uri.edu/grilli/COPRI_Babak_2015.pdf

ten Brink, U. S., Chaytor, J. D., Geist, E. L., Brothers, D. S., and Andrews, B. D. 2014. Assessment of tsunami hazard to the US Atlantic margin. *Marine Geology*, **353**, 31–54.

Viroulet, S., Sauret, A., Kimmoun, O., and C. Kharif 2013. Granular collapse into water: toward tsunami landslides. *Journal of Visualization*, **16**, 189-191.

Watts P, Grilli ST, Tapping DR and G Fryer 2005. Tsunami generation by submarine mass failure, II: Predictive equations and case studies. *J. Waterway, Port, Coast, Ocean Engng*, **131**(6), 298-310.

Ward, Steven N., and Simon Day 2001. Cumbre Vieja Volcano-Potential Collapse and Tsunami at La Palma, Canary Islands. *Geophysical Research Letters*, **28**(17), 3397–3400, doi:10.1029/2001gl013110.

Woodruff, I., Kirby, J. T., Shi, F. and Grilli, S. T. 2018. Estimating meteotsunami occurrences for the US East Coast. In *Proc. 36th International Conference on Coastal Engineering* (Baltimore, Jul 30 - Aug 3), https://doi.org/10.9753/icce.v36.currents.66.